THESIS

Characterisation of Bone Deformation Elicited by Artificial Muscles

Submitted as part of the requirements for the degree of

BACHELOR OF ENGINEERING (MECHANICAL)
AND BACHELOR OF MEDICAL SCIENCE

by

Natalie Bennell

Supervisor: A. Prof. Colin Dunstan

External Supervisor: Mr Andreas Kriechbaumer

June, 2014

School of Aeronautical, Mechanical and Mechatronic Engineering

University of Sydney

THE UNIVERSITY OF SYDNEY

DLR

Abstract

Bone mass reduction is highly prevalent in astronauts, osteoporosis sufferers and elderly people, diminishing quality of life due to an increased risk of injury and the fear of causing a bone fracture. The rate of deterioration is increased for astronauts in the microgravity environment of space missions. Consequently, long duration spaceflight, such as for exploration beyond low-earth and lunar orbit, is not feasible because of the abiding implications on astronaut health.

This thesis presents the design, construction and initial testing of a prototype test rack to simulate body movements and measure the resultant bone deformations. Physiologically accurate muscle forces of the lower limb were modelled using pneumatic actuators on a replica human tibia. These muscle forces were determined using finite element analysis (FEA) of data obtained from an in vivo study. This information can be used to determine how much each muscle in the lower limb contributes to bone deformation, and to develop effective methods to mitigate bone degradation for both space and terrestrial applications.

The test rack was constructed and functionality experiments were conducted. The performance of the anatomical lower limb model was assessed and many structural test rack components operated as expected. A number of design modifications are proposed for use prior to further experiments, and for future iterations of the test rack.

Acknowledgements

There are many people who I would like to express gratitude to for assisting me throughout this thesis.

I would like to thank my supervisor, A. Prof. Colin Dunstan, for all his positive encouragement and assistance through the year.

I extend a great amount of gratitude to my external supervisor, Mr Andreas Kriechbaumer, who kindly invited me to work on this interesting subject. I appreciate all the guidance and generous support.

I thank Manuela Paulina Trejo Ramírez for her detailed work on the control system for the test rack.

I would also like to thank Dr. Uwe Mittag, head of the Numerical Simulation of Physiological Systems working group at DLR, who provided valuable assistance and advice.

I thank all those in the Department of Space Physiology at DLR for the continual motivation given and for providing an enjoyable place to work each day. Also, thank you to my colleagues in the Institute of Aerospace Medicine workshop, who were patient with my attempts at speaking German and with my demanding deadlines.

Finally, I would like to express gratitude to all the people who supported me during my degree. A special thank you goes to my family who have never stopped encouraging me to pursue challenges and achieve my best.

Support

This thesis would not have been possible without the support from the University of Sydney and DLR, for which I am sincerely grateful.

Preface

The work documented in this thesis was carried out in the Department of Space Physiology, Institute of Aerospace Medicine at DLR (the German Aerospace Centre) in Cologne, Germany. The work took place between August 2013 and February 2014. Following this, I examined the results, devised recommendations and wrote the majority of my thesis whilst at the University of Sydney between March 2014 and June 2014.

Some data utilised in this project is sourced from work previously performed at DLR by Pengfei Yang, called the MUST study, and computer analysis by Andreas Kriechbaumber. The control system for the test rack was designed by Manuela Paulina Trejo Ramírez with requirements I developed.

I carried out the literature review to understand the physiological aspects of the lower limb, evaluate current research and establish the possible implications of my work. I devised the design requirements and specifications for the test rack, with guidance from my external supervisor, Andreas Kriechbaumer. I designed the assembly of the test rack and selected materials to use. I ordered the structural material, whilst the pneumatic system materials and devices were ordered by Manuela Paulina Trejo Ramírez. I designed additional components to be manufactured, with the manufacturing performed by the Aerospace Medicine Institute's workshop. I constructed the test rack, with the assistance of Andreas Kriechbaumer. I wrote test protocols for functionality testing. I performed tests with the assistance of Andreas Kriechbaumer and Manuela Paulina Trejo Ramírez, who regulated the pneumatic system. I analysed the results of the tests. The design recommendations devised are primarily my own, with some resulting from discussion with my external supervisor. Tests performed after my thesis were conducted by Andreas Kriechbaumer and Manuela Paulina Trejo Ramírez.

Natalie Bennell

Supervisor, A. Prof. Colin Dunstan

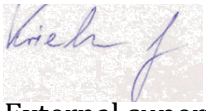

External supervisor, Mr Andreas Kriechbaumer

Table of Contents

Abstract ii

Acknowledgements iii

Preface iv

List of Figures x

List of Tables xiv

Abbreviations xvi

CHAPTER 1: INTRODUCTION 1

1.1 Bone Mass Reduction in Human Spaceflight 1

1.2 Thesis Project Objectives 1

1.3 Thesis Structure 2

CHAPTER 2. LITERATURE REVIEW 3

2.1. Anatomy and Physiology of the Lower Limb 3

2.1.1 Bone Mechanics 3

2.1.2 Bones of the Lower Limb 5

2.1.3 Muscle Location for the Tibia Bone 6

2.1.4 Muscle Contribution 7

2.2 Bone Atrophy 8

2.2.1 Occurrence of Bone Atrophy 9

2.2.2 Bone Mass Reduction in Space 9

2.2.2.1 Bone Atrophy in Previous Space Missions 10

2.2.2.2 Mitigation Methods 12

2.2.2.2.1 Pre-Flight Countermeasures 12

2.2.2.2.2 Resistance Exercise 12

2.2.2.2.3 Vibration 14

2.2.2.2.4 Pharmacologic Measures 14

2.2.2.2.5 Post-Flight Surveillance 15
2.2.3 Terrestrial Bone Mass Reduction 15
2.2.3.1 Health Complications Associated with Terrestrial Bone Atrophy 16
2.2.3.2 Mitigation Methods 17
2.3 Bone Deformation 18
2.4 Measurement Systems for Bone Deformation 21
2.4.1 In Vivo Measurement Procedures: In vivo Strain Gauge 21
2.4.1.1 In Vivo Strain Gauge Measurements 21
2.4.1.2 In Vivo Optical Measuring Systems 23
2.4.2 Ex Vivo Measurement Procedures 23
2.4.2.1 Scanning 23
2.4.2.2 Computer Modelling 24
2.5. Experimental Apparatus for the Lower Limb 25
2.6 Thesis Justification 27
CHAPTER 3. DESIGN AND CONCEPTS 28
3.1 Methodology Justification 28
3.1.1 Requirements 28
3.1.2 Design Considerations: Muscle Forces 30
3.1.3 Design Considerations: Angle of Muscles 31
3.1.4 Design Considerations: Body Force Impact 32
3.1.5 Design Selection 33
3.2 Experimental Apparatus 36
3.2.1 Materials and Devices 36
3.2.2 Test Rack Assembly 40
3.2.2.1 Test Rack Shell 40
3.2.2.2 Tibia Positioning 41

3.2.2.3 Top and Base Plates 41
3.2.2.4 Force Re-Direction and Actuator Positioning 42
3.2.2.5 Test Rack Assembly 43
3.3 Apparatus Setup 44
3.4 Control System 45
CHAPTER 4. ASSEMBLY AND TESTING METHODS OF PROTOTYPE 46
4.1 Test Rack Assembly 46
4.2 Problems Encountered and their Mitigations 48
4.3 Safety Measures 50
4.4 Testing Protocol 51
4.1.1 Initial Test 52
4.1.2 Tibialis Anterior Test 52
4.1.3 Soleus Test 53
4.1.4 Y-Direction Force Application Test 54
CHAPTER 5. RESULTS 55
5.1 Initial Test 55
5.2 Tibialis Anterior Test 56
5.3 Soleus Test 57
5.4 Y-Direction Test 60
5.5 Summary of Results 61
CHAPTER 6. DISCUSSION 63
6.1 Experimental Procedure 63
6.2 Test Rack Performance 65
6.3 Comparison of Design to Literature 68
6.3.1 Muscle Attachment 68
6.3.2 Knee and Ankle Joints 69

6.4 Recommended Design and Setup Modifications 70
6.4.1 Component Design Improvements 70
6.4.2 Construction Design and Setup Improvements 71
6.5 Limitation of Thesis 72
6.5.1 Testing Conditions 72
6.5.2 Component Conditions 73
6.6 Summary of Project 73
6.7 Future Directions 73
CHAPTER 7. CONCLUSION 75
REFERENCES 76
APPENDICES 84
Appendix A: Design Specification List 85
Appendix B: Isometric Forces of the Lower Leg 90
Appendix C: Beta Rack Specifications 91
Appendix D: List of Products 92
D1. Structural Components 92
D2. Support Components 93
D3. Devices Used 94
D4. Additional Components 94
D5 Safety Shielding Components 96
Appendix E: Specifications of Purchased Components 97
E1. Tibia Specimen 97
E2. Actuator Rope 98
E3. Safety Rope 98
E4. Bowline Knot 99
E5. Force Plate 100

E6. Pulley 101
Appendix F: Test Rack Engineering Designs 102
Appendix G: Control System 121
G1. Device Specifications 121
G.1.1 Actuators 121
G.1.2 Actuator Lever Arms 122
G.1.3 Actuator Mounting Support 123
G.1.4 Load Cells 124
G2. Pneumatic Control System Layout 125
Appendix H: Test Rack Results Summary 127
Appendix I: Validation Test Protocol 132

List of Figures

Figure 1: Hierarchical structural organisation of bone [10] 4

Figure 2: Osteocyte canalicular network [16] 5

Figure 3: Bones and joints of the lower limb, adapted from [17] 5

Figure 4: The tibia and fibula of the right leg. Left: anterior view, Right: posterior view [18] 6

Figure 5: Muscles of the right lower leg. Left: posterior superficial, Middle: posterior deep, Right: anterior [17] 7

Figure 6: The 21 muscles modeled, adapted from [19] 8

Figure 7: Trabecular network in a vertebral body: Left: from a young individual, with a dense network, Right: from an elderly individual, with a decrease in bone density [26] 9

Figure 8: Profile of 11 individual BMD changes in distal tibia relative to 6 month missions. Cumulative days spent in space before the document mission are shown in brackets for each cosmonaut [32] 11

Figure 9: Left: A crewmember performing a squat exercise on iRED [35]. Right: A crewmember performing a deadlift exercise on ARED [36] 13

Figure 10: Distribution of DXA aBMD as a percentage change in long-duration astronauts on Mir and ISS spaceflights [4] 14

Figure 11: Percentage change in DXA BMD, compared to preflight, in long-duration spaceflight [40] 15

Figure 12: Age-specific incidences of hip, vertebral and Colles' (wrist) fracture in Rochester, Minnesota [41] 16

Figure 13: BMC in the proximal tibia as a percentage of the mean of normal values [44] 17

Figure 14: Measurements from pQCT and DXA relating to the annual BMD percentage change in the TCC exercise group and control group (CON) [46] 18

Figure 15: Types of bone strain. (A) axial strain, (B) shear strain, (C) bending strain, (D) torsion strain [51] 19

Figure 16: Group means for: Left: axial, and; Right: shear components acting on the tibia. The lines represent the compressive contact forces (CompF), shear contact force (ShearF), net muscle force (MusF) and joint reaction force (JRF) [19] 20

Figure 17: Principal strains during exercise activities [54] 22

Figure 18: Left: Setup of the three-point bending experiment with 20kg of weight applied. Right: Deformation angle measure in the axis of weight application [62] 23

Figure 19: pQCT cross-sections obtained at 4 levels in the tibia. Differentiating between male, female and female athlete [63] 24

Figure 20: Different forms of meshing with FEA. Elements can be linear (a, b, c) or quadratic (d) [65] 25

Figure 21: Left: The knee simulator with a specimen fixed into the hip and tibia tubes [71]. Right: The Oxford rig used to simulate a weightbearing squat in cadaveric knee specimens [73] 26

Figure 22: A cadaver leg loaded onto the test rack. The numbers refer to pneumatic actuators linked to different muscles. 1: quadriceps, 2: semimbranosus, 3: biceps femoris, 4: gastrocnemius medialia, 5: soleus, 6: gastroncnemius laterialis, 7: tibialis anterior, 8: tibialis posterior [74] 27

Figure 23: Muscle attachment to tibia. Left: anterior view, Right: posterior view [17] 31

Figure 24: Vertical ground reaction forces during barefoot heel-toe running [76] 32

Figure 25: Force and moment (%BW) on the left knee when walking at a velocity of 3 km/h (subject K8L) [77] 32

Figure 26: Tibia specimen dimensions: a) 405 mm, b) 84 mm, c) 28 mm, d) 58 mm, e) 10 mm (canal) [80] 36

Figure 27: Layout of muscle simulation: 1) actuator arm, 2) rope clasp, 3) load cell, 4) rope tightener 38

Figure 28: Posterior muscle re-direction mechanism with three eye bolts fastened to item beams 38

Figure 29: Safety rope feeds through the top plate and the four eye bolts attached to the two vertical beams 38

Figure 30: Two ends of the safety rope connected with a bowline knot and a rope clamp 39

Figure 31: Y-axial force application from a pulley system 39

Figure 32: Test rack shell. Left: front view, Right: top angled view 40

Figure 33: Tibia alignment with pulleys on front of pillars 41

Figure 34: The top plates above the tibia specimen 42

Figure 35: Actuator lever arms align with the redirection eye bolts 42

Figure 36: Actuator positions on actuator plate 43

Figure 37: Test rack assembly 43

Figure 38: Four sunken head bolts drilled into the top grooves of the tibia specimen.....44

Figure 39: Muscle attachment to tibia: 1) Soleus, 2) Tibialis Posterior, 3) Tibialis Anterior, 4) Flexor Digitorum Longus 44

Figure 40: Tibia attachment to base plate.....45

Figure 41: Large brackets fastened between the two vertical beams and structural horizontal beam 48

Figure 42: Base brackets used to hold up long beams; Left: small brackets, Right: larger brackets 49

Figure 43: Left: bowline knots, Right: rope fasteners and rope tighteners 49

Figure 44: Temporary solution of inserting 40x40 mm beams under each corner of the test rack 50

Figure 45: PVC cylinder with bolts as muscle attachments 52

Figure 46: Tibialis Anterior Test actuator to muscle attachment rope connection.....53

Figure 47: Soleus muscle attachment on posterior side of tibia 54

Figure 48: Y-direction test setup 54

Figure 49: Temporary solution to prevent force plate from sliding.....57

Figure 50: Temporary load cell solution to measure forces 59

Figure 51: Slope of top plate; Left: before force application, Right: after force application.....61

Figure 52: Crack on the base of the tibia; Left: before testing, Centre: after testing' Right: Base of tibia showing the outermost thread worn away and tip minor indentation.....62

Figure 53: Comparison of slope direction between Anterior Tibialis and Soleus tests 66

Figure 54: The posterior (left) and lateral (right) views of the knee: (1) femur, (2) medial condyle, (3) lateral condyle, (4) medial meniscus, (5) lateral meniscus, (6) tibial collateral ligament, (7) fibular collateral ligament, (8) tibia, (9) fibula, (10) quadriceps tendon, (11) patella, (12) patellar ligament [85] 69

Figure 55: Approximate location of the marker clusters for the optical measuring system to detect tibia deformation; Left: front view, Right, side view 71

Figure 56: Secure additional item beams below the small platform (arrows) to raise the structure above the tibia base plate.....72

Figure 57: Actuator rope, layouts of material [90].....98

Figure 58: Steps to tie a bowline knot [92].....99

Figure 59: AMTI OR6-6-2000 Dimensions [93] 101
Figure 60: Harken 57 mm Cheek Block [94] 101
Figure 61: Materials of compact cylinders AEVU/AEVUZ [81] 122
Figure 62: Dimensions of the compact cylinders AEVU/AEVUZ) [81] 122
Figure 63: Rob eye SGS dimensions [83] 123
Figure 64: Mounting apparatus dimensions [82] 123
Figure 65: Dimensional drawing of burster load cell, model 8531 [95] 124
Figure 66: Individual components of the control system 125
Figure 67: LabView layout of the entire pneumatic system 126

List of Tables

Table 1: BMD and lean tissue change after 4-14.4 months of spaceflight [30] 10

Table 2: Requirements list 29

Table 3: Isometric force of muscles of the lower leg with force in the upwards direction [75] 30

Table 4: Isometric force of muscles in the lower limb with force in the downwards direction [75] 30

Table 5: QFD Analysis 33

Table 6: An overview of the differences between the Alpha and Beta test racks 34

Table 7: Is the movement feasible with the test rack design? 35

Table 8: Summary of test rack assembly 46

Table 9: A summary of safety measures 50

Table 10: Summary of the test rack components and their responses during the Initial Test 55

Table 11: Summary of the Tibialis Anterior Test observations 56

Table 12: Summary of the first Soleus Test observations 58

Table 13: Load Cell Test 59

Table 14: Summary of the second Soleus Test observations 60

Table 15: Component design modifications 70

Table 16: Design modifications for improvements to the construction and setup of the apparatus 71

Table 17: Alpha test rack specifications and design solutions 85

Table 18: Isometric forces of the muscles in the lower leg; yellow: modelled upward forces, green: modelled downward force. Adapted from [75] 90

Table 19: Beta Test Rack Specifications 91

Table 20: List of structural components of the test rack 92

Table 21: List of custom designed support components of the test rack 93

Table 22: List of devices used in the test rack 94

Table 23: List of other components used in the test rack 95

Table 24: Safety shielding components 96
Table 25: Simulated cortical bone (short fibre filled epoxy) 97
Table 26: Simulated cancellous bone (rigid polyurethane bone) 97
Table 27: Actuator rope specifications [90] 98
Table 28: Safety rope parameters [91] 98
Table 29: AMTI OR-6-6-2000 Force Plate specifications [93] 100
Table 30: AMTI OR6-6-2000 Force Plate Capacity, Sensitivity and Frequency [93] 100
Table 31: Harken Pulley Specifications [94] 101
Table 32: Muscle modelled compared with actuator piston size 121
Table 33: Dimensions for the four compact cylinders AEVU/AEVUZ used (mm). Adapted from [81] 122
Table 34: Dimensions for the four rob eyes SGS used (mm). Adapted from [83] 123
Table 35: Dimensions for the four actuators mounting apparatus (mm). Adapted from [82] 123
Table 36: Corresponding dimensions and specification for the load cell. Adapted from [95] 124
Table 37: Summary of test rack specifications and the results of this project 127

Abbreviations

Al	Aluminium
ARED	Advanced Resistive Exercise Device
BAP	Bone-specific Alkaline Phosphonate
BMC	Bone Mineral Content
BMD	Bone Mineral Density
BMU	Basic Multicellular Units
BW	Body Weight
CAD	Computer Aided Design
CT	Computed Tomography
DLR	Deutsches Zentrum für Luft- und Raumfahrt (the German Aerospace Centre)
DXA	Dual-energy X-ray Absorptiometry
FBM	Fat Body Mass
FEA	Finite Element Analysis
FEM	Finite Element Method
iRED	Interim Resistive Exercise Device
ISS	International Space Station
JAXA	Japan Aerospace Exploration Agency
LBM	Lean Body Mass
NASA	The National Aeronautics and Space Administration
NTX	N-teleopeptide
OST	Optical Segment Racking
pQCT	Peripheral Quantitative Computer Tomography
PVC	Polyvinhyl Chloride
QCT	Quantitative Computer Tomography
QFD	Quality Function Deployment
St	Steel
TCC	Tai Chi Chu
Zn	Zinc

CHAPTER 1: INTRODUCTION

1.1 Bone Mass Reduction in Human Spaceflight

Prolonged exposure to microgravity in space causes bone mass reduction, which increases the risk of bone fractures and early onset osteoporosis. The significant health risk to astronauts limits current mission durations, and restricts advancements in future human spaceflight endeavours.

Skeletal recovery from bone atrophy requires significantly more time than the spaceflight itself. It is estimated that an astronaut's bone mass takes up to three years to return to pre-flight levels [1]. Aside from spaceflight, people in the global population also suffer from bone degradation and are at high risk of injury. People with osteoporosis, suffering from paralysis or patients requiring limb immobilisation experience bone mass reduction.

It is necessary to develop countermeasures to limit bone degradation in order to both increase productivity of current geocentric manned missions, and to allow more rapid progress in development of manned missions further into the solar system. These methods will also benefit the wider community. Numerous studies have been performed to develop countermeasures that reduce bone atrophy, ranging from resistive exercises to pharmaceuticals [2-4] However, none have been effective in completely preventing bone mass reduction.

1.2 Thesis Project Objectives

The purpose of this project was to design and manufacture experimental apparatus, called the 'test rack', for musculoskeletal experiments. These experiments will establish how muscles and bones work together to maintain skeletal health, with a focus on the load-bearing tibia bone of the lower leg, which experiences an increased rate of bone loss when unloaded. A replica human tibia was used, with muscle forces simulated using pneumatic actuators. The test rack reproduces body movements by modelling muscle forces and body weight, and determines the resulting tibia bone deformation. The design process aimed to generate a physiologically accurate model of the lower leg. Tests were

performed to evaluate appropriate safety measures and determine accurate functionality of the apparatus.

The thesis is a follow-on study from a previous project at DLR (the German Aerospace Centre), called the MUST study [5, 6]. In MUST, researchers inserted three screws into the tibia of five living healthy males, and performed in vivo measurements to determine how the tibia deforms during different movements. This information was put into a computer model using the Ansys software suite (Ansys, Inc., PA, USA). The software then determined the magnitude of muscle force from the bone deformation. The test rack developed in this project was designed to produce the same tibia deformation as the MUST study, using simulated muscle forces on a model human tibia. The data can then be used to support and verify the computer model, and improve its accuracy based on empirical measurements.

1.3 Thesis Structure

The following chapter presents an in depth analysis of bone mechanics, bone loss and bone deformation, focusing particularly on aspects relevant to spaceflight. The current literature is analysed, and the state of research is discussed, including mitigation methods to reduce bone loss, measuring systems to detect bone deformation and test racks that examine cadaver legs and knee joints.

The design of the test rack is justified in Chapter 3, inclusive of the structural mechanics of the test rack and physiological model of the lower limb. The testing procedure encompasses the test rack assembly, safety measures and the test protocol. Results are presented in Chapter 5, including additional tests to address issues arising with certain components.

Chapter 6 discusses in detail the completed test rack and presents the initial measurements. Design modifications for future tests are proposed, along with recommendations for complementary future work. A conclusion is then drawn on the suitability of the apparatus design and experimental results. Appendices are provided for the apparatus design specifications, isometric forces of materials in the lower leg, list of materials,specifications of purchased products technical drawings of components designed and manufactured during the project, control system layout, design specification compared with results and test protocol for the intended future validation of the test rack.

CHAPTER 2. LITERATURE REVIEW

This literature review presents and discusses the current research and findings on the field of bone mechanics, bone atrophy and measures to counteract bone loss. Key contributing studies discussed and evaluated include both those performed on Earth and in space. A large area of the research focuses on the tibia bone. Due to being a weight bearing bone, a decrease in movement and corresponding forces consequently impairs bone strength. Therefore, alterations in the tibia bone can be attributed to bone atrophy and an increased risk of fractures.

2.1. Anatomy and Physiology of the Lower Limb

2.1.1 Bone Mechanics

Bone mass is the most commonly examined factor of bone structural behaviour [7] because of its close relation to bone strength. Bone is composed of cortical bone and cancellous bone. The microstructure of these varies immensely. Cortical bone is dense bone arranged in osteons, in which the matrix lamellae are laid down in a concentric circular pattern around a central Haversian canal containing blood vessels (Figure 1). These arise due to remodelling of the original bone by basic multicellular units (BMU). Cancellous bone is porous bone. It is made up of rods and plates of bone, forming an open sponge-like architecture. Consequently, the two behave differently when exposed to stimuli. Much research supports this fact. For instance, Goldstein *et al.* [8] found that in one subject alone, the spatial variations in cancellous bone stiffness within the tibial metaphysis can have a 100-fold difference, ranging from 4 to 430 MPa in the load bearing area. This illustrates the vast behavioural difference within the cancellous bone. Also, Ulrich *et al*. [9] found that bone exhibiting similar bone mineral density (BMD), yet having diverse bone architectures, can have a strength and stiffness difference of up to 53%.

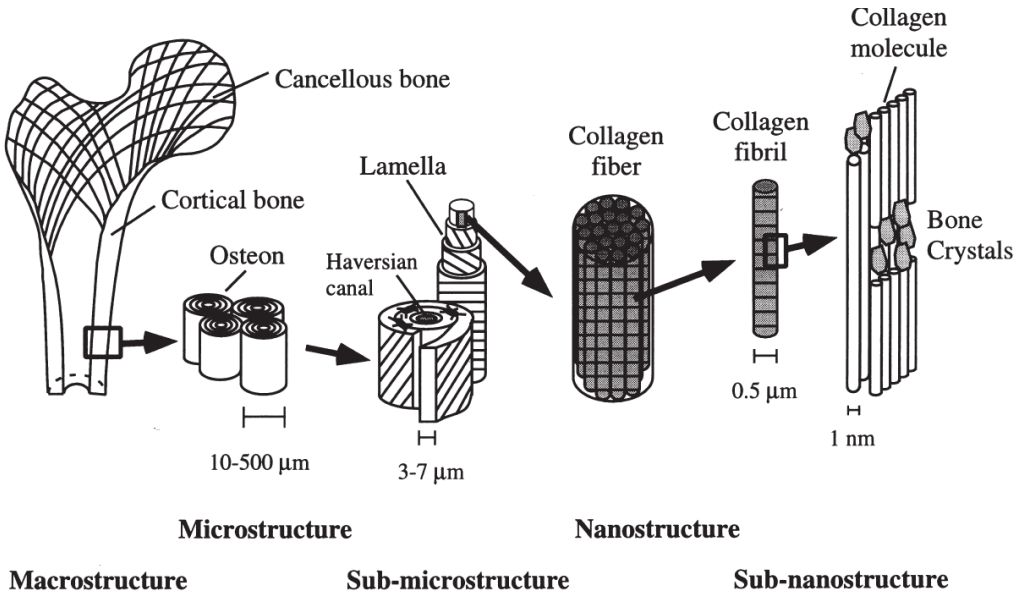

Figure 1: Hierarchical structural organisation of bone [10]

Bone remodelling typically occurs to either maintain mineral homeostasis, adapt to mechanical changes or repair damage [11]. BMU is a term used to describe a functional cohort of cells that control the process of bone remodelling: osteoblasts, osteoclast, osteocytes, bone lining cells and capillary blood supply [12].

Bone continues to renew itself with bone formation, induced by osteoblasts, and bone degradation or resorption, induced by osteoclasts. In modelling, these processes are not directly coupled, however either or both may be involved depending on the stimulus. In unloading, bone modelling can result in bone loss whereas in reloading, it can result in bone gain. In growth, osteoblasts and osteoclasts act on different sides of cortical bone to enable bone drift, sculpting the shape of the bones. Osteocytes (Figure 2), which are mature osteoblasts embedded within the bone matrix, are prevalent throughout the skeletal system and are involved in the regulation of bone remodelling [13]. They actively secrete growth factors that simulate bone formation as well as secrete sclerostin that inhibits bone formation [11, 14]. In elderly people, the bone remodelling process becomes disturbed due to a shortage of osteoblast formation in relation to osteoclast absorption [15]. In space, bone resorption increases at a rapid rate due to the reduced stress on bones from lower gravity levels.

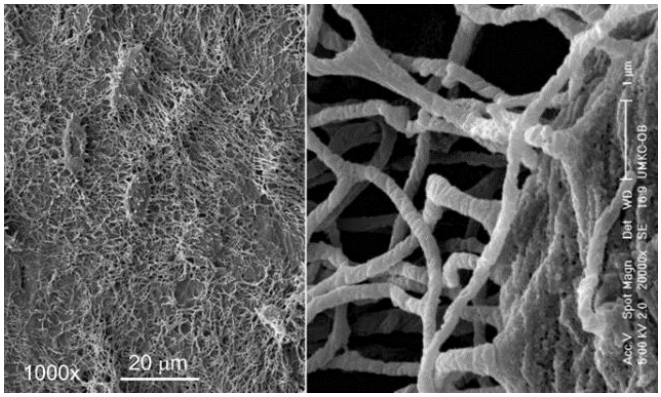

Figure 2: Osteocyte canalicular network [16]

2.1.2 Bones of the Lower Limb

As the lower limbs support the weight of the body and are subjected to high forces, the bones are thicker and stronger when compared to those of the upper limbs. The lower limbs also function as the mechanism to move the body through space [17, 18]. The bones of the lower limb include the pelvic bone, femur, patella, tibia, fibula and foot bones (Figure 3).

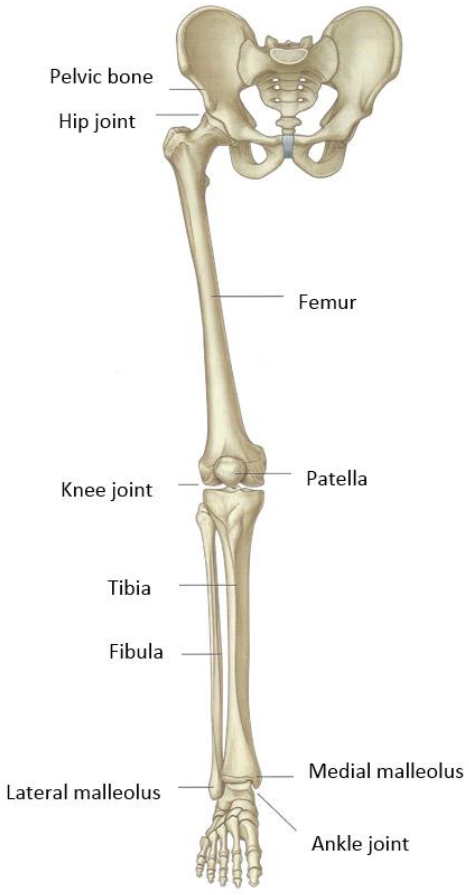

Figure 3: Bones and joints of the lower limb, adapted from [17]

This thesis investigates tibia displacement from muscle simulation. The tibia bone receives force from the femur and transmits it through to the foot. The tibia shaft has a triangular cross-section and expands at both the upper and lower ends of the bone to support the weight of the body at the knee and ankle. In contrast, even though several muscles originate from the fibula bone, it is not involved in weight bearing (Figure 4) [17, 18].

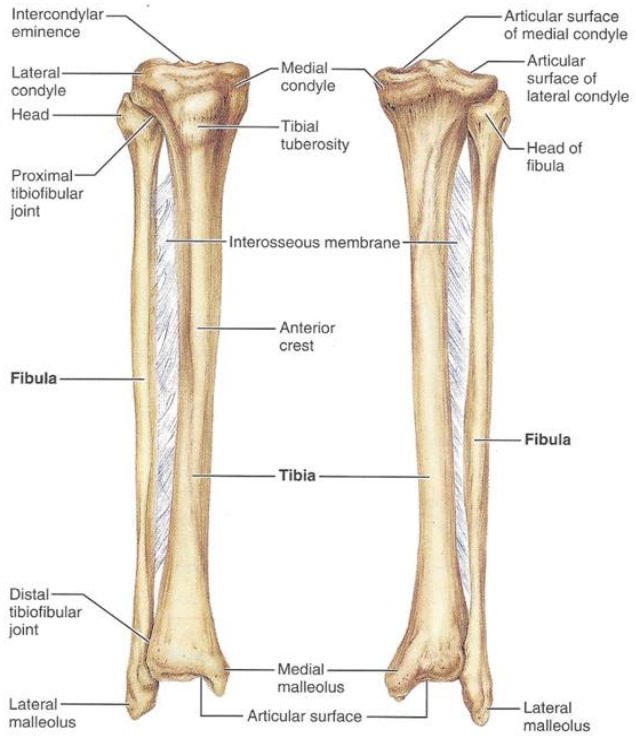

Figure 4: The tibia and fibula of the right leg. Left: anterior view, Right: posterior view [18]

2.1.3 Muscle Location for the Tibia Bone

Skeletal muscle tissue attaches to and covers the skeletal system. It consists of parallel bundles of long fibres with transverse stripes, called striations. Through somatic and branchial motor nerves, the muscle is compelled to move bones and gives support to the body. Individual skeletal muscles are typically named on the bases of shape, attachments, position or fibre orientation [17].

Muscles of the posterior compartment of the leg are arranged in two groups, superficial and deep, and are separated by a layer of fascia. The three superficial muscles in the posterior compartment of the leg, the gastrocnemius, plantaris and soleus (Figure 5, left), all connect to the calcaneus bone and cause plantar flexion of the ankle joint. There are four muscles in the deep compartment of the leg (Figure 5, middle). The popliteus acts on

the knee, whereas the flexor halluces longus, flexor digitorium longus and tibialis posterior all act mainly on the ankle. The four muscles in the anterior compartment (Figure 5, right) of the leg collectively dorsiflex the foot at the ankle joint, extend the toes and invert the foot [17].

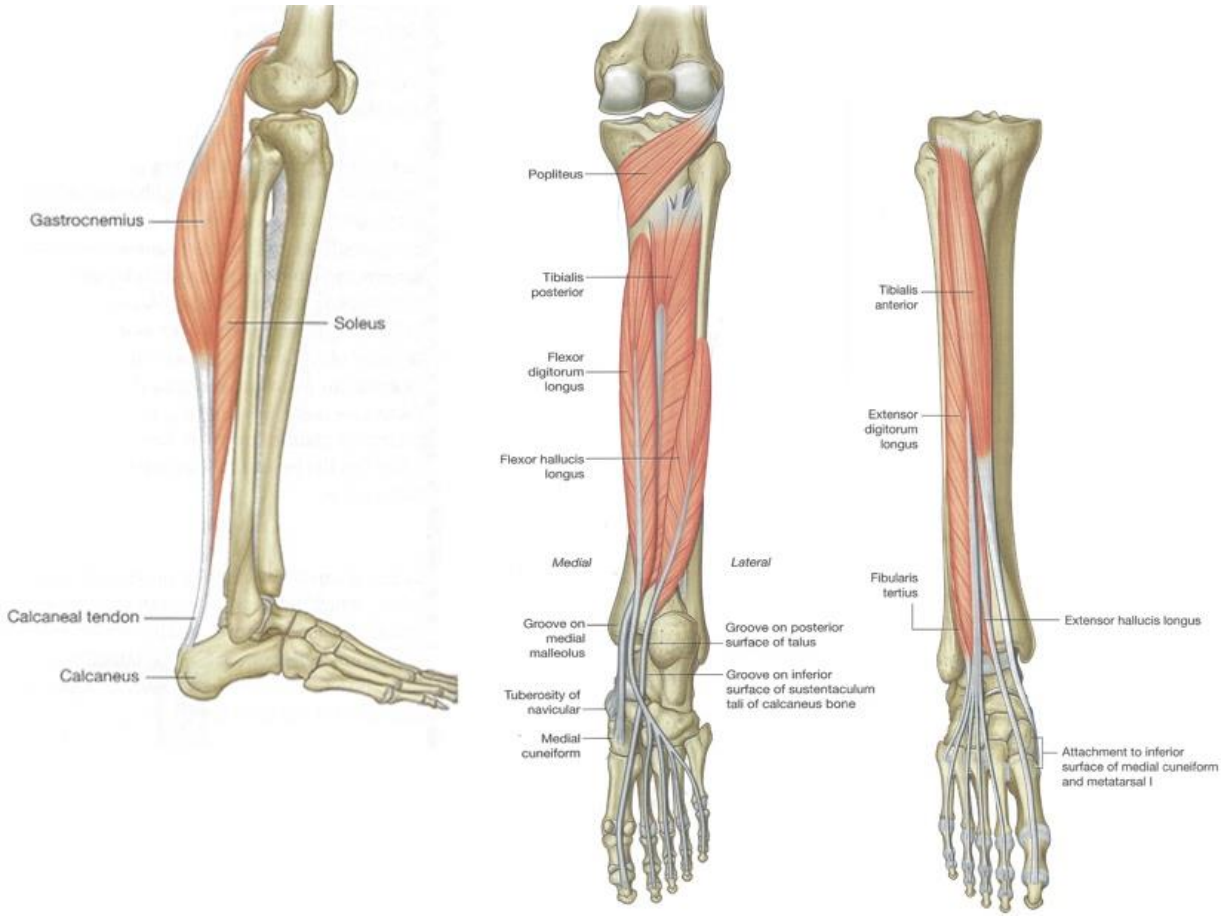

Figure 5: Muscles of the right lower leg. Left: posterior superficial, Middle: posterior deep, Right: anterior [17]

2.1.4 Muscle Contribution

The movement and force of muscles affects the deformation of bones. Across the research of bone and whole extremity movement, muscles are required to be included in models for valid conclusions to be drawn. An example of note is that of Sasimontonkul *et al.* [19], who optimised a model of the lower limb with 21 attached muscles (Figure 6).

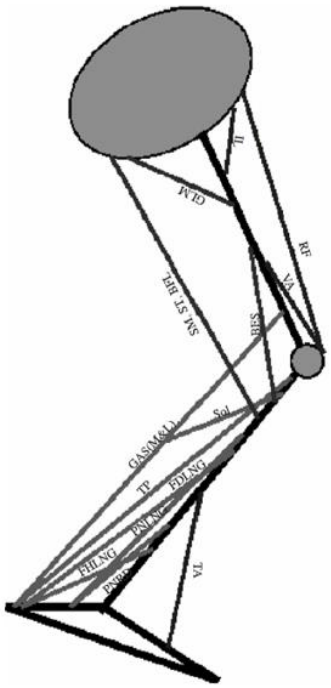

Abbreviation	Muscle
GASM	medial gastrocnemius
GASL	lateral gastrocnemius
FDLNG	flexor digitorum longus
PNBR	peroneus brevis
Sol	soleus
TP	tibialis posterior.
FHLNG	flexor hallucis longus
PNLNG	peroneus longus
TA	tibialis anterior
BFS	biceps femoris short head
BFL	biceps femoris long head
ST	semitendinosus
SM	semimembranosus
RF	rectus femoris
VA	vastii is composed of vastus mediallis (VAM), vastus intermedius (VAI), and vastus laterallis (VAL)
GLM	gluteus maximus is composed of superior, middle, and inferior components.
IL	iliacus

Figure 6: The 21 muscles modeled, adapted from [19]

Similarly, Arnold *et al.* [20] utilised a new computer model of the lower limb based on the layout and architecture of 21 cadaver subjects [21]. The investigation used a musculoskeletal modelling package [22] to construct the geometry of a single lower limb and placed axis coordinates at the joints. Additionally, they added 35 muscles of the lower limb to further model the movement. Predictions of fibre length and muscles forces can be obtained from the model. It is available to the public [23] and can be further examined in the software OpenSim (Stanford, CA, USA).

2.2 Bone Atrophy

Bone has the ability to adjust its internal structure as a result of varying mechanical demands. This mechanism is proposed to involve localised electric fields induced by piezoelectric effects resulting from forces in bone crystal [24]. These changes allow for humans and animals alike to adapt to environmental fluctuations. Therefore, promotion of frequent loading situations increases bone mass, whilst disuse impedes bone growth. Bone atrophy resulting from impedance of bone growth is a silent illness without symptoms until a fracture occurs. Two factors that provide a hindrance to daily life is a fracture itself and the fear of fracture once bone loss is diagnosed.

2.2.1 Occurrence of Bone Atrophy

Bone atrophy results in reduced bone mass and modified microstructure of bone (Figure 7). It can be induced in a number ways, and is classified into two groups: primary osteoporosis and secondary osteoporosis [25]. Primary osteoporosis is typically associated with an increase in age and decrease in gonad function, for example low levels of oestrogen. It is extremely common amongst post-menopausal women and leads to an increased likelihood of bone fractures. Secondary osteoporosis is a result of other health problems, commonly disuse. Disuse osteoporosis is classified through a decrease in mechanical loading in such areas as lower limbs due to a great decline in weight bearing. It affects astronauts, people with paralysis, those on prolonged bed rest or have a bone immobilised due to fracture or other injury. Bone

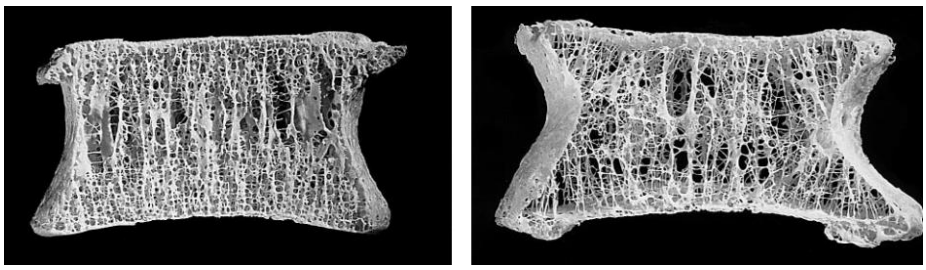

Figure 7: Trabecular network in a vertebral body: Left: from a young individual, with a dense network, Right: from an elderly individual, with a decrease in bone density [26]

2.2.2 Bone Mass Reduction in Space

Decreased forces and reduced movement as a result of microgravity is believed to be the primary driver accelerating bone loss in astronauts. Due to weightlessness in space, bone resorption increases and bone formation is suppressed, thus leading to progressive bone mass reduction [1].

Following the Apollo program, NASA founded the Skylab space station. Focusing on life science missions, three 3-man crew Skylab missions took place between 1973 and 1974. Subsequent combined and individual manned space missions followed from the American and Russian space programs. Both organisations performed numerous studies and collected data related to the musculoskeletal system. In 1999, construction of the International Space Station (ISS) commenced, and continues today. The missions to the ISS are usually mid to long duration, thus creating an excellent test bed for microgravity studies [27].

2.2.2.1 Bone Atrophy in Previous Space Missions

Bone loss associated with the microgravity of spaceflight is a well-recognised problem for astronauts. It poses risks not only during spaceflight, but also once astronauts are returned to Earth because the recovery time is significant, potentially leading to long-term health impacts. Astronauts experience the highest amount of bone loss in their primary load bearing bones: the long bones of the leg, pelvis and lower spin. It is widely considered that muscle strength is much more likely to restore before bone mass following microgravity [28], hence increasing the potential of bone fractures [29]. Additional risks include bone fracture whilst in space and early onset osteoporosis.

In 1989, the American and Russian space agencies established a collaboration to study bone changes during flight in-situ in space. An accumulation and analysis of measurements performed on 18 cosmonauts on the Russian Mir station between 1990 and 1995 is presented by LeBlanc *et al.* [30]. Apart from two individuals with flight durations of 311 and 438 days, the duration range for spaceflight was between 126 and 197 days. An exercise countermeasure protocol was followed whilst on-station, involving: cycle-ergometer, treadmill (with bungee cords for attachment) and strengthening exercise with elastic expanders. The crew had dual-energy X-ray absorptiometry (DXA) scans pre-flight and post-flight. It can be seen from the measurements collected (Table 1) that BMD was reduced by an average of 1-1.5 % per month. Furthermore, an important point was that bone losses in the weight bearing skeletal regions are high. This trend can similarly be seen in bed rest study subjects [31]. It was suggested that the flight exercise program was not sufficient in reducing the amount of bone loss.

Table 1: BMD and lean tissue change after 4-14.4 months of spaceflight [30]

Variable	N	%/Month	SD
BMD Spine	18	-1.06*	0.63
BMD Neck	18	-1.15*	0.84
BMD Troch	18	-1.56*	0.99
BMD Total	17	-0.35*	0.25
BMD Pelvis	17	-1.35*	0.54
BMD Arm	17	-0.04	0.88
BMD Leg	16	-0.34*	0.33
Lean Total	17	-0.57*	0.62
Lean Leg	16	-1.00*	0.73
Lean Arm	17	0.00	0.77
Fat Total	17	+1.79	4.66

*$p<0.01$

Similarly, BMD measurements were accumulated from 15 Russian MIR cosmonauts from 1994 to 2000 [32]. Figure 8 graphs the tibia measurements before and after spaceflight and 6 months following return to Earth on a peripheral quantitative computer tomography (pQCT) system. It shows the cancellous bone of the tibia having a greater BMD reduction (mean -1.8%) compared to the cortical bone (mean -5.4%). BMD did not return to pre-flight values after six months recovery, emphasising the length of the recovery process.

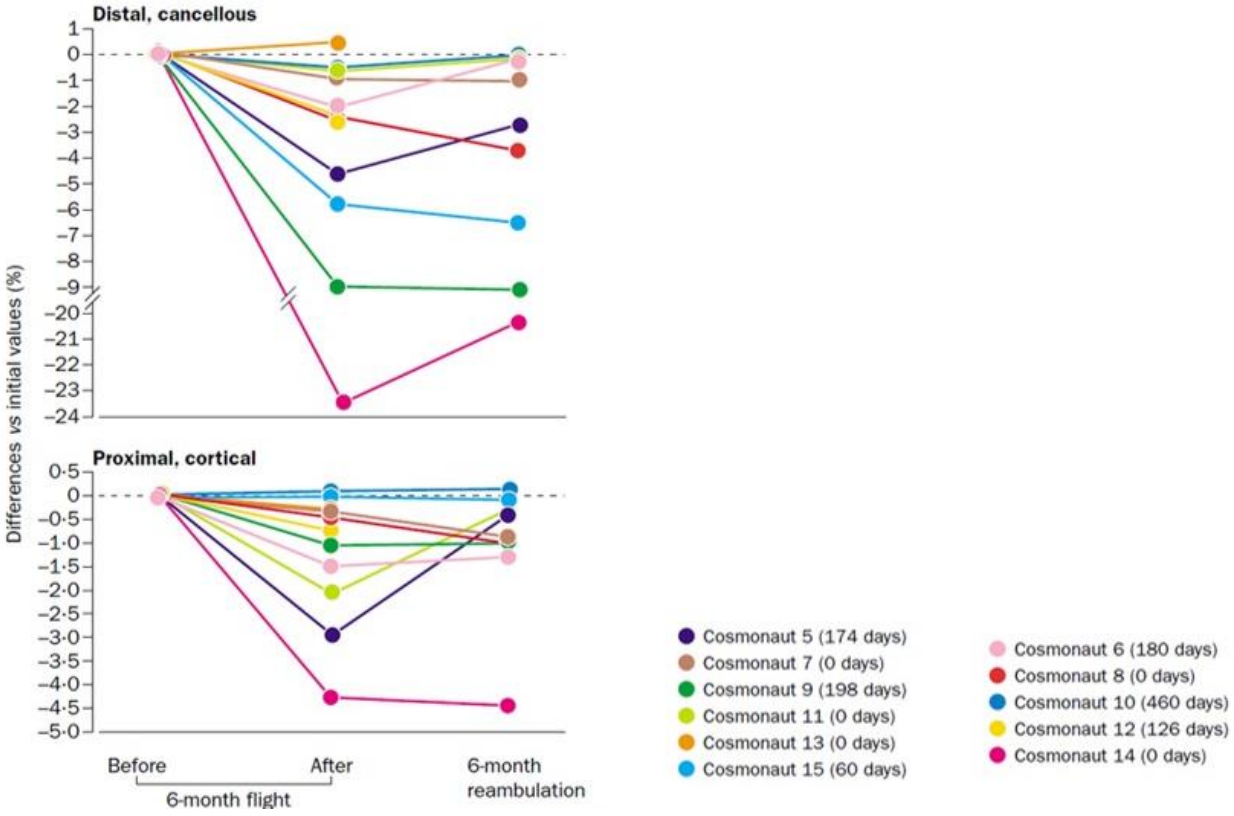

Figure 8: Profile of 11 individual BMD changes in distal tibia relative to 6 month missions. Cumulative days spent in space before the document mission are shown in brackets for each cosmonaut [32]

A further method to measure bone loss is through bone turnover biomarkers. Studies were performed as part of the Shuttle-Mir Science Program on astronauts and cosmonauts who were in space for 4-6 months [33]. The results found an increase in N-telopeptide (NTX) early in spaceflight, signifying an increase in bone resorption. This level remained elevated throughout the mission but returned to pre-flight levels on landing and samples collected up to four months post-flight. In contrast, bone-specific alkaline phosphatase (BAP), a biomarker for bone formation, was slightly reduced or remained

unchanged for the duration of spaceflight, indicating the occurrence of bone resorption and formation uncoupling.

2.2.2.2 Mitigation Methods

Much research has been performed in an attempt to develop countermeasures for bone atrophy. Although there is as yet no sufficiently performant device or method to eliminate bone loss identified, exercises have shown promise in counteracting decline of the musculoskeletal system of astronauts, especially when combined with medication and dietary guidelines.

2.2.2.2.1 Pre-Flight Countermeasures

Certain protocols for pre-flight should be modified, according to recent research. NASA standards state that long-duration astronauts are permitted a 10-15% decline in areal bone mineral density (aBMD) during spaceflight [34]. Since 1998, NASA has medically required DXA measurements of aBMD on all astronauts. They use T-score cut-points to determine bone health, with a low initial T-score serving as a reason for disqualification from long-duration spaceflight. This criterion can beneficially be used to watch over astronauts who have a high risk of bone strength loss and thus an increased chance of fracture. However, the dependence on DXA as the only method of assessing spaceflight outcomes and countermeasure effectiveness may offer insufficient information to NASA. The NASA Bone Summit [34] therefore recommends NASA additionally uses QCT-based FEM estimates of hip strength as pre-flight measurements for understanding bone health. Furthermore, they advise that QCT measurements be performed as close as possible to launch and re-entry dates.

2.2.2.2.2 Resistance Exercise

Resistive exercise is currently the sole countermeasure regularly employed to mitigate bone loss in all long-duration astronaut flights. The first long-duration ISS crew launched in late 2000 with a cycle ergometer and treadmill exercise equipment. The Interim Resistive Exercise Device (iRED) was assembled six weeks later, and these three forms of exercise have been used since. Yet, even with resistive exercise, significant bone losses were still experienced and recorded.

The Advanced Resistive Exercise Device (ARED) was put onto the ISS to supplement the iRED in December 2008 [34]. The ARED is a robust device able to maintain a constant load

over its ranges of motion. It has a maximum load of 2675 N in comparison to the iRED's 1337 N [3]. Resistive exercise, including squats, heel raises and deadlifts on the iRED or ARED, and aerobic exercise, on the cycle ergometer or treadmill, are performed on the ISS for up to 2.5 hours a day, six days a week [3] (Figure 9).

Figure 9: Left: A crewmember performing a squat exercise on iRED [35]. Right: A crewmember performing a deadlift exercise on ARED [36]

Bone mass has been measured in a variety of ways to compare the effectiveness of iRED and ARED. A comparison of aBMD using DXA was plotted between Mir, ISS Pre-ARED (therefore only involving access to iRED as weight-bearing exercises) and ISS ARED missions (Figure 10) [4]. It can be seen that the use of ARED has more beneficial outcomes in comparison to iRED use, with a decrease of aBMD from an average monthly loss of roughly 1% to 0.3-0.5% per month. This demonstrates that higher force loading has a more beneficial impact on negating bone atrophy.

It should be noted that since the introduction of ARED, astronauts have been complaining of vision impairment [37]. This may be a result of the linkage between high intensity resistive exercise and increases in blood pressure due to microgravity [38]. Considerations for this will have to be made in developing future countermeasures for bone atrophy in space.

In addition to usual activity in spaceflight, an increase in resistance exercise force can also lead to injuries, which in turn can inhibit an astronaut's exercise regime. To avoid health

degradation, further countermeasures must be investigated to supplement exercise in the case of an astronaut injury being too extensive to continue exercise.

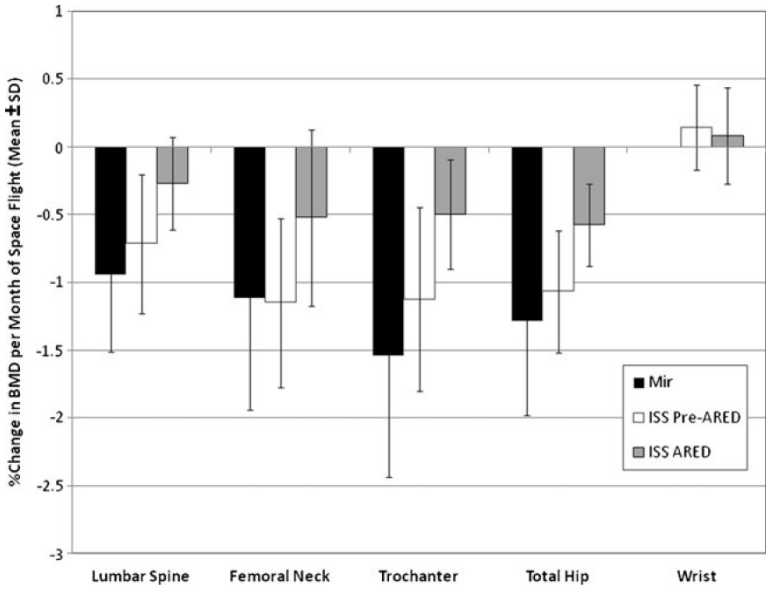

Figure 10: Distribution of DXA aBMD as a percentage change in long-duration astronauts on Mir and ISS spaceflights [4]

2.2.2.2.3 Vibration

It is hypothesised that a combination of artificial gravity and vibration may prove to have a beneficial effect on bone and muscle preservation in comparison to current exercise countermeasures. Goel *et al.* [39] studied the effects of one-legged and two-legged squats on a vibrating platform. The four subjects' movements were captured by the Vicon motion capture system (Vicon Motion System Ltd, LA, USA) and then modelled on OpenSim (Stanford University, CA, USA), with the use of Matlab (The MathWorks, Inc., MA, USA) code for conversion between the two systems. Results from the study were compared to iRED exercises performed in parabolic flight. The vibration study ground reaction forces in a one-legged squat were 144% greater, and two-legged squat 33% greater, than the two-legged squat using iRED. It was concluded that simulated vibration exercises is highly effective in simulating both bone and muscle.

2.2.2.2.4 Pharmacologic Measures

An international partnership between NASA and the Japan Aerospace Exploration Agency (JAXA) were made to investigate the potential of antiresorptive agents for mitigation of bone atrophy [40]. Seven ISS astronauts agreed to take a 70 mg dose of alendronate, a bisphosphonate, per week, commencing three weeks prior to launch. As exercise is

considered essential during spaceflight, the study could not be performed with a subject group being only administered bisphosphonates. Comparison can be seen in Figure 11 between percentage change DXA BMD from pre-ARED exercise, and only ARED exercise and bisphosphonate consumption plus ARED exercise. A combination of the existing exercise program and bisphosphonate was proven to reduce bone loss, sustain bone strength, inhibit resorption marker increase and reduce calcium urinary excretion.

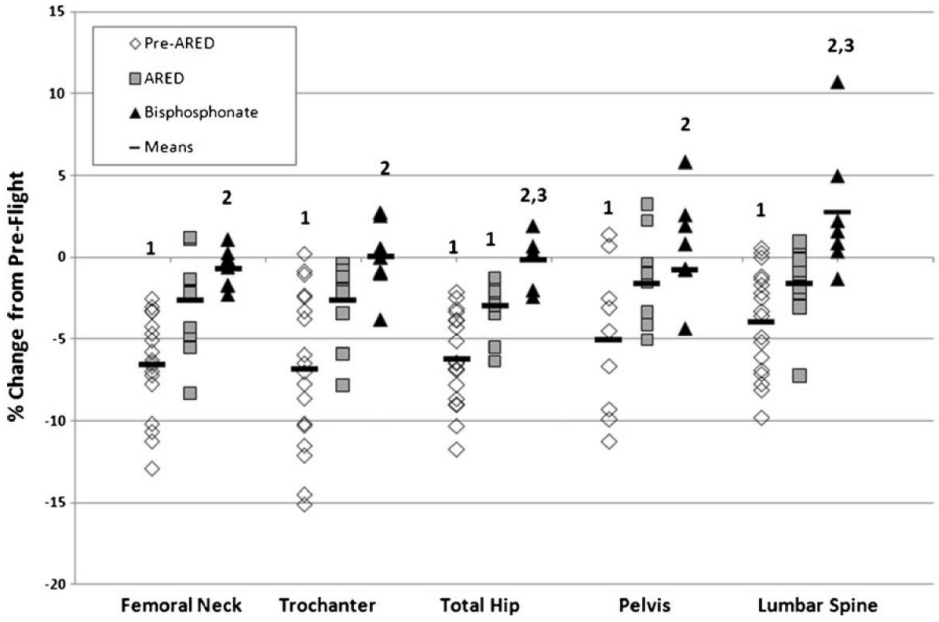

Figure 11: Percentage change in DXA BMD, compared to preflight, in long-duration spaceflight [40]

2.2.2.2.5 Post-Flight Surveillance

Information regarding the recovery period and influence of post-flight osteoporosis is very limited. Due to an abundance of aBMD data from terrestrial studies, the NASA Bone Summit [34] recommends to continue surveillance on returned astronauts. DXA and QCT measurements should both be used in post-flight measurements. Additionally, it is recommended that an osteoporosis specialist assess astronauts.

2.2.3 Terrestrial Bone Mass Reduction

People with paralysis, osteoporosis and those volunteering for bed rest studies all experience bone loss. The amount and styles of exercise have been investigated to determine if any have an advantages consequence for BMD.

2.2.3.1 Health Complications Associated with Terrestrial Bone Atrophy

Similar to space, terrestrial evidence of bone mass reduction has an increased risk of bone fracture and reduction of quality of life due to the fear of a fracture. Women over the age of 35 years have overall fracture rates twice that of men (Figure 12). The onset of osteoporosis and the decline in BMD with aging is an outcome of hormonal interactions, environmental, genetic and nutritional factors.

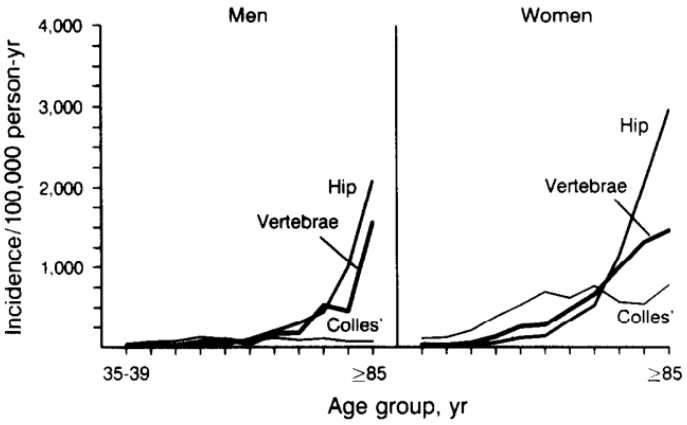

Figure 12: Age-specific incidences of hip, vertebral and Colles' (wrist) fracture in Rochester, Minnesota [41]

A major problem for people with spinal cord injury is osteoporosis [42, 43]. Immobilisation and neurological lesion prompt early bone loss. Biering-Sørensen *et al.* [44] investigated the long-term effects of spinal cord injury in a variety of locations in the body. Notably, the most intense bone mineral content (BMC) decrease occurred in weight-bearing bones, firstly the proximal tibia (Figure 13), followed by the femoral neck. This compares to lumbar spine, where the BMC remains relatively unchanged. Therefore, the study illustrates that normal muscle function and load bearing is required to avoid bone loss.

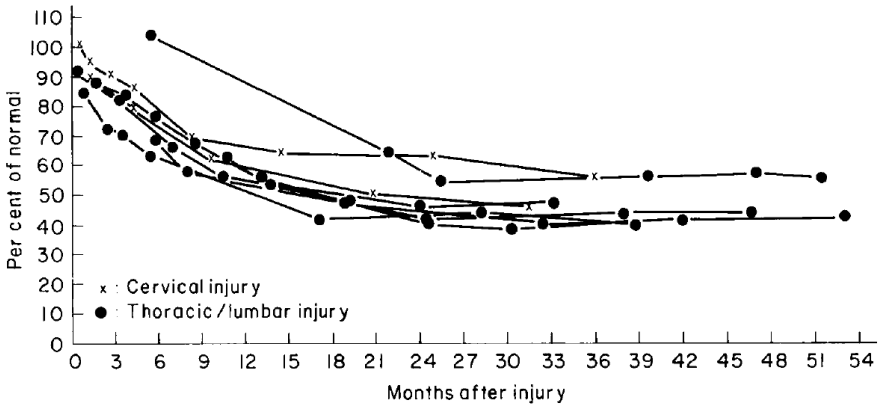

Figure 13: BMC in the proximal tibia as a percentage of the mean of normal values [44]

Bed rest, presently the only human-based ground analog for microgravity, investigates both the role of bone loss and possible countermeasures in spaceflight. Bed rest unloads the skeleton whilst maintaining mobilisation similar to space. The length of time for bone mineral recovery is a pressing concern. The recovery following a 17-week bed rest study demonstrated positive, yet not sufficient, recovery over 6 months in the majority of regions tested [31]. Therefore, further investigations are required to account for recovery time.

2.2.3.2 Mitigation Methods

Due to the high occurrence of terrestrial osteoporosis, and the resultant impact on quality of life, the need for countermeasures is inevitably high. Many of the investigations undertaken in this field have resulted in varying degrees of success.

Walking and leisure time activates have been investigated to determine if they have a favourable effect on reducing the risk of hip fractures [45]. The study, commencing in 1976, comprised of 121,700 registered female nurses in the U.S. Of these, 61,200 women were involved in the follow-up in 1998. Over the two decades, the women were asked to perform a certain quantity of exercises and activities. It was found that an increase in leisure time activity corresponds with a lower risk of hip fractures. Therefore, women of any weight or fitness level can reduce their chance of fracture by escalating their amount of exercise.

The effects of Tai Chi Chu (TCC), a low-impact, weight-bearing exercise, have been proven to be beneficial for reducing the rate of bone loss in weight bearing bones for people with osteoporosis [46]. In this study, the exercise considerably reduced the amount of BMD

change in weight bearing bones (Figure 14). Due to the exercise's high demand for neuromuscular coordination, slow movement of limbs and low impact factor, TCC has been recommended for the elder generation or people with rheumatoid arthritis.

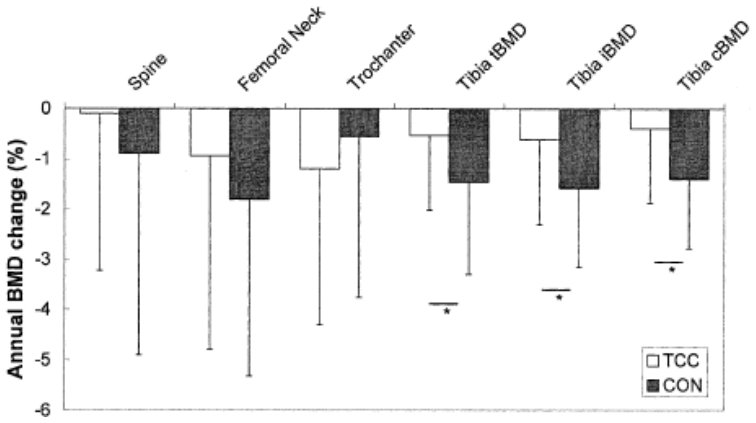

Figure 14: Measurements from pQCT and DXA relating to the annual BMD percentage change in the TCC exercise group and control group (CON) [46]

Bone loss from spinal cord injury is difficult to treat due to the individual's limited range of motion. However, physiotherapy and electrodes to induce muscle movement can slow the rate of BMD loss in these patients.

The countermeasures for bed rest do not necessarily mitigate spaceflight bone atrophy. Many bed rest studies have found that a protocol of either intense, on-going resistance exercise or vibration exercise has the potential to reduce, or even prevent, bone loss [47-49]. This contrasts with the more recent [4, 34] above literature that demonstrates exercise can slightly reduce, though not completely eradicate, the problem of bone atrophy. This thesis, by providing a test rack in which such hypotheses can be measured, should ultimately contribute to this debate.

2.3 Bone Deformation

Research on bone deformation mechanics has been on-going for decades, with the field rapidly advancing in the 1970s. However, according to Currey [50], it was at the beginning of the 1980s that saw the study really flourish, attributing recent development and understanding to an increase in technology.

A bone can deform in a number of ways (Figure 15). Axial strain, including tensile and compressive strain, deforms the bone in the same direction as the load being applied and occurs during most physical activities. Shear strain arises from a load applied at a certain

angle and similarly results from day-to-day activities. Bending strain may be simulated from the application of a perpendicular force, whilst torsional strain may be simulated from a twisting load along the axis of the bone [51].

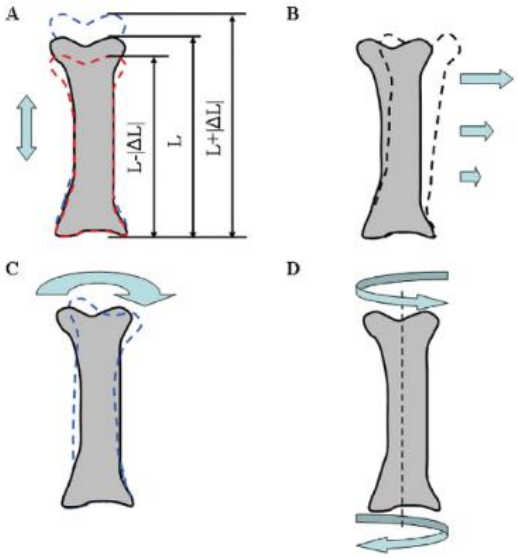

Figure 15: Types of bone strain. (A) axial strain, (B) shear strain, (C) bending strain, (D) torsion strain [51]

Much research has been focused on investigating the effects of exercise on bone mass and risk of fracture. Bennell *et al*. [52] performed a one year study on track and field athletes to document any incidences of stress fractures. Their findings stated that almost three quarters of the athletes sustained injury, with 46% of those occurring at the tibia. Fractures mostly occur when the applied load is greater than the structural strength of that particular bone [7]. Sasimontonkul *et al.* [19] found that whilst running, tibial stress fractures are most likely due to the large compressive forces and small posterior shear force during mid-stance rather than at ground impact (Figure 16). These fractures can be caused by continual high loading over time. It is important to note that a bone is able to undergo a large quantity of force and bending before break. Evidence suggests that limb bones can withstand forces which enforce up to four times more deformation than that as a result of high physical activity before the bone will fracture [53].

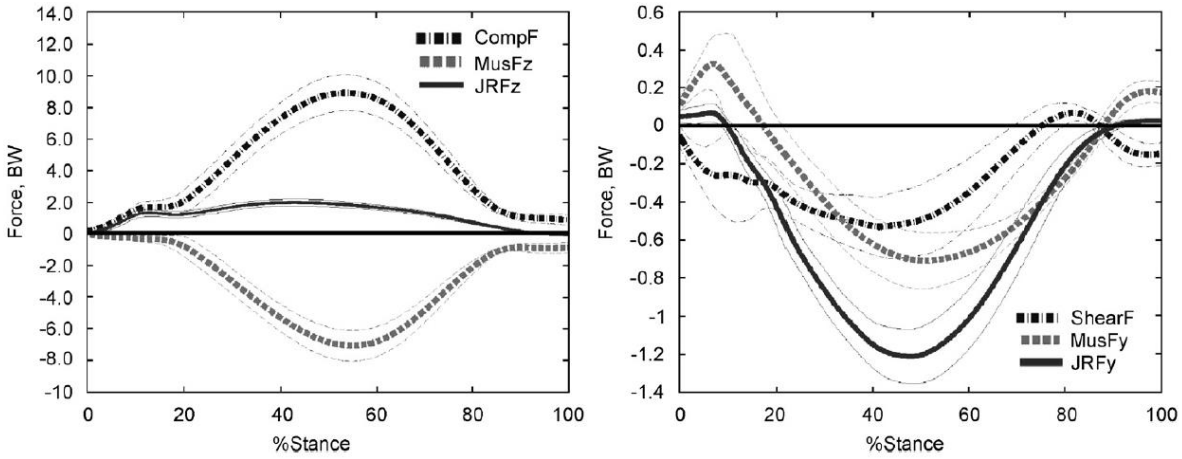

Figure 16: Group means for: Left: axial, and; Right: shear components acting on the tibia. The lines represent the compressive contact forces (CompF), shear contact force (ShearF), net muscle force (MusF) and joint reaction force (JRF) [19]

Although exercise poses a high likelihood of bone fracture, strong evidence suggests that exercise also strengthens bones. Milgrom *et al*. [54] evaluated different types of exercise to determine if any caused significant strain on the tibia to improve bone strength. No statistical differences of tibial strains were found between the exercises of walking, leg presses and using a stepmaster. Yet, strains were much higher in running and considerably lower in stationary bicycling. Thus, from the exercises explored in their study, running is the only exercise that will promote tibial bone strengthening. Bone loading as a result of exercise and/or other stimuli consequently causes an increase strain and initiates a rise in early bone formation markers, thus resulting in an increase in osteoblast activity and reduction of osteoclast recruitment [55].

Similarly, a person's level of fitness and style of exercise greatly affect the modelling and remodelling bone cycle. Yet, it is more to do with relative levels of activity from loading and disuse, rather than purely fitness. An adept and clear analogy was documented by Skerry [55]. He explains that an Olympian weightlifter, or any professional sportsperson, will have a skeletal bone system habituated to their particular activities. However, once retired, bone mass will reduce immensely, even if exercise is still maintained above a 'normal' level. On the other hand, if a non-athlete commences exercising, even at levels lower than the weightlifter, they would see greater bone adaptations to their skeletal system.

2.4 Measurement Systems for Bone Deformation

Over time, measurement techniques used to evaluate forces on bones, deformation and movement have progressed through a series of innovative and diverse approaches. Each with its own advantages and limitations, their results accumulate to give a comprehensive explanation into the mechanics of bone. To date, no study has been performed that specifies the mechanical response for bone adaption. However, with the findings made from the procedures detailed following, a sound start can be made to further investigate the area.

2.4.1 In Vivo Measurement Procedures: In vivo Strain Gauge

2.4.1.1 In Vivo Strain Gauge Measurements

In vivo 'inside the body' bone studies involve the use of strain gauges to measure the deformation of the bone.

The application and study of in vivo tests for measuring bone strain was first conducted in 1943, when strain gauges were used in a live animal [56]. The year 1975 saw the first revolutionary in vivo study in humans and from 1996 the quantities of these studies multiplied rapidly. However, there still remains little understanding of in vivo bone strains during physical activity because of its high level of invasiveness and consequential limitation of research for movement [51]. There have been reported side-effects of swelling and tenderness at the surgical site along with the risk of infection [51, 57], leading many studies to avoid their use.

Despite these issues, due to the significance of the information able to be deduced from these sensors, there are still some studies currently being performed, with many of these discussed in the following paragraphs.

A typical strain gauge only measures strain in one direction. Therefore, to account for the various types of strains, a rosette strain gauge is typically used for in vivo measurements. More recently a new procedure has been developed to reduce the level of invasiveness associated with inserting a strain gauge directly onto bone: K-wires are inserted into the bone and a strain gauge attached externally. Similarly, a bone staple can be used. Improvements to this technique are needed, with the aim of being less invasive and more accurate. Digital image correlation and ultrasound wave assessment were performed on

animals and bone specimens, respectively [51, 58]. Nazer *et al.* [59] have documented a thorough systematic review of direct bone strains in humans. They focused on 24 studies involving in vivo measurements spanning across numerous sites around the body and the outcome of physical activity on the bones. They suggest a combination of in vivo and computational methods to advance the field; such as improving bone strength by creating exercise procedures.

The outcome of muscle fatigue on tibial bone strain has been studied via the in vivo methodology. Milgrom *et al.* [57] studied four male volunteers following a strict protocol of running for 2 km at a minimum speed of 12 km/h, along with a 30 km march through a hilly desert at a minimum pace of 6 km/h. Only half the subjects completed the entire march due to excessive muscle fatigue. It was found that there is an increase in bone strains at the fatigue state, thus proving to be a major influence for stress fracture formation and propagation.

As mentioned in section 2.1, exercise through the use of applied loads plays a fundamental role in maintaining bone mass and strength. This theory was investigated by Milgrom *et al.* [54] with in vivo strain measurements (Figure 17). Whilst wearing strain-gauged staples, six subjects performed the exercises of walking, leg presses, bicycle riding, step master and running. A dose-response relationship between the physical loading activities and the mechanical capability of bone [60] clarifies the results of this study. Running produced the highest strain rate, consequently it may be deduced that it is a suitable strengthening activity for the tibia bone.

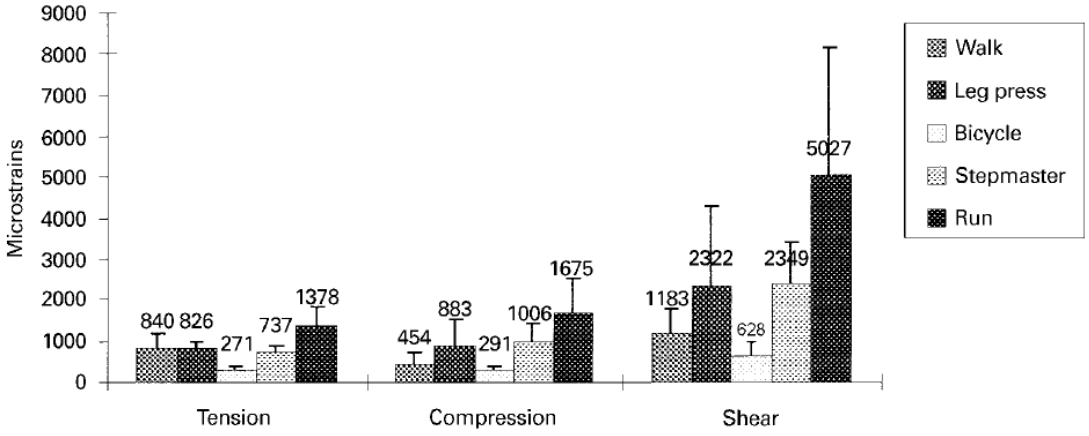

Figure 17: Principal strains during exercise activities [54]

2.4.1.2 In Vivo Optical Measuring Systems

Optical measuring systems are becoming increasingly more accurate for measuring small movements. Yang *et al.* [61] explored the utilisation of an optical segment tracking (OST) system to determine if it is appropriate for measuring in vivo bone-segment deformation. A Vicon motion capture system was used to determine the most suitable calibration, camera distance and marker size along with the highest achievable resolution. It was concluded that the optical measuring system is suitable and sufficiently performant to capture small displacements from a large specimen volume.

Ganse *et al.* [62] performed three-point bending tests using OCT, with the purpose of validating the measuring technique. Prior to this study, no in vivo three-point bending tests of the human tibia had been done before. Reflecting marker clusters were inserted into the tibia bone of five healthy subject and weights were applied between the proximal and medial screws (Figure 18). The three-point bending test confirmed that OCT is feasible for in vivo bone deformation measurements.

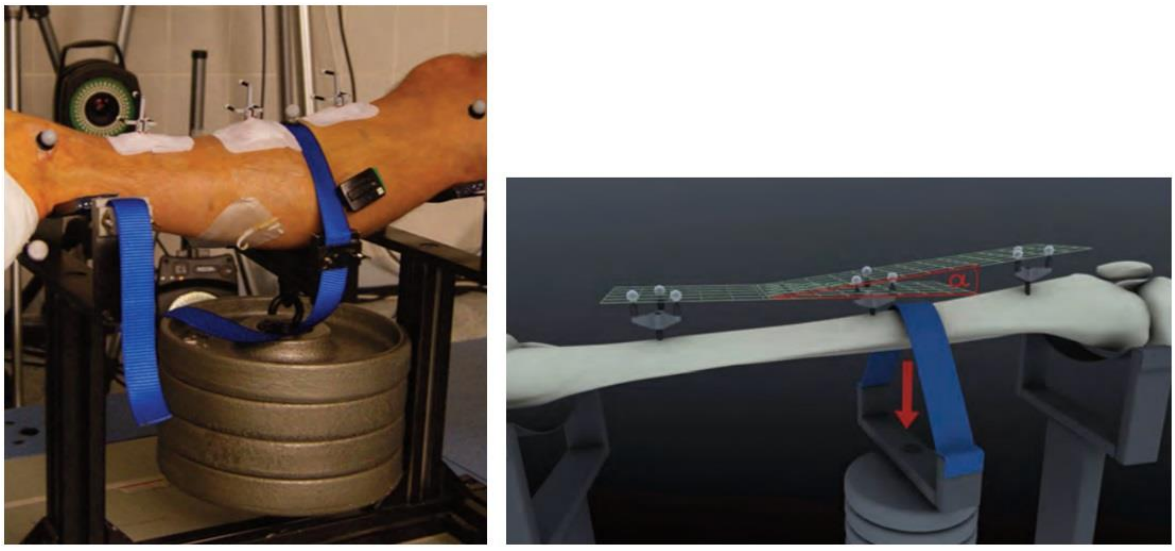

Figure 18: Left: Setup of the three-point bending experiment with 20kg of weight applied. Right: Deformation angle measure in the axis of weight application [62]

2.4.2 Ex Vivo Measurement Procedures

2.4.2.1 Scanning

Advancements in scanning technology have advanced considerably in recent years, allowing for a vast range of newer, higher resolution measurements. DXA is commonly used to measure bone mass of individuals, including pre- and post-flight scans for

astronauts and those with high risk of osteoporosis. It separates the body into distinct sections, including: bone mineral content (BMC), fat body mass (FBM) and lean body mass (LBM) [63]. Another growing field is pQCT. Rittweger *et al.* [63] used this methodology to study the relationship between muscle and bone. The tibia bone was split into four components and an analysis of each cross-section was performed (Figure 19). The study concluded that both the force applied and the length of the tibia bone significantly impact upon the deformation in hollow bones.

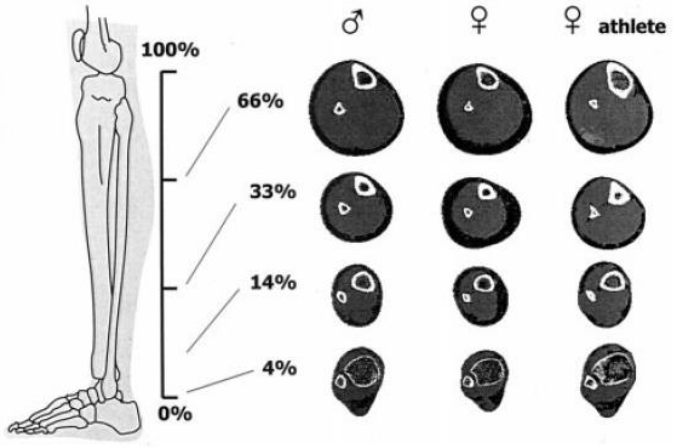

Figure 19: pQCT cross-sections obtained at 4 levels in the tibia. Differentiating between male, female and female athlete [63]

Techniques involving X-ray and CT scans have advanced to measure strains in trabecular bone [64]. Images are taken of the bone specimen being loaded and unloaded, following which a texture correlation is performed to determine strains. This methodology is advantageous as no assumptions regarding tissue mechanical properties are required.

2.4.2.2 Computer Modelling

Computer modelling systems can be used to predict the deformation of a bone from certain loads and/or model the motion of the entire low extremities. In 1943, the finite element method (FEM) was initially devised as a mathematical technique and was not practical for use in bone modelling [65] until the invention and improvement of computers saw the methodology advance in 1970 [50]. By 1995, 310 general purpose computer programs for FEA had been developed [66]. This technique is used to create lifelike biological models, integrate multiple strain gauge information to interpret strains over a cross-section and to test the morphology of fossils. A key part of the FEA process is

meshing, which involves dividing the specimen into a 'finite', and typically a large, number of elements connected to each other. A 3D element characteristically has several types of mesh structures, those being: four-node tetrahedral, five-node pyramids, six-node wedges and eight-node bricks (Figure 20). A load or number of loads are applied at a certain location or area directed at a specific angle. The geometry and material properties of the specimen as well as the boundary conditions of the system are inputs into the model. When the process is run, FEA measures the applied loads to the specimen, like springs, which deform in prescribed ways.

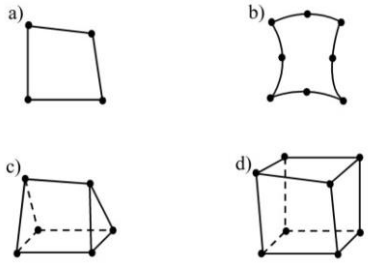

Figure 20: Different forms of meshing with FEA. Elements can be linear (a, b, c) or quadratic (d) [65]

Computer modelling can also be employed to develop musculoskeletal models of the lower extremities. This method was utilised by Wehner *et al.* [67] to determine internal forces and moments during gait through the longitudinal tibia bone axis. They expanded on the AnyBody Research Group's model of the musculoskeletal system and used a gait analysis dataset based on 15 markers and a ground reaction force plate. The study resulted in successful measurement of the internal forces on the tibia, which could later be used to improve implantation designs and in vivo studies.

2.5. Experimental Apparatus for the Lower Limb

There are many examples of experimental apparatus that experiment on cadaver legs and specifically the knee or ankle joints [68-70]. However, a test rack simulating body movement with artificial materials to measure bone displacement has not been constructed prior to this thesis.

Test racks described in literature were investigated to determine if any specific design elements or 'lessons learned' could also be incorporated into the design of this thesis' test rack.

Mueller et al [71] constructed an apparatus that held knee cadaver specimens simulated with five knee muscles to control a variable amount of body weight [72]. The knee simulator (Figure 21, left) consists of a hip and knee joint, allowing for six degree of freedom knee joint movement. Another similar rack, called the Oxford testing rig (Figure 21, right), also studied the knee with cadaver specimens and compared the effects of medialisation and anteromedialisation of the tibial tubercle on patellafemoral contact measures. They used hip and ankle joints to simulate a continuous weightbearing squat for the tests [73]. These racks illustrate design concepts that can be used for implementing ankle, knee and hip joints.

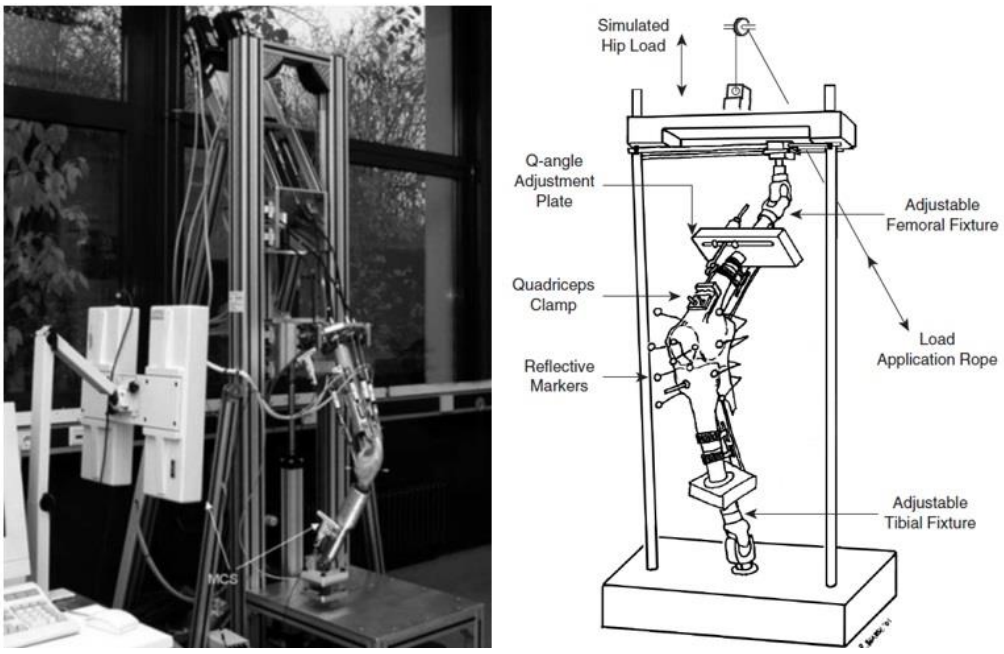

Figure 21: Left: The knee simulator with a specimen fixed into the hip and tibia tubes [71]. Right: The Oxford rig used to simulate a weightbearing squat in cadaveric knee specimens [73]

Another test rack, developed by the German Sports University (Cologne, Germany), simulated physiological muscle contractions using actuators attached to muscles of a cadaver leg (Figure 22). The ankle and knee joints were still intact and the foot was secured to the base just below the toes. Tibia displacement was measured by tracking relative movement between marker clusters on the bone using the OST approach [74]. A similar approach is used in this thesis' test rack, with actuators simulating muscle forces. However, an artificial tibia is used and specific sections of a movement are modelled under static conditions.

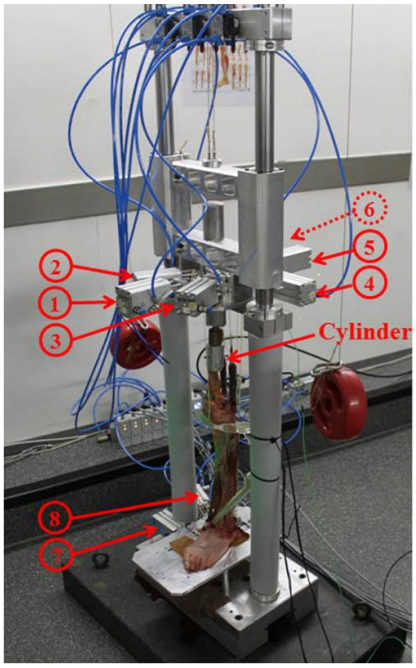

Figure 22: A cadaver leg loaded onto the test rack. The numbers refer to pneumatic actuators linked to different muscles. 1: quadriceps, 2: semimbranosus, 3: biceps femoris, 4: gastrocnemius medialia, 5: soleus, 6: gastroncnemius laterialis, 7: tibialis anterior, 8: tibialis posterior [74]

2.6 Thesis Justification

The objective of this thesis is to design and create a test rack that can simulate different movements by modelling muscle forces and applying body weight to the tibia with the aim that the strain, as indicated by applied load and pattern of displacement, can be characterised. As supported in this literature review, exercise and muscle loading have encouraging outcomes for preventing bone atrophy. Therefore, identifying which muscles simulate certain bone movement can lead to promotion of bone growth.

There is little research performed in this area, subsequently FEA computer models lack verification of methodology. The thesis, and future work based upon it, will investigate the extent of bone displacement from muscle simulation, and hence a reduction in bone degradation, from a variety of static and dynamic movements.

Furthermore, countermeasures need to be developed to reduce bone atrophy for astronauts as well as terrestrial cases. Employing muscle simulation and exercise protocols at certain muscle sites that, from this thesis and future studies, are known to produce high bone displacement, can consequently impede bone resorption and mitigate bone atrophy.

CHAPTER 3. DESIGN AND CONCEPTS

3.1 Methodology Justification

The aim of the thesis was to design and create a test rack to hold a model human tibia, with muscle forces simulated using pneumatic actuators. Preliminary stage tests were performed to evaluate appropriate safety measures and determine accurate functionality.

The overall purpose of the test rack, governed by a previous study performed at DLR [5], was to simulate different movements of the tibia. This involved analysing a range of activities following insertion of three screws in the right tibia. The resulting tibia deformation was then uploaded into a computer model which determined the amount of muscle movement, and these forces are to be modelled in the test rack. It is hypothesised that the muscle forces applied experimentally will cause the same tibia deformation achieved from the in vivo study.

Prior to this thesis, bone deformation has never been measured by simulating movements with artificial materials. Consequently, innovative approaches were developed to overcome design challenges. A strong emphasis was placed on the lower limb physiology and replicating muscle forces accurately.

3.1.1 Requirements

The first step in the design phase was to establish a requirements list. All conditions on the list (Table 2) should be fulfilled. Due to time and cost restrictions, some requirements were not achieved in this design. However, further improvements are discussed in the Recommendations Section. Additionally, a table providing the design solutions to addresses these requirements can be found in Appendix A.

Table 2: Requirements list

Attachment of tibia/mounting	
Proximal Fixture	Proximal tibia moveable, similar to physiology.
Distal Fixture and Mounting	Distal tibia head firmly fixed to prevent any movement or rotation. May be positioned on a force plate. Mechanical decoupling of tibia fixation and any downward pulling force source.
Forces/Control	
Forces and Muscles	Four downward forces, modelling the muscles Soleus, Tibialis Posterior, Tibialis Anterior and Flexor Digitorium Longus, applied using pneumatic actuators. Orientation of muscle force vectors close to anatomical orientations. Magnitude of force in range zero to maximum isometric force of each muscle. Speed and force with respect to time behaviour close to physiological conditions.
Tendon	Force transfer to one point on tibia for each muscle to replicate tendon attachment point.
User Interface	Test rack setup simple. Labels on test rack*.
Control System	Actuator vibration caused by stroke should not affect tibia deformation. Easily regulated pneumatic control system.
Specimen	
Type of bone	Validation using simple structure with known mechanical properties that is straightforward to model on a computer and has known mechanical properties. Tibia bone replica that is physiologically similar to bone.
Number of joints	No joints.
Optical Measuring System*	
Axis and Accuracy	High accuracy and can measure displacement along the x, y and z axis. Mechanism for optical measuring system to detect bone deformation.
Visibility	High visibility.
Force Measurement System	
Reaction Force	Measure forces and moments along the x, y and z axis.
Muscle Force	Mechanical load cells to measure actuator force.
Test Rack	
Support Structure	Allow for various size elements. Be able to withstand the high forces applied to it.
Safety	Implementations to prevent injury in case of malfunction.
Whole Test Rack	Simple disassembly. Cost kept at minimum.

*Requirement not fulfilled in this design and testing

3.1.2 Design Considerations: Muscle Forces

The muscle forces simulated will differ for various body movements. To account for all possibilities, the maximum isometric force for each muscle was predetermined. These values were used when deciding what size pneumatic actuators to use and the force magnitude to validate the test rack.

A total of 14 muscles attached to the tibia were replicated. These included ten muscles in the upward force direction (Table 3) and four muscles in the downwards direction (Table 4). Muscle that are attached to the fibula or the interosseous membrane, and not the tibia, were not included in the design. As some muscles are bunched together, their corresponding isometric forces are a combined value.

As the current test rack was measuring the force reaction at the ankle, the gastrocnemius was not incorporated into the design.

Table 3: Isometric force of muscles of the lower leg with force in the upwards direction [75]

Muscle	Force (N)
Rectus femoris	1,169
Vastus medials	1,294
Vastus lateralis	1,871
Vastus intermedius	1,365
Tensor fascia latae	233
Sartorius	156
Gracilis	162
Biceps femoris	896
Semitendinosus	1,228
Semimembranous	410
Total:	*8,784*

Table 4: Isometric force of muscles in the lower limb with force in the downwards direction [75]

Muscle	Force (N)
Tibialis anterior	905
Extensor halluces longus	162

Muscle	Force (N)
Soleus	3,549
Tibialis posterior	1,588
Flexor digitorum longus	310
Flexor halluces longus	322
Total	*6,836*

Therefore, the muscles in the lower extremity have an isometric force total of 15,620 N. Appendix B presents a spreadsheet of all isometric forces of the muscles of the lower leg.

3.1.3 Design Considerations: Angle of Muscles

The attachment to the tibia was established using diagrams. Bolts were inserted into the tibia at the location of muscle attachment, which was estimated to be in the centre of the tendon area. The opposing end of the muscle was situated extremely close to the bone. This is due to the muscles being directed around the ankle joint to their corresponding endpoints.

Figure 23 displays the attachment points of the muscle to the tibia. It should be noted that a left tibia specimen was used in the test rack (supplied did not offer right). Therefore the tendon positioning was flipped around the longitudinal axis.

Figure 23: Muscle attachment to tibia. Left: anterior view, Right: posterior view [17]

3.1.4 Design Considerations: Body Force Impact

In addition to measuring the specific muscle forces, body weight was also included in the model. To validate the test rack, the maximum possible downward force must be applied to ensure the tibia and the rack, structurally and the individual components, could withstand the force. When walking and running, the impact force can be between 1.5-3 times body weight at the heel (Figure 24).

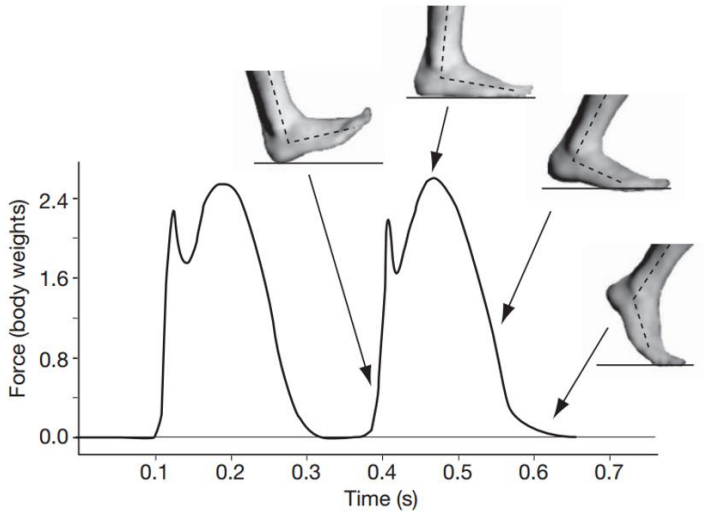

Figure 24: Vertical ground reaction forces during barefoot heel-toe running [76]

Similarly, the force measured at the knee joint whilst walking can be as high as three times body weight [77]. The maximum moment is measured at approximately 3.5% body weight (Figure 25). Therefore, moment at the knee has minimal effect.

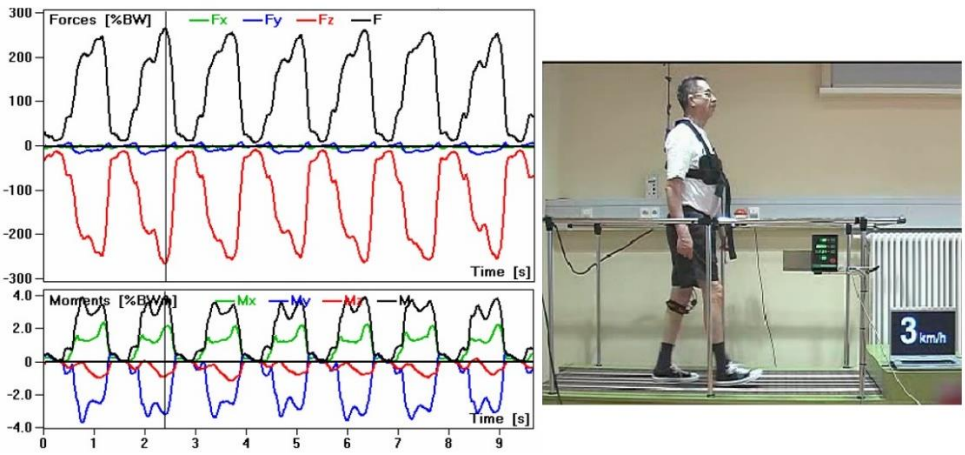

Figure 25: Force and moment (%BW) on the left knee when walking at a velocity of 3 km/h (subject K8L) [77]

When walking at a velocity of 3 km/h (Figure 25), a subject experienced a maximum force in the x-direction, side to side, at the knee ranging from -3 to 6% BW and the y-direction,

forwards and backwards, from -19 to 9% BW. This illustrates that the forces in the x- and y- directions are minimal in comparison to the downward direction.

When validating the test rack, the maximum possible forces must be used. Therefore, the downward body weight force was estimated at three times body weight.

3.1.5 Design Selection

The test rack must be able to model various types of body movements. A quality function deployment (QFD) trade off spreadsheet was constructed to analyse and select a top mechanism for the test rack (shown in Table 5). This mechanism was the apparatus above the tibia that induced forces and moments onto the specimen. A weighting was given to each requirement, with cost being the highest. It was deduced that the direct force application was the most feasible design option.

Table 5: QFD Analysis

Weighting (%)	Mechanism Options / Requirements	Direct force application	Mechnical joint with a gliding mechanism platform	Mechanical joint with hexapod	Real joint (incl. distal femur) with gliding mechanism platform	Real joint (incl. distal femur element) with hexapod
9	Move top of specimen in doward direction	5	3	5	5	5
9	Move top of specimen across plane motion	1	5	5	5	5
9	Withstand large amounts of force	5	4	4	4	4
9	Controlled movement	1	3	5	3	5
7	Adjust to external forces	2	3	5	3	5
9	Low degree of difficulty to control motion	1	1	5	2	4
9	Low degree of difficulty to install	5	3	4	2	3
5	Does not obstruct pulley system	4	2	2	2	2
5	High stability	5	5	5	3	3
5	Low weight	4	3	1	3	1
9	Similar to physiology of tibia	2	3	4	4	5
15	Cost	5	3	-10	3	-10
	Total Sum	**40**	**38**	**35**	**39**	**32**
	Weighted Sum (% of total)	**24.1**	**22.7**	**15.37**	**23.9**	**14.0**

From this, two test rack designs were formulated. The first, simplified design (Alpha) allowed testing under static conditions, whereas the second, more advanced design (Beta) aimed at achieving dynamic motion across a vast range of movements. The Alpha design was selected for construction as it can be usefully utilised for testing and fit into the scope of this project, with lower costs requirements and less construction time than the Beta design. It is the intention for the test rack to be extended to the Beta design in the future. Table 6 gives an overview of the design specifications for both the Alpha and Beta test rack. Further specifications are presented in Appendix A (Alpha) and Appendix C (Beta).

Table 6: An overview of the differences between the Alpha and Beta test racks

Specification		Alpha	Beta
Motion	Static motion	√	√
	Dynamic motion	x	√
Joints	Ankle	x	√
	Knee	x	√
	Hip	x	√
	Patella	x	√
Measuring System	Force Plate	√	√
	Vicon	√	√
Forces	Upwards with weights	√	x
	Upwards with actuators	x	√
	Downwards with actuators	√	√
	Bodyweight with weights	√	x
	Bodyweight with actuators	x	√
	Gastrocenemius muscle	x	√
Force redirection	Pulley system	x	√
	Smooth surface	√	√/x
Structural	Two pillars	√	√
	Structure above force plate	√	√
	Safety lines	√	x
	Safety brackets	x	√
	Pulley system on pillars	√	x
	Specimen rotation	√	x

The Alpha design did not take into account the foot. Therefore, the base of the tibia represents the ankle joint. Table 7 illustrates the analysis to determine whether the types of movements were feasible with the Alpha design.

Table 7: Is the movement feasible with the test rack design?

Movement	Feasible?	Description
Standing	Feasible	Muscle positioning predetermined from diagrams. The base of the tibia should be locked and the top of tibia free to move.
Walking	Feasible	Multiple stages of gait will be tested: Heel strike – same as standing Toe-off – slight ankle in tibia, must adjust the redirection system
Running	Feasible	Same as walking, but with larger forces. A foot should be included with the future design (Beta).
Hopping (one and two legs)	Feasible	Some motions are the same as standing, but with higher magnitude. At the bottom of the jump (knees highly bent), the camera system will need to be adjusted accordingly with the tibia specimen. In future design, have a joint to open and close for stabilisation.
Climbing stairs	Feasible	Camera position may need to be adjusted. In future designs, it is recommended that an adjustable top mechanism to model movement whilst it is occurring.
Climbing spiral stairs	Not Feasible	The body twists when climbing spiral stairs, causing torsion. Torsion cannot be modelled in the current design
Squats	Feasible	Have the top of the tibia open (moveable). If the tibia is tilted to the extent that the visibility for the optical system is greatly reduced, then the specimen and the redirection mechanism should be adjusted.
Plantar flexion and dorsiflexion	Feasible	Reduce force exerted at the top of the tibia specimen (perhaps remove top plate). In future design, with a large mechanism above the specimen, use a load cell and/or spring scales to ensure no weight is enforced onto the specimen.

The structural design took into consideration the specifications for both racks. Essentially, the base structure of the rack will remain the same whilst individual components and the setup will be modified in future designs and tests.

3.2 Experimental Apparatus

3.2.1 Materials and Devices

It was imperative that test rack requirements (see Table 2) were followed when choosing materials and devices. Wherever possible, parts for the test rack were reused from DLR stock to minimise cost and delivery time. Many materials were purchased from companies who have an affiliation with DLR.

This test rack was not designed to accommodate cadaver legs. This is as firstly, they require an extremely long preparation and setup time, with every muscle needing to be sutured to an actuator. Secondly, muscle fibres reduce in strength after a person dies, thus they are not capable of withstanding high forces and are likely to tear [78, 79]. Thirdly, bones vary in mechanical strength from person to person. As the muscle forces are being determined using a computer model, the bone properties must be known and entered into the program. Therefore, the test rack used an artificial bone and artificial muscles to simulate movements.

The model tibia, sourced from Sawbones (Pacific Research Laboratories, WA, USA), had mechanical properties similar to human bone (Figure 26). The model bone consisted of simulated cortical bone, properties in longitudinal and transverse directions, and cancellous bone, with solid and cellular properties (Appendix E1). The computer-aided design (CAD) model of the bone was also purchased with the specimen.

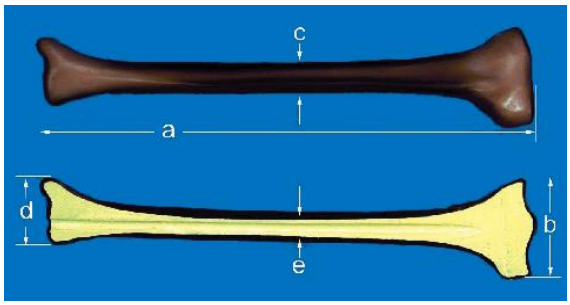

Figure 26: Tibia specimen dimensions: a) 405 mm, b) 84 mm, c) 28 mm, d) 58 mm, e) 10 mm (canal) [80]

Construction beams were purchased from the company item (item Industrietechnik GmbH, Solingen, Germany). Profile 8 80x80 (mm) anodised aluminium beams were used for structural sections of the rack. These were supported by brackets, whose size depended on the magnitude of forces at that section. See Appendix D1 for an overview of item products used in the test rack.

Four pneumatic actuators simulated downward muscle forces. Each was selected according to the muscles' isometric forces (see Table 4). All actuators required a load cell to measure each force magnitude. Ropes with minimal elasticity and a substantial braking load (FSE Coppa 3000 Dyneema) connected the actuators to the specimen. An M8 bolt acted as the tendon attachment with the bone specimen, with the rope tied around the bolt using a bowline knot (Appendix E4) The forces and moments experienced at the base of the tibia, representing measurements at an ankle joint, were read using an AMTI force plate (OR6-6-2000) (Advanced Mechanical Testing, Inc., MA, USA) (Appendix E5). The force plate measured forces in the x, y and z directions and their corresponding moments. Gecko tape attached and held the base plate, connected to the base of the tibia with a M10 bolt, to the force plate.

For the actuators to perform as required and expected, the rope must be on the same plane as the actuator lever arm. Therefore, rope tighteners were used to even out the load cells and ensure all connections were secure. Similarly, the rope could not go directly from the actuator to the tendon attachment, as this angle causes inaccurate force application. The setup is displayed in Figure 27. Ropes were redirected through eye bolts and up to the tibia attachment. As all four muscles go to the ankle or calcaneus, the redirection point is extremely close to the tibia. The eye bolts, cut at their respective lengths and held by small beams, shown in Figure 28, were employed to redirect the actuator forces along the rope and to the tibia specimen.

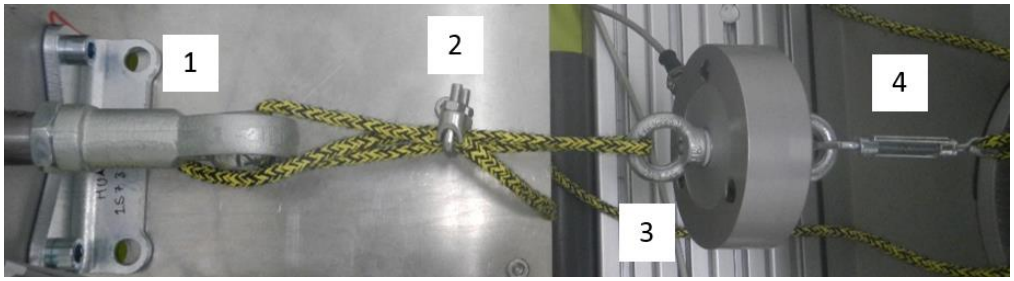

Figure 27: Layout of muscle simulation: 1) actuator arm, 2) rope clasp, 3) load cell, 4) rope tightener

Figure 28: Posterior muscle re-direction mechanism with three eye bolts fastened to item beams

A combination of body weight and muscles in the upward direction were exerted onto the tibia. Force application was achieved using weights. To account for the substantial size of the weights, a large plate was positioned on top of the tibia. The weight of the plate was taken into consideration when applying force.

Safety ropes were tied between the top plate and through four eye bolts located within two supporting beams. This was to ensure that the weights and top plate stayed in place (Figure 29). The rope (FSE Rio 8mm) was selected for its high breaking load and capacity to stretch under load. A bowline knot and a rope clamp were used to fasten the two ends of the rope (Figure 30).

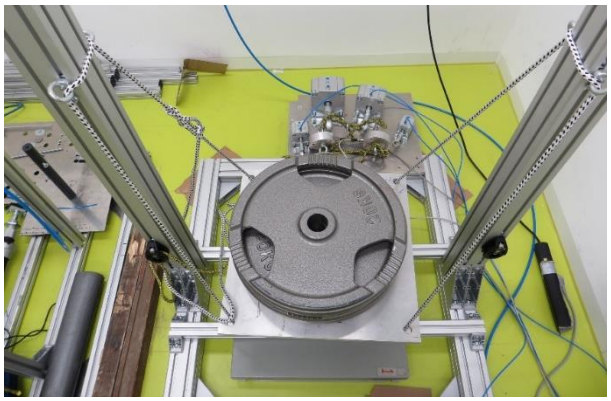

Figure 29: Safety rope feeds through the top plate and the four eye bolts attached to the two vertical beams

Figure 30: Two ends of the safety rope connected with a bowline knot and a rope clamp

The y-axial force was administered to the top plate via a pulley system. As mentioned, the tibia specimen was turned so its orientation changed to the y-direction moving from left to right of the rack (when viewed from the front). A pulley was positioned on each of the two vertical pillars at the same level as the top plate. These pulleys, Harken Carbo AirBlocks 57mm Cheek Block, (Harken, Inc., WI, USA), were selected due to their very high breaking load (1080 kg). A rope ran from the top plate, through the pulley, to a weight balancing beside the pillar (Figure 31). The forces in the x-direction were minimal, and therefore were not considered in the Alpha rack design. However, the Beta rack will simulate all forces in the future.

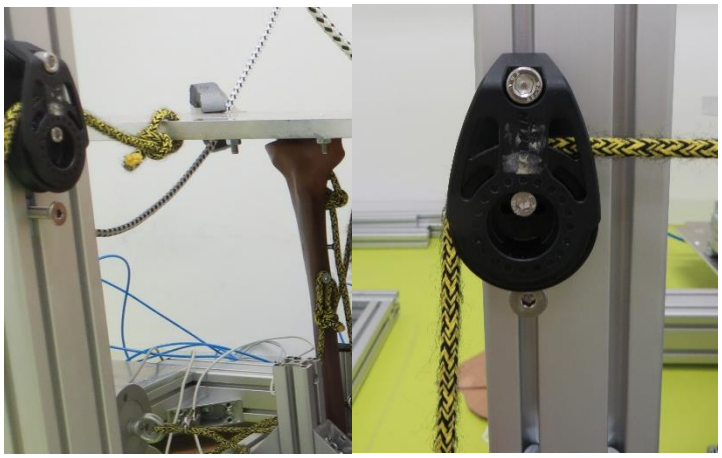

Figure 31: Y-axial force application from a pulley system

For a full list of materials used for the rack, please refer to Appendix D.

3.2.2 Test Rack Assembly

The test rack was drawn on the CAD program CATIA (Dassault Systéms, Paris, France). The designed layout was intended for test rack validation. The muscle orientation was modelled in the standing position. Specific re-direction positioning may have to change in the future as different movements are simulated.

3.2.2.1 Test Rack Shell

The shell of the test rack was designed to be robust and versatile to handle a large range of tests. Therefore, large beams were used and numerous brackets were utilised to take into account large forces. Also, two tall vertical beams were used to support the structure so maximum visibility was available for the optical measuring system.

The force plate is slightly greater in depth than the large item beam. Therefore, base brackets were designed and manufactured to raise the test rack above the force plate. A bracket was secured to each of the four corners of the rack. Also, an item bracket was fastened between each of the base beams to fix them together. Small item beams ran across the main structure to hold the muscle force re-direction mechanism (Figure 32).

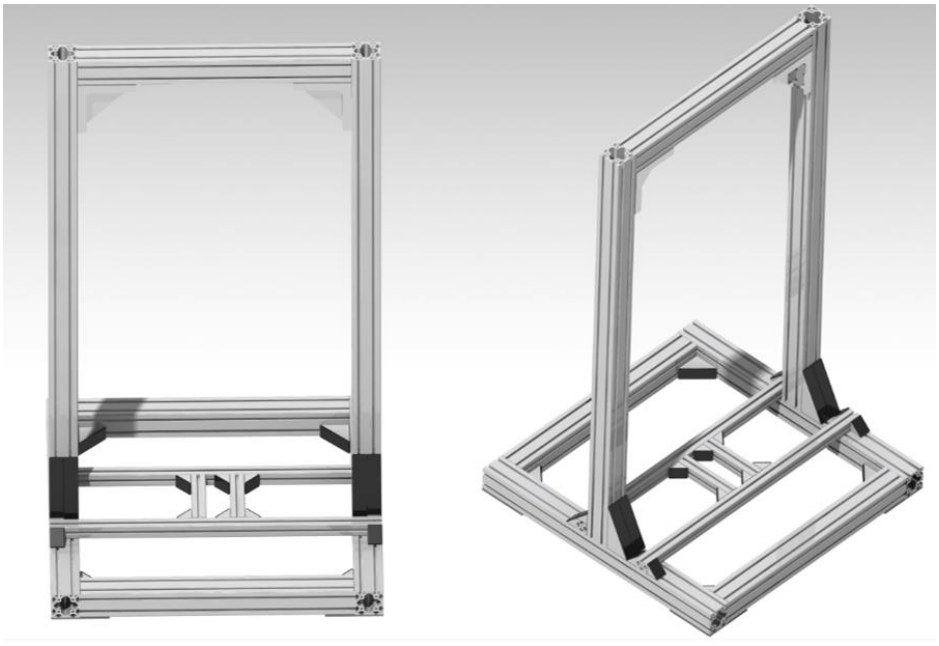

Figure 32: Test rack shell. Left: front view, Right: top angled view

3.2.2.2 Tibia Positioning

The y-axial forces were enforced along the centreline of the tibia. As the pulleys and weights to induce this y-axial force are located on the front surface of the vertical beams, the tibia must be moved forward. Consequently, as the tibia must be standing in the middle of the force plate, the force plate is also forward of the centre of the test rack (Figure 33).

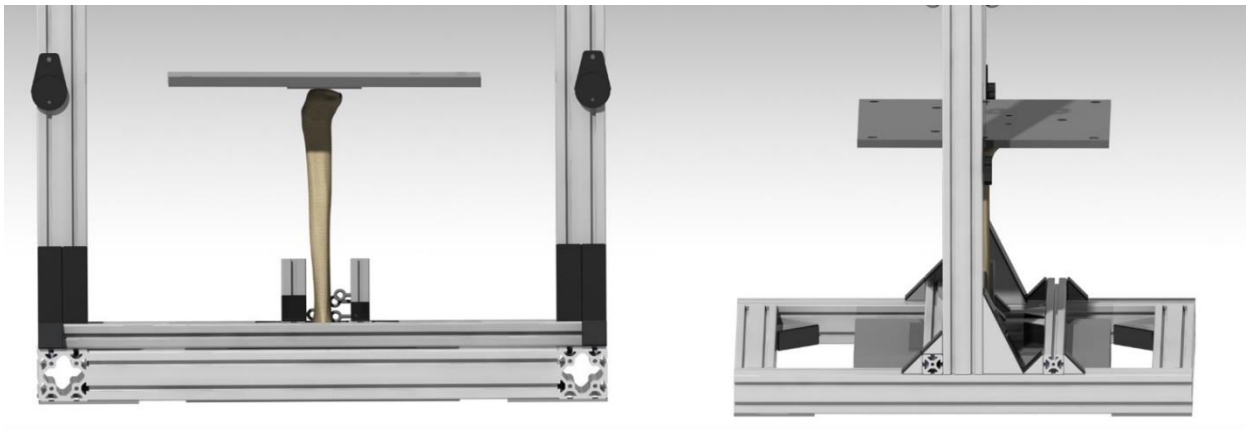

Figure 33: Tibia alignment with pulleys on front of pillars

3.2.2.3 Top and Base Plates

A base plate and two top plates were employed in the test rack. The base plate had one M10 sunken hole in the centre, accommodating the sunken head M10 bolt that goes through the plate and into the tibia base. Two top plates were designed to allow for a simple and quick setup and assembly. A large aluminium top plate sits above the tibia. It is large enough to carry weights and has holes for ropes to feed through. This large plate is not connected directly to the tibia. A smaller plate is wedged between the tibia and large top plate. This has four holes on the perimeter, one sunken hole in the centre and four sunken holes close to the centre. The outside holes connect the two plates, the inner hole connects the small plate to a PVC specimen and the four inner holes connect the small plate and the tibia (Figure 34).

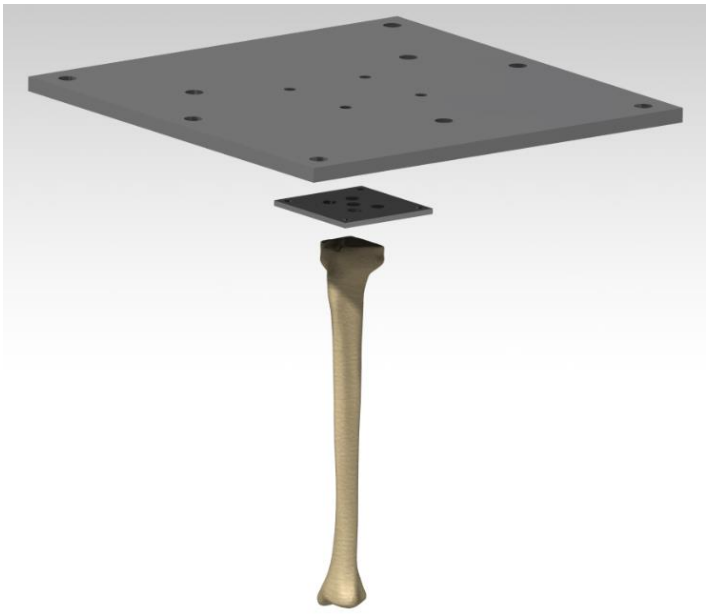

Figure 34: The top plates above the tibia specimen

3.2.2.4 Force Re-Direction and Actuator Positioning

When determining the re-direction positions for the eye bolts, the actuator orientation and height and the muscle location must be considered (Figure 35). The artificial tibia is configured to simulate a standing position for the feasibility and validation testing. This is due to its simplified muscle orientation and a vertical tibia alignment.

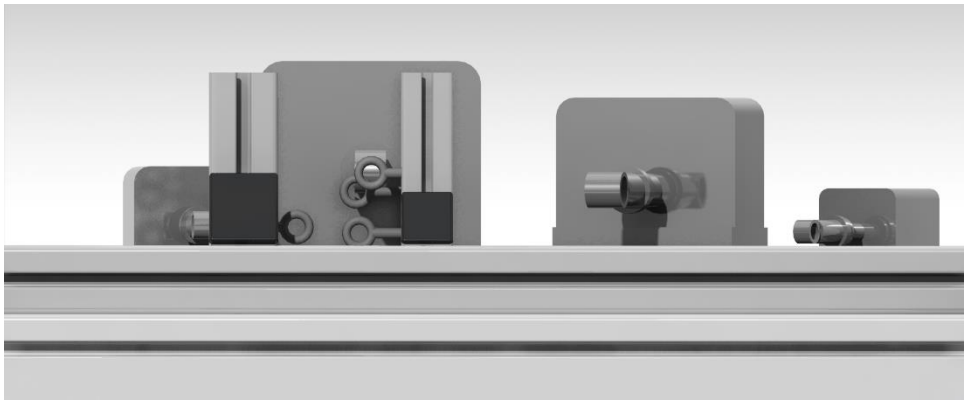

Figure 35: Actuator lever arms align with the redirection eye bolts

The actuators each have brackets to raise the body up. Each bracket also has holes for fastening. The positioning of the actuators was determined using CATIA. The re-direction bolt locations and the plate's orientation to the test rack were all considered when establishing the actuator orientation (Figure 36). The hole locations were designed and drawn, and given to the DLR workshop to cut.

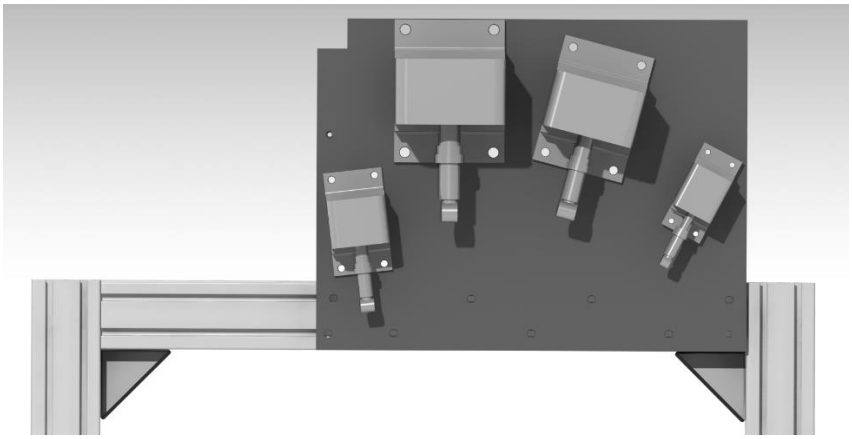

Figure 36: Actuator positions on actuator plate

3.2.2.5 Test Rack Assembly

Figure 37 shows the 3D model of the test rack assembly (left) and the overall size of the test rack (right).

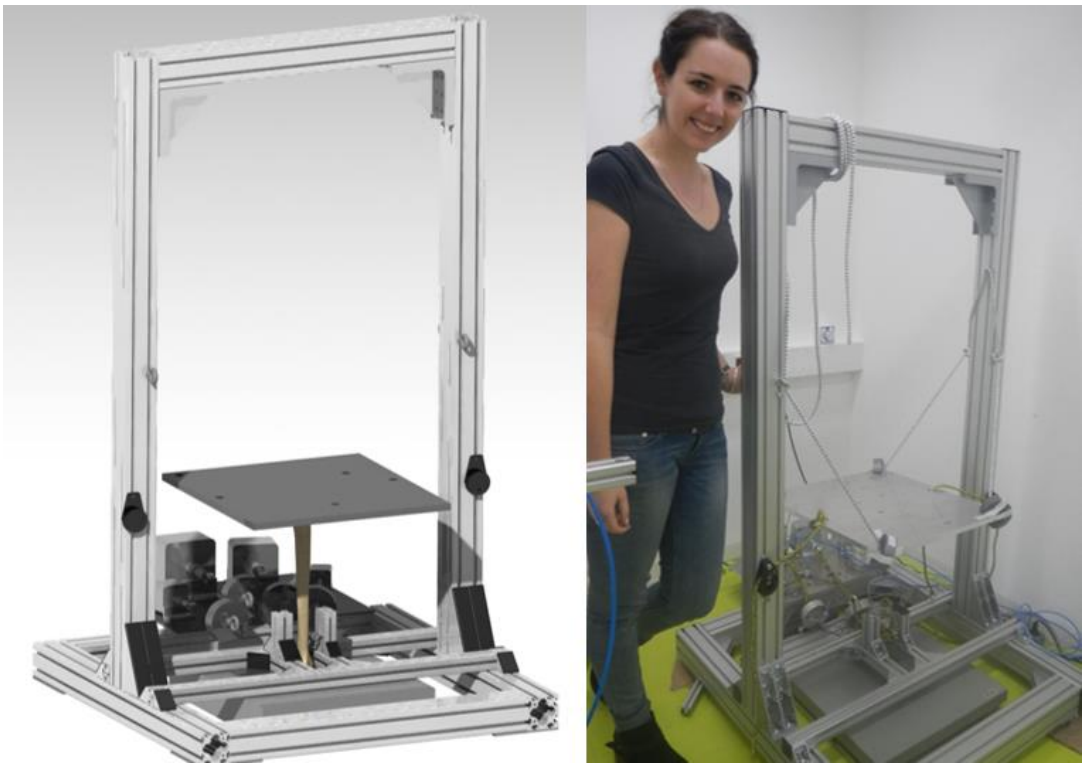

Figure 37: Test rack assembly

Technical drawings of the test rack assembly and individual components are available in Appendix F.

3.3 Apparatus Setup

The tibia specimen was manipulated before being placed in the test rack. The two grooves at the top of the tibia, where the tibia and femur would touch, is where maximum force transfers. Therefore, four M8 threads were drilled into these grooves. The sunken bolts, shown in Figure 38, attach the small top plate to the tibia.

Figure 38: Four sunken head bolts drilled into the top grooves of the tibia specimen

M8 threads were drilled into the four tendon locations on the anterior and posterior of the specimen. M8 bolts, longer than the hole, were hand tightened into each hole. These correspond to the four muscle attachments (Figure 39).

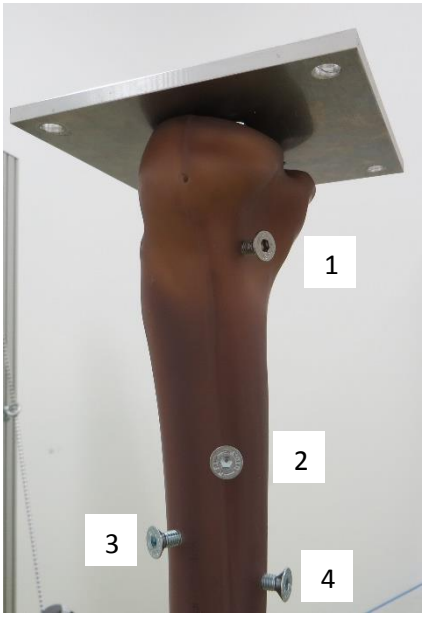

Figure 39: Muscle attachment to tibia: 1) Soleus, 2) Tibialis Posterior, 3) Tibialis Anterior, 4) Flexor Digitorum Longus

An M12 thread was drilled into the pre-existing hole, located in the centre of the tibia. A sunken head M12 bolt connected the base plate to the tibia. The bolt attachment has a large gap between the base plate surface and the tibia. This results from the shape of the tibia base, forming a groove to fit into the talus. Therefore, three washers were used to support the bolt and lift up the tibia (Figure 40).

Figure 40: Tibia attachment to base plate

3.4 Control System

The control system of the test rack is provided in Appendix G and is summarised here, for a generalised understanding. It was designed by Manuela Paulina Trejo Ramirez in parallel to this thesis, based on requirements provided by this project to model the muscle forces simulated on the test rack.

To develop a physiologically accurate model of the lower limb, force application was designed to be similar to muscles with fast reaction times and force ranges from zero to maximum isometric force of each muscle. Consequently, the largest actuator must be capable of applying a force of 3.5 kN (see Table 4). Four compact cylinders AEVU/AEVUS [81] (Festo, Esslingen, Germany), all with small strokes (10 mm) and various piston sizes, were implemented to model the four downward muscle forces. Their corresponding mounting accessories [82] and rod eyes [83], acting as lever arms, were purchased to accomplish a complete actuator setup. Additional air tubing, solenoid valves, air controllers and an emergency stop button were acquired to regulate the pneumatic system. Control of the actuators and pneumatic airflow was performed using the software program LabView (National Instrument, NI, USA). The program additionally graphed the actuator force magnitude recorded by burster load cells (models: 8531-2000 and 8531-5000) (Burster Präzisionsmesstechnick Gmbh & Co kg, Gernsbach, Germany), which were setup in the rope connection between the actuators and tibia specimen.

CHAPTER 4. ASSEMBLY AND TESTING METHODS OF PROTOTYPE

4.1 Test Rack Assembly

Once the materials were manufactured and delivered, the test rack assembly began. The construction process, in the order executed, is summarised in Table 8.

Table 8: Summary of test rack assembly

Assembly Step	Description
1. Test Rack Base  	The large base beams were held together by custom designed base brackets (Appendix F). Additional item brackets (80x80) were fixed in each corner.
2. Test Rack Vertical Beams	The two 1.5 m long vertical beams were attached to the top beam with two large (80x80) brackets in each corner.
3. Test Rack Small Platform 	The small platform, positioned above the base structure, was assembled. At this stage in the assembly, the positioning of the two inner beams was random. Therefore, these two beams were loosely fixed for later adjustments.
4. Test Rack Shell Assembly 	The components of steps 1-3 above were secured together using numerous brackets.
5. Force Plate 	The test rack was manually tilted, allowing the force plate to slide underneath the small support platform.

Assembly Step	Description
6. Eye Bolts and Pulleys 	Four eye bolts were inserted into the long vertical supports to hold a safety rope. Similarly, the redirection pulley for the y-direction force was attached to both vertical pillars. As shown in the picture on the left, the eye bolt was attached to the inner groove and the pulley to the outer groove of the item beam.
7. Actuator Platform and Actuators 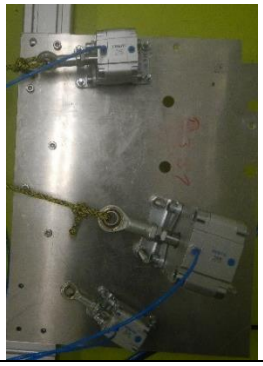	The custom designed actuator plate (Appendix F) was secured to the back base beam with nine M8 bolts. The four actuators were fixed to their predetermined position (photo on left shown with only three actuators attached).
8. Re-Direction Points  	The pre-cut eye bolts were screwed to support beams at set heights (left most picture). These beams were then fixed to the small raised platform inner beams (right picture). The inner beams were relocated to predetermined positions (Appendix F).
9. Test Specimen 	The base plate (Appendix F) was covered in Gecko Tape. The Gecko Tape had high friction, therefore the base plate should not slide over the force plate. The tibia base and small top plate were initially secured firmly to the tibia specimen. The rack was then tilted to place the specimen, and its corresponding plates, onto the centre of the force plate and between the small raised platform.
10. Large Top Plate	The large tibia top plate was secured to the small top plate with four M8 bolts. Ropes were tied through holes on the perimeter of

Assembly Step	Description
	the plate and attached to the corresponding safety eye bolts and redirection pulleys.
11. Actuator/Re-direction/Specimen Rope	The ropes were tied using a combination of bowline knots and rope fasteners. The ropes were attached to the actuator and a load cell. From there, another rope fed from the load cell through the re-direction eye bolt and tied around the tibia specimen's muscle attachment point.
12. Actuator Setup	During this setup, the actuator, air ways and control system was prepared.

4.2 Problems Encountered and their Mitigations

Several problems were encountered during the test rack assembly. These issues, however, were investigated and resolved as part of the design process.

- The large vertical test rack beams were fixed at the top with a horizontal beam and four medium size (80x80 mm) brackets (two in each corner). Upon assembly, it was noticed that the supports moved slightly and vibrated when pushed strongly. Therefore, larger, stronger brackets, shown in Figure 41, were purchased and secured at the top of the vertical beams.

Figure 41: Large brackets fastened between the two vertical beams and structural horizontal beam

- Another problem that arose concerned the attachment of the two vertical beams to the base structure. These long beams are extremely heavy and encountered strong forces during tests. Two small 80x80 mm brackets (Figure 42, left) were replaced with two larger 160x80 mm brackets (Figure 42, right) at the base of each vertical beam.

Figure 42: Base brackets used to hold up long beams; Left: small brackets, Right: larger brackets

- There was also an issue with tightening the ropes. Initially, bowline knots and rope fasteners secured both ends of the rope connecting the actuator to the load cell and the load cell to the tibia specimen (Figure 43, left). However, the knots were not tight enough and the load cell lagged and pulled the rope down. Rope tighteners (Figure 43, right) were introduced on each line of rope to ensure the rope was taut.

Figure 43: Left: bowline knots, Right: rope fasteners and rope tighteners

- A structural design flaw was noticed during the assembly. To account for the force plate being larger in depth than the 80x80 (mm) base beams, the base brackets raised the whole test rack up 5 mm. Yet, this only allowed for a 4 mm tibia base plate to slot between the force plate and the small platform. Instead, a larger base plate (20 mm) was designed so the simulated forces would not cause the plate to

bend. Therefore, the whole test rack had to be elevated further. Item profiles were inserted underneath the base brackets (Figure 44) to raise the rack and provide a temporary solution.

Figure 44: Temporary solution of inserting 40x40 mm beams under each corner of the test rack

- When securing the tibia to the base plate with the large bolt, a small crack was produced. As the primary purpose of the test was to determine functionality rather than specific tibia deformation, the crack does not impact on the results.

4.3 Safety Measures

Safety measures were taken prior to testing. These are outlined in Table 9.

Table 9: A summary of safety measures

Safety Issue	Safety Measure	Figures and Equations
Pressurised air drove the actuators. Also, large magnitudes of force were applied to the test rack. There was a risk that objects could spontaneously detach from the rack and fly around the room.	Safety shielding was designed (Appendix F) and assembled. A stability test, where objects were propelled at the PVC glass, confirmed the shielding could handle high forces and will protect those positioned behind it.	
The large tibia top plate could fall as a result of high forces or the tibia specimen breaking. This would likely damage the test rack and cause objects to detach and project around the room.	A safety rope (FSE Rio 8mm) was fed through holes positioned in the four corners of the tibia top plate and four eye bolts on the edges of the two vertical beams. The ropes would hold the top plate if	

Safety Issue	Safety Measure	Figures and Equations
	it tilts excessively. The ropes can withstand the high forces, as demonstrated in a test that resulted in the ropes and top plate holding 140 kg.	
The actuator ropes could snap when holding high forces.	The safety factor for the actuator was determined using the equation on the right. The rope had a large safety factor of 2.8. Therefore, the rope would sufficiently tolerate the high forces.	$Safety\ Factor = \frac{Material\ Strength}{Design\ Load}$ Where: Material strength = 17 kN (rope's breaking load) Breaking load = 6 kN (largest actuator's maximum output)
The test rack has many sharp edges, causing hazardous obstacles.	Shield caps were put onto the end of the beams and the brackets. The top plate temporarily had foam taped to each corner.	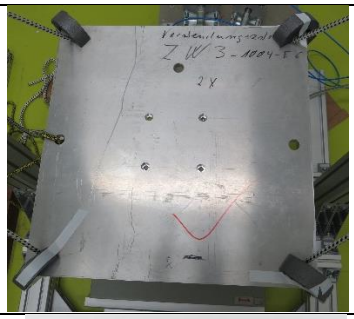
The pneumatic control has large amounts of pressurised air travelling through numerous valves. If the test rack encountered a serious problem, the air should immediately be switched off.	A stop button was positioned next to the controller. The button can instantly stop all air flowing into the actuators.	

4.4 Testing Protocol

A number of experiments assessed the functionality of the rack and components. Each experiment progressed consecutively, with qualitative observations recorded.

Due to human error when drilling the threaded holes into the top of the tibia, the top plate had a natural slant prior to testing. This was measured using a spirit level before each test.

4.1.1 Initial Test

An initial test was performed on a PVC cylinder (Figure 45), with the purpose of confirming that the actuators worked, the ropes and knots held the forces and the whole rack remained standing.

The test rack was assembled as outlined in Section 4.1. However, instead of the tibia specimen, the PVC cylinder, with the attached base and top plates, was positioned on the test rack. The Tibialis Anterior actuator (second smallest) and Soleus actuator (largest) were used to simulate forces. Bowline knots tied the rope connecting the actuator to the load cell and the load cell to the muscle attachment. Separately, each actuator transmitted approximately half its maximum force (around 400 N and 1000 N respectively), which was held for 10 seconds. The force application was repeated two times. All observations were noted including any errors in the setup for improvements for future tests.

Figure 45: PVC cylinder with bolts as muscle attachments

4.1.2 Tibialis Anterior Test

Functionality testing must examine how the test rack (structurally and all components) adapts to the highest possible forces. However, to ensure the high loads do not damage the tibia specimen in the first run, a smaller actuator, mimicking the tibialis anterior muscle, was initially used. The test rack setup was performed as outlined in Section 4.1. A rope fastener connected the rope to the second smallest actuator and to a rope tightener, which joined with the load cell. On the other side of the load cell, another rope attached with a rope fastener went through the redirection eye bolts and around the muscle tibia attachment point, connected by a bowline knot. The rope setup is shown in Figure 46.

The pressurised air flow speed to the actuator was controlled and measured by the number of turns of the air control valve. Each flow speed, increased by one turn for each test, was held for 5 seconds and subsequent observations were recorded.

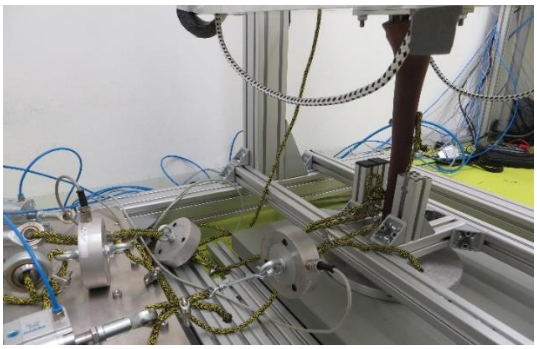

Figure 46: Tibialis Anterior Test actuator to muscle attachment rope connection

4.1.3 Soleus Test

The Soleus Test modelled the large muscle of the lower leg, the Soleus muscle, which attaches to the posterior side of the tibia (Figure 47).

The objective of this test was to determine if the test rack components could tolerate the highest expected forces. As such, the corresponding actuator was capable of applying forces up to 4000 N.

The Tibialis Anterior Test rope and test rack setup was also used for this test. Upon completion of the Tibialis Anterior Test, with the tibia specimen still intact, ropes were untied from the corresponding actuator and reconnected with the largest one.

The air flow (in bar) was progressively increased, by one turn in the valve, and held for 5 seconds at each magnitude. Any rack alterations observed were recorded. The test was repeated once.

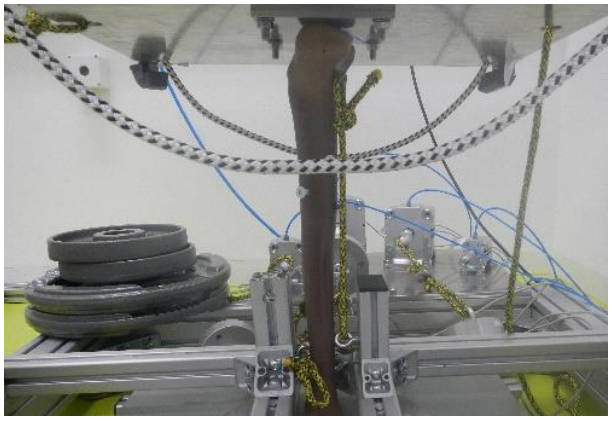

Figure 47: Soleus muscle attachment on posterior side of tibia

4.1.4 Y-Direction Force Application Test

When moving, force from body weight is exerted predominantly in the z-direction, but also in the y-direction and minute amounts in the x-direction (see Section 3.1.4). As the test rack aims to provide an anatomically accurate model of the lower limb, body forces in the y-direction must also be replicated. The purpose of the Y-Direction Test was to determine if the test rack and lower limb setup can withstand forces applied to the top of the tibia in the y-direction. No forces were applied using actuators, so all actuator connections were untied. A force was applied to the top plate, which was attached to the top of the specimen. A rope was tied (bowline knot) to the top plate and fed through the pulley positioned on the left pillar (Figure 48). A 5 kg weight was secured to the other end of the rope and slowly released. The change in angle of the top plate was measured using a spirit level. Any qualitative findings were also recorded.

Figure 48: Y-direction test setup

CHAPTER 5. RESULTS

5.1 Initial Test

The initial test aimed to verify that all components operate as expected: the actuators apply forces, the ropes and knots can withstand these forces and all structural components of the test rack remain secure. Table 10 outlines the test rack components and how they responded to the application of high forces.

Table 10: Summary of the test rack components and their responses during the Initial Test

Component	Observation
PVC Cylinder	Deformed with each force application, as expected. The PVC cylinder did not break.
Muscle Attachment Bolts	The bolts stayed in the PVC cylinder. Following the experiment, the bolts were extracted and there were no visible signs of thread deterioration.
Base Plate and Gecko Tape	The base plate stayed attached to the force plate. Therefore the Gecko Tape has sufficient friction to hold the forces.
Rope	There was no visible elastic stretching or deformation in the actuator ropes.
Knots and Fasteners	Unexpectedly, the bowline knots slipped while the fasteners held the ropes. Also, it was difficult to tie the ropes tightly. Therefore, rope tighteners were implemented for later tests.
Actuators	Air flowed to the actuator, after which the lever arm moved to exert force. Therefore, it functioned as expected.
Test Rack Structure	Small vibrations were observed in the vertical beams. The test rack structure stayed intact during the experiment.

The test confirmed that everything but the bowline knots, which slipped under force, worked as expected for medium force application. Therefore, the only change required to prepare for the following test was to secure the actuator ropes with rope fasteners and tighteners.

5.2 Tibialis Anterior Test

The Tibialis Anterior Test was the first test performed on the tibia specimen. The second smallest muscle was modelled to clarify that the structural test rack components worked as expected and that the tibia specimen and fixation points could tolerate forces.

When the force was applied, the slope of the top plate was +2.5˚ in the x-direction and -1.5˚ in the y-direction. This was the first measurement of the slope of the top plate. These angles imply that the top of the tibia experienced a small additional uneven force.

Table 11 provides a summary of the test rack changes observed at different force magnitudes. At this initial stage in testing, no device was installed to measure the air flow for each turn of the valve. Each turn signifies that the air flow to the actuator progressively increased. The test rack experiment room had access to 6 bar of pressurised air. The maximum air flow into an actuator was 5.8 bar, with the remaining 0.2 bar being lost amongst the pneumatic control system and air tubing.

Table 11: Summary of the Tibialis Anterior Test observations

Air Flow (Number of turns)	Observations
1-5	No noticeable change/movement.
6	Small movement in load cell.
7	Small movement in actuator and small vibration.
8	- Vibration of whole actuator platform. - Actuator plate moved approximately 2-3 mm.
9	As per 8 turns.
10	- Top plate slight movement (hence, tibia specimen movement). - Actuator platform movement again.
12	Vibration of rack and top plate movement.
14	Top plate movement.
14.5 (max – 5.8bar)	Large movement of top plate.

No observations were made in the 1-5 number of turns (low air supply to actuators). This suggests the test rack and components could withstand forces at a low magnitude. It was only when the higher forces were applied that the significant changes in the rack were noted.

The bending of the actuator plate was the most significant result from the Tibialis Anterior Test. A thicker, more stable actuator plate was designed (Appendix F) following the experiment. Due to time restraints, it was manufactured after completion of this thesis and will be used in future tests.

Additional noteworthy experimental outcomes include the force plate sliding backwards towards the actuators (+ x-direction) and, although not observed, it was highly probable that the small item profiles holding the re-direction eyebolts also bent. Therefore, a mechanical fixation between the force plate and the rack framework was required. A temporary solution, shown in Figure 49, was implemented where spare item profiles and PVC cylinders were slotted between the force plate and base item structure to prevent the force plate from moving.

Figure 49: Temporary solution to prevent force plate from sliding

5.3 Soleus Test

The Soleus Test modelled the forces applied to the largest muscle of the lower limb. Consequently, the largest actuator, which can apply forces up to 4000 N, transmitted force to the Soleus muscle attachment bolt. The test objectives were to determine if the test rack components could handle these high forces and continue to function as expected.

The Soleus Test was only repeated once as a substantial problem was noticed in the test rack setup during the first test. This issue was then corrected prior to the second test.

Table 12 lists the observations for the few air flow varieties performed in the first test. The initial slope of the top plate was +1.6 in the x-direction and -1.4 in the y-direction. Compared with the measurement taken prior to the Tibialis Anterior Test, the slope has shifted considerably towards the positive x-direction and only a small amount in the y-

direction. The possible reason for this change is justified in Section 6.2. The weight of the top plate in the Soleus test thus continues to exert force in the x and y directions. A pressure metre was setup for this test enabling air flow to be recorded in bars. The test ceased when it was realised that the load cell was reading the force magnitude incorrectly.

Table 12: Summary of the first Soleus Test observations

Air Pressure (bar)	Observations
0.54	- No change.
0.99	- The actuator plate moved. - Movement was observed in the actuator attachment. This movement probably resulted from the actuator, which modelled the Soleus, only being secured to the actuator plate with two bolts instead of four. - The top plate, and therefore the tibia specimen, moved.
1.58	Same as observed above, but with more movement.

Like the Tibialis Anterior Test, the test rack operated as expected when force was applied at low levels. As the force magnitude increased, an increase in movement was observed in the test rack.

The measurements from the load cell were viewed in LabView. When the actuators were operational, the load cell should have read the corresponding force output. During the first Soleus test, the load cell fluctuated between -10 N and 10 N (oscillations caused by external noise). The test was stopped and the load cell untied from the test rack. After further consideration, it was realised that the axial load cells were setup incorrectly. The attachment of rope on both sides of the load cell cancelled out the forces.

Tensile and compressive tests were performed to confirm that the low force readings resulted from the load cell setup and not from the load cell themselves or from the computer control system. The force readings were positive, but still incorrect. The force from the load cell was recorded as approximately half that of the applied force. Therefore, scaling of the load cells was required. As the oscillations occurred on the computed force magnitude graph, the maximum force reading was recorded. The results are listed in Table 13.

Table 13: Load Cell Test

Test Type	Weight Applied (kg)	Corresponding Force Applied (N)*	Load Cell Reading (N)
Compressive	88	863	420
Compressive	66	647	320
Tensile	55	-540+	-250+

*Rounded to zero decimal places and obtained using the equation $Force = kg \times 9.81$

+A negative value was recorded as force was applied in tension

The Soleus Test rope setup, with the actuator held by two ropes connected to the actuator and tibia specimen respectively, could no longer be used. Consequently, a temporary solution was employed to continue the Soleus Tests whilst measuring the force magnitude. The new setup had wire rope tied around the load cell, as shown in Figure 50. Hence, only the one side of the load cell was then transmitting force output and the system did not cancel forces out.

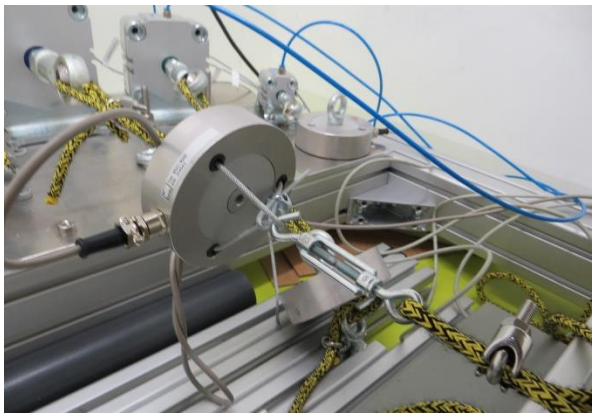

Figure 50: Temporary load cell solution to measure forces

Table 14 shows the second Soleus Test observations, with the load cell held in the new setup. The slope of the top plate was the same as the first Soleus Test. A tensile force was applied to the load cell in this setup. Thus, the force was recorded as a negative magnitude. As stated above, the load cells required scaling. Precise computer scaling was not completed for this test due to time constraints. Consequently, for this setup the force value recorded by the load cell was doubled.

Table 14: Summary of the second Soleus Test observations

Air Pressure (Bar)	Force Application (N)	Observations
0.57	-188	- The rope slackened due to the knot and wire around the load cell loosening.
1.03	-206	- The specimen and actuator moved.
1.59	-168	- The specimen moved. - The force reading was lower than the previous two tests. This likely resulted from the wire apparatus pushing against the side of the load cell transmitting force output.
5.37	-132	- The total rope length, from the actuator to the specimen, increased due to wire deformation. This lead to a decrease in the maximum applied force.

It was expected that an increase in the air supplied to the actuators would result in a higher load cell force reading. Table 14 illustrates that this did not happen. The low force recorded likely resulted from the load cell mounting apparatus deforming, thus lengthening the distance between the actuator and tibia specimen. As the actuators had a small stroke of only 10 mm, any variation in the setup of the connection between the actuator and specimen generates lower force application. This signifies that the test rack setup must be accurate to deliver the intended forces.

No measurements to compare the amount of air flow to the actuators and the corresponding force exerted were conducted prior to these tests. Nevertheless, as the actuators were setup and controlled as recommended by the supplier, it was expected that they transmitted the desired high forces when supplied with a high air flow. To support this, the test rack structure reacted to forces when the actuators were operational, with the majority of tests performed resulting in vibrations in the vertical pillars and actuator plate as well as force plate movement. Overall, the actuators likely performed as required but the test rack was not sufficiently setup to transfer the entire forces from the actuator to the tibia specimen.

5.4 Y-Direction Test

The Y-Direction test was designed to determine if the specimen and test rack could withstand force application in the positive y-direction.

The initial slope of the top plate was +1.9 x-direction and -1.9 y-direction. After 5kg of weight was applied in the positive y-direction, the slope changed to +1.7 x-direction and +2.8 y-direction. The top plate slopes are illustrated in the diagram of Figure 51.

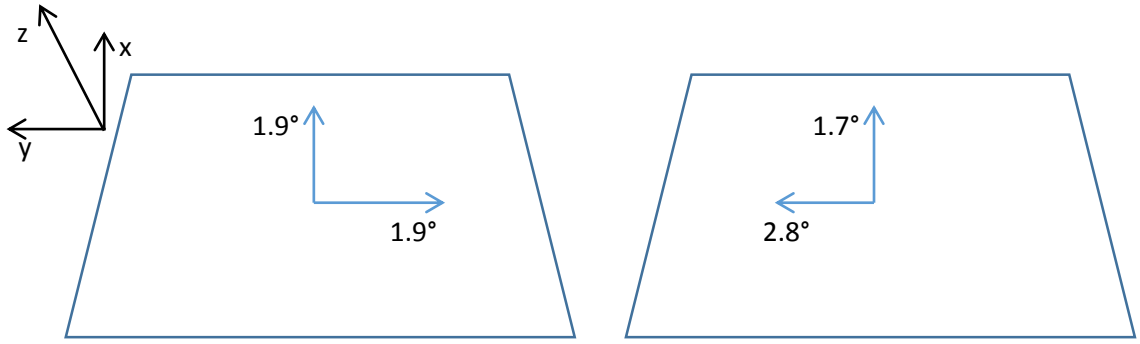

Figure 51: Slope of top plate; Left: before force application, Right: after force application

The top plate moved by 4.7˚ in the positive y-direction. Thus, the tibia specimen bent in the direction of force application as expected. The slope changed in the x-direction by 0.2˚, indicating that the tibia specimen was not aligned correctly.

The test was to consist of applying the force for 10 seconds. However, the force was applied only for a few seconds as a loud cracking sound came from the tibia specimen. The experiment was stopped and not repeated. It was noticed after disassembling the components that the crack was expanding along the base hole of the tibia, where the tibia was attached to the base plate with a M12 bolt. This showed that there was too much pressure at this particular point. In addition, the cracking that extended from this site demonstrated that the tibia did not bend as expected in the middle to upper sections.

5.5 Summary of Results

After all tests were performed, it was noticed that:

- The structural support beams of the test rack withstood high forces.
- The actuators operated when supplied with air. However, due to the unanticipated setup limitations, the entire force transmitted by the actuators was not applied to the tibia specimen.
- The muscle attachment bolts stayed inserted in the specimen through all tests and did not cause any damage.
- The pulley redirected force in the y-direction test.

- The Gecko Tape secured the base plate to the force plate.
- The crack at the base of the tibia propagated, shown in Figure 52.

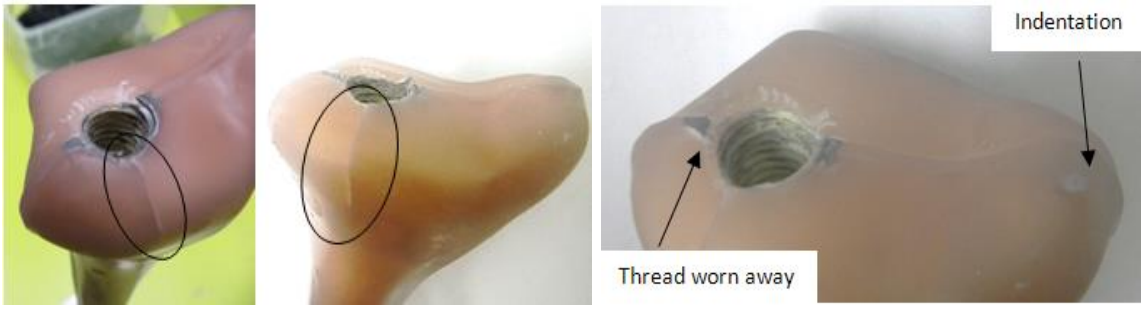

Figure 52: Crack on the base of the tibia; Left: before testing, Centre: after testing' Right: Base of tibia showing the outermost thread worn away and tip minor indentation

- In the base hole of the tibia, at least one entire thread had worn away (Figure 52, rightmost image).
- There was a minor indentation on the base tip of the tibia specimen (Figure 52, rightmost image).
- The front edge of the top plate no longer aligned with the test rack. The tibia specimen had moved due to the loosening of the bottom fixation screw.
- The rope/wire for the soleus actuator (Soleus Testing) had dropped approximately 1.5cm. This is likely due to the wire deforming under load. In addition, the rope knots loosened slightly.
- The actuator platform bent.
- The re-direction eyebolts bent when force was applied.
- The rack moved and slid over the item profiles in the corners.

For an overview of the results compared with the corresponding requirement specifications, please refer to Appendix H.

CHAPTER 6. DISCUSSION

6.1 Experimental Procedure

This thesis comprises four experiments that tested the functionality of the test rack. All tests generated valuable preliminary results that have assisted in developing and improving the rack for future experiments. The test first used a PVC cylinder to examine the performance of the test rack components. The second and third tests, the Tibialis Anterior and Soleus Tests, applied forces onto the tibia specimen at the corresponding muscle attachment point. The final test, the Y-Direction Test, assessed whether the test rack and specimen could withstand forces transmitted to the top of the tibia in the positive y-direction. The experimental procedure offered qualitative results and air flow measurements. Observing the functionality of the test rack was essential to examine how it was working, if it operated as expected and if any necessary adjustments were required.

In the Tibalis Anterior and Soleus Tests, force was progressively increased. The test rack functioned as predicted when a small force magnitude was applied. At higher forces, the tests exposed aspects that worked and elements that experienced problems. Yet, whether the components operated as expected or not, the results from the tests have the potential to assist in the development of improvements for future work. Specifically, components that fulfilled the requirements can either remain as they were or have minor alterations for improvement whilst solutions to overcome specific design limitations should be developed. The recommended design variations are summarised later in this chapter (Section 6.4).

The unforeseen technical challenges to address in the time available affected the amount of tests performed. No tests were performed on the smallest actuator and the second largest actuator, which were modelling the Flexor Digitorum Longus and Tibialis Posterior respectively. It would have been beneficial to include these actuators into the Initial Test phase to see if they, the redirection components and the muscle attachments worked correctly with a PVC cylinder. Additionally, having all actuators working at maximum performance concurrently on the tibia specimen, modelling an isometric

exercise, would have verified that the test rack, tibia and all components could endure high loads. To overcome these uncertainties, the isometric exercise was modelled on Ansys at DLR and it was revealed that the tibia specimen would not break under this high load. Furthermore, the experimental procedure included the highest force from the largest actuator (maximum 4000 N), thus demonstrating that the ropes and redirection eyebolts could withstand forces applied by all of the actuators. However, the mechanical stability of the components could still be affected by creeping and fatigue. These possibilities were not tested as future experiments intend to apply forces for a short period of time, around 5 seconds, with a small amount of repetitions. Consequently, creep and fatigue criteria, respectively, are not required to be met with the intended use of the rack. There was not sufficient time to improve the test rack following the functionality testing nor make any physical modifications. However, potential and proposed improvements resulting from these tests are discussed in this chapter.

Another factor that restricted the quality and repeatability of the tests was the incorrect installation of the load cells, which affected readings of force magnitude. To overcome this issue, adequate supporting equipment, such as load cell flanges, are recommended for future tests.

During the Y-Direction test, a large crack spread from the base of the tibia. Due to this damage, and potential further damage that could occur if testing was continued, the test was stopped and the components of the test rack were disassembled for inspection. There was not sufficient time to amend the crack in the tibia specimen nor prepare a new specimen. Before further experiments are performed, the tibia specimen should be repaired or replaced.

Validating the test rack was originally intended for this thesis. However, due to essential equipment being unavailable in the timeframe, the validation process was not completed. However, the process was designed. To validate the test rack, an optical measuring system is required to measure the displacement of a PVC cylinder in one place on the front plane. The displacement recorded on the optical measuring system must equal that simulated on a computer model. If the two measurements do not match, adjustments would need to be made to either the test rack or the computer model (depending on the error found and the reasons for this error). Once the test rack and computer model displacements

correlate, then experiments simulating body movements could be performed. The test protocol for the validation of the test rack is provided in Appendix I.

The force plate is critical in future tests in order to record the reaction forces at the base of the tibia. The force plate takes force and moment measurements along three axes. It can additionally assist with the alignment of the weights above the specimen to ensure the correct forces and moments are being applied to the tibia head. The force plate was part of the current test setup despite not being used but did illustrate that all components could be set up as per the original design.

6.2 Test Rack Performance

The test rack's performance clearly identified some successful design points as well as portrayed areas of weakness in the design and setup.

All structural beam, bracket and bolt components of the test rack successfully stayed secured throughout the tests. However, the entire rack did move and slide over the item profiles, relative to the force plate and specimen, which were temporarily positioned under each corner to accommodate for a thick base plate. This unwanted movement shortened the distance between the specimen and actuators resulting in the maximum force not being applied. Subsequently, the results only displayed the effect of partial force application. It is likely that with a high force magnitude more observations would be noted. Additionally, if quantitative measurements were taken, it is expected that large differences would have been recorded. Consequently, a simple design adaptation to raise and fix the test rack to the ground is essential for validation and future tests.

Movement and tilting of the top plate was observed when force was applied to the attachment points. Also, the base of the specimen stayed firmly secured to the force plate. Consequently, the tibia specimen must have deflected during testing. The angle of the top plate, which was already tilted prior to testing, was measured before each testing condition and noted to have changed over the course of experiments. The slope of the top plate changed in the x-direction between the Tibialis Anterior test and the Soleus test from 2.5˚ to 1.6˚ respectively. Figure 53 compares the changes in the slope of the top plate in the x-direction and the y-direction for both tests. As only minor forces were applied in the x-direction in the Tibialias Anterior testing, the difference in top plate movement, and hence the tibia movement, is likely attributed to the tibia shifting at its base attachment

point by twisting anti-clockwise and slightly leaning less towards the positive x-direction. Additionally, one thread was completely worn away at the base of the tibia after testing, thus corroborating that the tibia shifted and moved at the base with force application.

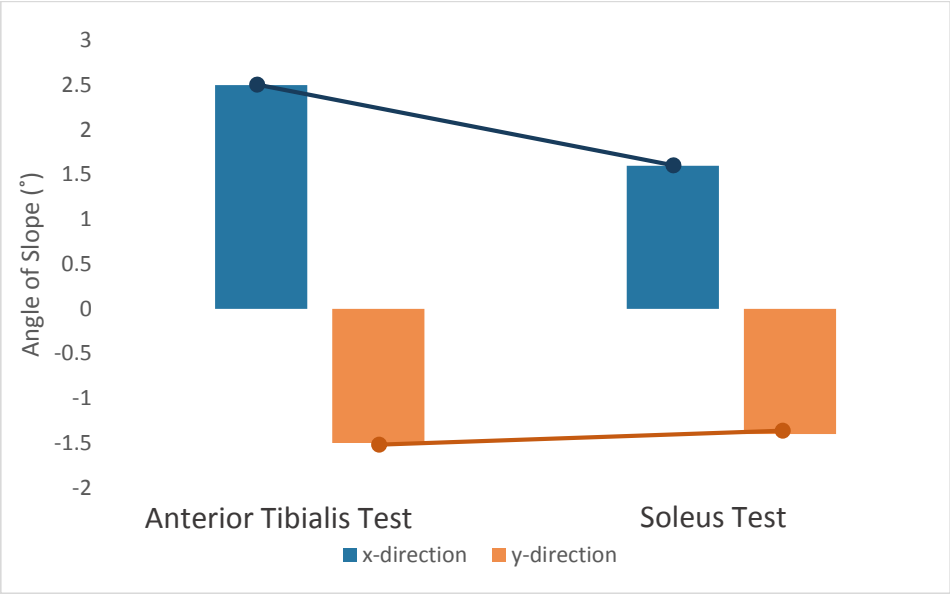

Figure 53: Comparison of slope direction between Anterior Tibialis and Soleus tests

Following the Y-Direction test, the crack obtained prior to testing propagated along the base of the tibia. As mentioned in the Results section, this shows that there was too much pressure at the base tibia attachment. Additionally, the crack suggests there was undesired movement between the specimen and bolt resulting in less than expected tibia deformation. There was also a minor indentation at the base tip of the tibia specimen, indicating that this part was touching the base plate and producing a reaction force. This not only damaged the tibia specimen, but signifies that the force distribution was incorrectly transferred through the tibia. Therefore, a new attachment mechanism is required at the base of the tibia to amend these issues.

Testing revealed that the load cells were not reading the force magnitude correctly. Ensuring that the load cells accurately measure the designated magnitude of force to the tibia is essential for further tests.

The plate holding the actuators lifted and bent when the actuators were in use. The length between the actuator lever arm and the tibia was decreasing, thus altering the total force magnitude. This bending and shortening would be expected to increase further when all four actuators are operating at the same time. Consequently, a new thicker actuator plate

with more attachment points is required. This has been designed and is provided in Appendix F.

The rope connecting the actuator to the tibia attachment did not visibly stretch or deform, which supports the specifications provided by the supplier (Appendix E2). It was essential that the ropes were secured tightly and had a relatively large preload as the actuators had a small stroke. However, the initial rope connections did have faults. Firstly, it was extremely difficult to tie a bowline knot tightly. So, at least one rope fastener was used for each rope. Yet, this also proved difficult, even with two people working cooperatively. To counteract this, a rope tightener was used to add a preload to the rope. The Tibialis Anterior test verified a rope connected with rope fasteners and a rope tightener worked effectively. Therefore, more rope tighteners should be implemented for future tests to ensure the ropes do not slacken due to knot or fasteners loosening.

A test performed outside of this thesis determined that friction between the ropes and eyebolts caused approximately 20% of forces to be lost. This signifies the importance of designing a new approach for low friction force redirection. Using pulleys, like those used for y-directional force application to the top plate, is a promising alternative option.

The top plate above the tibia specimen was very large and heavy (made from aluminium) in order to carry weights representing body forces. Like the force plate, the top tibia plate was attached in this test setup to depict the same layout as future tests. It was also needed in the Y-direction test to add lateral forces to the top of the tibia. The top plate force application design, although inexpensive and simple, is expected to cause some functional and safety issues. The weights sitting on the top plate have the potential to slide around or be positioned incorrectly, instigating unwanted moments, and they could even slide off the top plate onto the test rack below. Therefore, it is recommended to invest in an actuator that can model the body forces. Furthermore, the prior work and time required to setup the specific movements for testing will reduce with an actuator in comparison to calculating the amount of weights required and manually placing them on the top plate.

Finally, the Gecko Tape held the base plate in position. Hence, the friction of the tape was sufficient enough to prevent movement and can confidently be used in later tests.

6.3 Comparison of Design to Literature

A test rack that evaluates the effect of body movements on a model tibia bone by applying muscle forces with actuators has not been constructed prior to this thesis. As such, all individual elements of the test rack, designed to be as physiologically accurate as possible, are unique to this thesis. This section evaluates the similarities and differences of the components of the test rack to literature and physiological attributes.

6.3.1 Muscle Attachment

The muscle attachment points at the tibia were represented at one point. Anatomy of the tibia was used to predetermine these points at approximately the centre of the muscle attachment area [17]. This generated a simplistic model of the tibia and muscles. Modelling force over an area of the tibia will reduce the pressure at one particular point and result in either an equally distributed force or a high force in the centre, with force dissipating out across the area. Regarding the displacement of the bone, it is hypothesised that the changes will not be significant in the lower section of the tibia, although the middle and upper sections may experience minor changes.

Further experiments can determine the influence of the type of muscle attachment. Once the test rack is validated, the deformation at three sensor locations observed from the test rack can be compared to a computed model of the tibia with muscle areas instead of points of attachments. If the difference is insignificant, the muscle attachment at the points can be confidently used for future tests. Otherwise, analysis must be made to determine the most appropriate solution. Either the corresponding change can be calculated and later deducted from the test rack findings, or a new method for muscle attachment over an area must be designed. Key design challenges for distributed force across areas of the tibia include: not causing unwanted moments or unequal forces, a non-permanent, adjustable material that can adapt to different force magnitudes and directions, high enough properties to hold high forces and a process of attaching rope to the area. In the design phase of this thesis, sugru (FormFormForm, London, UK) [84] and glue were used to explore options of muscle attachment materials. These were not utilised in the original design as they did not address the challenges listed above. If a new design is required for muscle attachment to the tibia, it should take into consideration these numerous challenges.

6.3.2 Knee and Ankle Joints

No knee or ankle joints were incorporated into the test rack design and setup. Instead, the top of the tibia was free standing with force applied in the downwards direction, thus restricting full movement. This compares to the knee in a physiological setting, which is a modified hinge joint and is composed of a tibiofemoral and patellofemoral joint. It is supported by cartilage (menisci), tibial collateral, fibular collateral, and patella ligaments and the quadriceps tendon (Figure 54) [85]. Additionally, the tibia does have some rotation about the knee. As mentioned in the body force impact section (Section 1.2.4), this moment is minor for gait. Consequently, it was excluded for these tests. In future, positioning the weights off centre on the top tibia plate will cause a moment for the alpha test rack design. The Beta test rack design (Appendix C) does account for this movement with a one degree of freedom knee joint and a five degree of freedom hip joint.

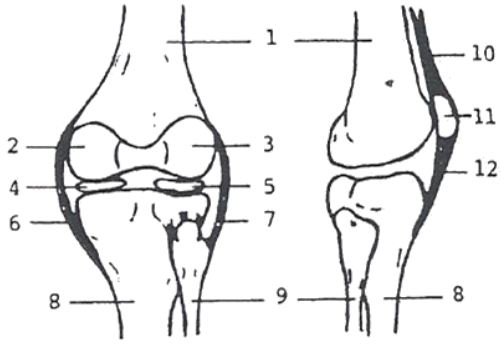

Figure 54: The posterior (left) and lateral (right) views of the knee: (1) femur, (2) medial condyle, (3) lateral condyle, (4) medial meniscus, (5) lateral meniscus, (6) tibial collateral ligament, (7) fibular collateral ligament, (8) tibia, (9) fibula, (10) quadriceps tendon, (11) patella, (12) patellar ligament [85]

The bottom of the tibia was secured to the base plate, which was secured to the force plate that was positioned on the ground. Consequently, the force plate will read forces at the ankle, not the foot. This differs to the DLR predecessor study [74], which determined the reaction forces at the foot during movements. The ankle joint is a stable hinge joint that can perform only dorsiflexion and plantar flection movements in the sagittal plane. It can also execute inversion and eversion, inward and outward rotation and pronation and supination movements [85]. The test rack simulated individual moments of a body movement with static conditions, by the foot positioned flat on the ground with the tibia upright, keeping the base of the ankle secured thus ensuring no possible movement. Including a foot in the design was considered, however due to its complexity with a large

quantity of bones, muscles and tendons, the idea was discontinued. In the future Beta test rack design, the ankle joint will have two degrees of freedom (rotation x and rotation y), with possible additional movement in the y direction to allow for dynamic movement.

6.4 Recommended Design and Setup Modifications

Many potential design modifications were highlighted in Section 6.2. These are again emphasised here along with further improvements that were noticed during the setup phase.

6.4.1 Component Design Improvements

Table 15 outlines issues observed during testing and corresponding design modifications.

Table 15: Component design modifications

Component	Issue	Recommended Design Modification
Tibia attachment distal	The current screw holding it in place cannot withstand high forces, thus causing damage to the specimen, and instigates incorrect force transfer through the bone.	A mould fitted into the base of the tibia should be designed to act like the Talus bone and attached to the force plate.
Tibia attachment proximal	Four screws are currently positioned in the grooves at the top of the tibia causing incorrect force transfer.	A mould should be made for the top of the tibia that will transfer most of the forces onto the two grooves of the tibia bone.
Load cells	The load cells read the force magnitude at approximately half the actual value.	Scaling and adequate setup equipment is required.
Rope connections	Knots loosen resulting in less force application to the tibia.	Each rope should incorporate a rope tightener in the attachment.
Force redirection	Friction between the rope and eyebolt is high, resulting in less force being applied to the tibia.	A new system should be used that eliminates or reduces friction, such as pulleys. The new design should be tested for losses prior to permanent implementation.
Downward body force	Positioning weights above the tibia top plate leads to potential safety issues and high complexity for determining the quantity and position.	Use an actuator to apply the downward body force.
Optical measuring	Currently no sensors attached.	For future optical measurements, marker clusters must be attached to the tibia via bone screws at three locations (Figure 55),

Component	Issue	Recommended Design Modification
system sensors		similar to those used in the MUST study. Differences are acceptable as the tibia specimen in not the same geometry as all the subjects in the MUST study.

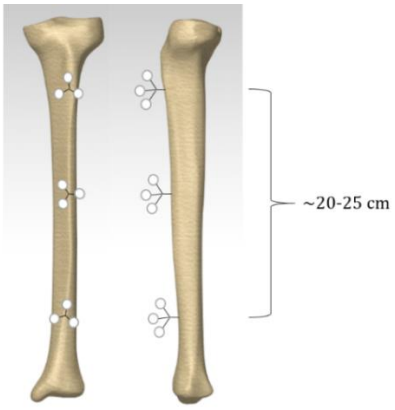

Figure 55: Approximate location of the marker clusters for the optical measuring system to detect tibia deformation; Left: front view, Right, side view

6.4.2 Construction Design and Setup Improvements

Proposed design modifications for the tibia base plate, actuator plate, specimen alignment and force plate are described in Table 16.

Table 16: Design modifications for improvements to the construction and setup of the apparatus

Component	Issue	Recommended Design Modification
Thick tibia base plate	The test rack was temporarily raised using four item profiles to allow enough space for the tibia base plate.	A permanent solution must be devised to raise and secure the test rack. One possibility is to secure an additional item beam below the small platform holding the redirection eyebolts (or later pulley system) to raise the structure above the tibia base plate (Figure 56).
Actuator plate	The actuator plate bent and vibrated when an actuator was operational.	A thicker plate has been designed and is detailed in Appendix F.
Tibia alignment	It was often difficult to accurately align the tibia with certainty.	Two lines should be drawn in cross configuration originating in the centre and expanding to the middle of each edge. These lines can align the top plate, and thus tibia, parallel with the vertical pillars.

Component	Issue	Recommended Design Modification
Force plate	As discussed in the Results section, item beams and a PVC cylinder were slotted between the force plate and the test rack's base to ensure the force plate did not slide towards the actuators.	A more permanent device should be designed and manufactured to fit into this space and prevent movement. Another recommendation is to firmly attach the force plate and test rack to a wooden plate underneath the structure.

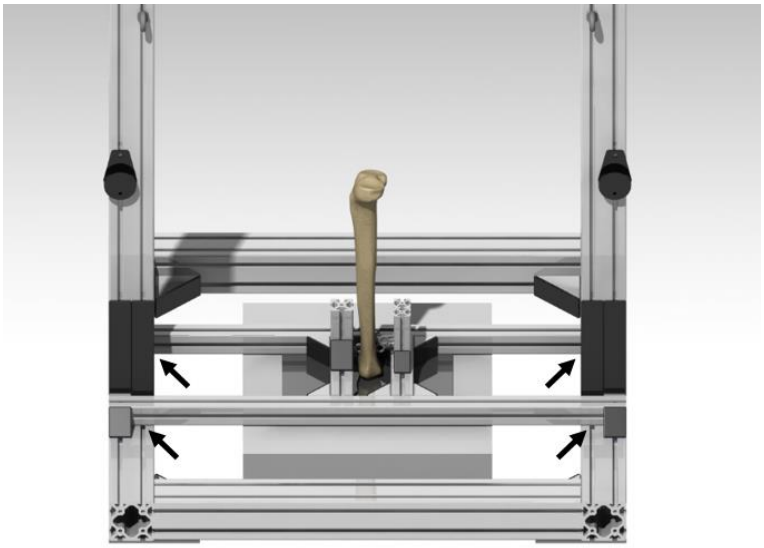

Figure 56: Secure additional item beams below the small platform (arrows) to raise the structure above the tibia base plate

6.5 Limitation of Thesis

6.5.1 Testing Conditions

Due to the time constraints and the available resources, there were several limitations to this thesis. Firstly, the test rack was not validated. No validation tests could be performed as an optical measuring system was unavailable. Nevertheless, validation would not have been completed in the time frame as numerous changes to the design of the test rack and components must be completed prior to further tests.

Another limitation to this thesis was that no quantitative results were obtained because there was no optical measuring system. Subsequently, tibia displacement obtained from the test rack could not be compared between computer models nor the predecessor DLR MUST study. Once an optical measuring system is chosen and installed, significant

advancements in understanding the test rack performance, and in obtaining experimental data, will be swiftly accomplished.

6.5.2 Component Conditions

To verify the test rack against the MUST study and computer model, so that in the future the results can be generalized and relevant across a number of conditions, only a single large tibia specimen was used. This means that the functionality experiments only observed the impact of muscle simulation on the selected large tibia specimen. Nevertheless, the test rack was designed with the capability to also handle a variety of tibia replica sizes in future studies, such as those on astronauts and osteoporosis sufferers. This is achieved through the tall pillar components, which take into consideration a range of tibia specimen sizes, such as the small and medium size replicas available from the company Sawbones.

As the pneumatic actuators have a short stroke of 10 mm, to allow for a fast response time, the test setup had to be precise. Otherwise, as a consequence of unwanted movement in the force plate, base plate, actuator plate or test rack completely, or if there is any slack rope connections, the intended force magnitude would not be transmitted to the tibia specimen. Observations from the functionality tests found that many of these irregularities previously mentioned did occur, resulting in a lower force application than expected. Actuators with larger strokes would be more appropriate for these, and future, tests to account for any variability in the setup.

6.6 Summary of Project

Overall, the test rack testing presented positive outcomes that suggest many design concepts can remain as originally proposed. The results also exposed design faults and identified specific components that did not function as expected. However, all observations and conclusions made from this project have been utilised to improve the rack and to develop new design concepts.

6.7 Future Directions

Design variations, outlined in the section above, should be made and verified for functionality. To ensure the new design alterations succeed, initially only small magnitudes of force should be applied so any minor issues can be observed and changed.

Additionally, markers must be attached to the tibia and PVC cylinder at specific locations, which correspond to the positions used in the DLR MUST study, so optical measurements can determine the deformation. The next step is to validate the test rack (Appendix I). Successful validation signifies the test rack is operating as expected and correlates with the computer model.

After the above procedure has been accomplished, tests to simulate the numerous movements predetermined from the DLR MUST study can be performed. The exercises include standing, walking, running, hopping, climbing straight and spiral stairs and performing plantar flexion and dorsiflexion. The muscle forces simulating these movements are to be obtained using the previous study's results. If required, the test rack can be extended to the proposed Beta Test Rack to include dynamic movement and knee, ankle and hip joints.

Furthermore, the results from this test rack and successive studies can be applied to determining which specific muscles produce the highest amount of bone deformation. This knowledge has the potential to create new countermeasures for space and terrestrial applications, most notably for bone atrophy experienced by long-duration astronauts, osteoporosis suffers and those with paralysis.

CHAPTER 7. CONCLUSION

A unique test rack prototype was designed, manufactured and tested. The test rack, which is the first of its kind, simulates muscles forces on a replica human tibia bone. Downward muscles forces were simulated using pneumatic actuators connected to bolts in the model tibia, which represent human tendon attachment locations.

Effective safety measures were recommended and implemented prior to and during test setup. Static load experiments were performed on the Alpha model to examine the functionality of both the mechanical components of the test rack and the anatomical structure of the model. The structural component of the test rack took into account the forces applied, high visibility and overall lower limb modelling. The lower leg model took into consideration a variety of anatomical attributes to ensure physiological accuracy. The test rack remained intact and rigid throughout the experiment. The high friction Gecko tape secured the base plate to the force plate and pneumatic actuators applied forces to the muscle attachment bolts, which stayed inside the specimen without causing damage.

A number of modifications have been recommended to overcome design limitations that were identified during the testing phase. The test rack is proposed to be extended to the Beta design version, and with implementing the design modifications, it promises an upgraded and more robust experiment setup in the future.

It is possible to perform bone deformation experiments using the test rack, which were previously only possible to model using computer simulations and cadaver specimens. Empirical data from physical models will confirm computational models, which will assist investigations into the effects of muscles on bone health conditions including bone atrophy. Increased knowledge gained from this data will allow for improvements in bone atrophy mitigation for both space and terrestrial applications. Thus, leading to increased human mission durations in space, allowing manned spaceflights further into the solar system with reduced risk to astronaut bone health, and to a lower risk of bone fractures in the general population.

REFERENCES

1. Sibonga, JD, Evans, HJ, Spector, ER, Maddocks, MJ, Smith, SA, Shackelford, LC & LeBlanc, AD 2005, *What Happens to bone health during and after spaceflight?* Available from: http://ntrs.nasa.gov/archive/nasa/casi.ntrs.nasa.gov/20060013245.pdf.

2. Lang, T. 2013, *Bone loss in long-duration spaceflight: measurements and countermeasures*. in *2nd Annual ISS Research and Development Conference*. Denver, Colorado.

3. Smith, SM, Heer, MA, Shackelford, LC, Sibonga, JD, Ploutz-Snyder, L & Zwart, SR 2012, 'Benefits for bone from resistance exercise and nutrition in long-duration spaceflight: Evidence from biochemistry and densitometry'. *Journal of Bone and Mineral Research*, vol 27(9): p. 1896-1906.

4. Sibonga, JD 2013, 'Spaceflight-induced Bone Loss: Is there an Osteoporosis Risk?'. *Current osteoporosis reports*, vol: p. 1-7.

5. Yang, P-F, Sanno, M, Ganse, B, Koy, T, Brüggemann, G-P, Müller, LP & Rittweger, J 2014, 'Torsion and Antero-Posterior Bending in the In Vivo Human Tibia Loading Regimes during Walking and Running'. *PloS one*, vol 9(4): p. e94525.

6. Ganse, B, Yang, P-F, Brüggemann, G-P, Koy, T, Rittweger, J & Müller, LP. 2013, *Deformation stimulates bone - feasibility of an innovative surgical approach for in-vivo measurements of bone deformation*. in *19th IAA Humans in Space* Cologne, Germany.

7. Cole, JH & Van der Meulen, MC 2011, 'Whole bone mechanics and bone quality'. *Clinical Orthopaedics and Related Research®*, vol 469(8): p. 2139-2149.

8. Goldstein, SA, Wilson, DL, Sonstegard, DA & Matthews, LS 1983, 'The mechanical properties of human tibial trabecular bone as a function of metaphyseal location'. *Journal of biomechanics*, vol 16(12): p. 965-969.

9. Ulrich, D, Hildebrand, T, Van Rietbergen, B, Müller, R & Rüegsegger, P 1997, 'The quality of trabecular bone evaluated with micro-computed tomography, FEA and mechanical testing'. *Studies in health technology and informatics*, vol: p. 97-112.

10. Rho, J-Y, Kuhn-Spearing, L & Zioupos, P 1998, 'Mechanical properties and the hierarchical structure of bone'. *Medical engineering & physics*, vol 20(2): p. 92-102.

11. Burr, D 2002, 'Targeted and nontargeted remodeling'. *Bone*, vol 30(1): p. 2-4.

12. Kular, J, Tickner, J, Chim, SM & Xu, J 2012, 'An overview of the regulation of bone remodelling at the cellular level'. *Clinical biochemistry*, vol 45(12): p. 863-873.

13. Heino, TJ, Kurata, K, Higaki, H & Väänänen, HK 2009, 'Evidence for the role of osteocytes in the initiation of targeted remodeling'. *Technology and Health Care*, vol 17(1): p. 49-56.

14. Graham, JM, Ayati, BP, Holstein, SA & Martin, JA 2013, 'The role of osteocytes in targeted bone remodeling: a mathematical model'. *PloS one*, vol 8(5): p. e63884.

15. Van der Linden, J, Homminga, J, Verhaar, J & Weinans, H 2001, 'Mechanical consequences of bone loss in cancellous bone'. *Journal of Bone and Mineral Research*, vol 16(3): p. 457-465.

16. Lu, Y, Xie, Y, Zhang, S, Dusevich, V, Bonewald, L & Feng, J 2007, 'DMP1-targeted Cre expression in odontoblasts and osteocytes'. *Journal of dental research*, vol 86(4): p. 320-325.

17. Drake, R, Vogl, AW & Mitchell, AW 2009, *Gray's anatomy for students*. Elsevier Health Sciences.

18. Marieb, EN & Hoehn, K 2007, *Human anatomy & physiology*. Pearson Education.

19. Sasimontonkul, S, Bay, BK & Pavol, MJ 2007, 'Bone contact forces on the distal tibia during the stance phase of running'. *Journal of biomechanics*, vol 40(15): p. 3503-3509.

20. Arnold, EM, Ward, SR, Lieber, RL & Delp, SL 2010, 'A model of the lower limb for analysis of human movement'. *Annals of biomedical engineering*, vol 38(2): p. 269-279.

21. Ward, SR, Eng, CM & Smallwood, LH 2009, 'Are current measurements of lower extremity muscle architecture accurate?'. *Clinical orthopaedics and related research*, vol 467(4): p. 1074-1082.

22. Delp, SL & Loan, JP 1995, 'A graphics-based software system to develop and analyze models of musculoskeletal structures'. *Computers in biology and medicine*, vol 25(1): p. 21-34.

23. SimTK *Enabling grounbreaking biomedical research via open access to high quality simulation tools, accurate models and the people behind them*. Available from: https://simtk.org/xml/index.xml.

24. Shackelford, LC 2008. *Musculoskeletal response to space flight*, in *Principles of clinical medicine for space flight*. Springer. p. 293-306.

25. Lau, RY-c & Guo, X 2011, 'A review on current osteoporosis research: with special focus on disuse bone loss'. *Journal of osteoporosis*, vol 2011.

26. Mosekilde, L 2000, 'Age-related changes in bone mass, structure, and strength–effects of loading'. *Zeitschrift für Rheumatologie*, vol 59(1): p. I1-I9.

27. LeBlanc, A, Spector, E, Evans, H & Sibonga, J 2007, 'Skeletal responses to space flight and the bed rest analog: a review'. *Journal of Musculoskeletal and Neuronal Interactions*, vol 7(1): p. 33.

28. Cavanagh, PR, Licata, AA & Rice, AJ 2007, 'Exercise and pharmacological countermeasures for bone loss during longduration space flight'. *Gravitational and Space Biology*, vol 18(2): p. 39-58.

29. Androjna, C, McCabe, N, Cavanagh, P & Midura, R 2012, 'Effects of Spaceflight and Skeletal Unloading on Bone Fracture Healing'. *Clinical Reviews in Bone and Mineral Metabolism*, vol 10(2): p. 61-70.

30. LeBlanc, A, Schneider, V, Shackelford, L, West, S, Oganov, V, Bakulin, A & Voronin, L 2000, 'Bone mineral and lean tissue loss after long duration space flight'. *J Musculoskelet Neuronal Interact*, vol 1(2): p. 157-60.

31. Leblanc, AD, Schneider, VS, Evans, HJ, Engelbretson, DA & Krebs, JM 1990, 'Bone mineral loss and recovery after 17 weeks of bed rest'. *Journal of Bone and Mineral Research*, vol 5(8): p. 843-850.

32. Vico, L, Collet, P, Guignandon, A, Lafage-Proust, M-H, Thomas, T, Rehailia, M & Alexandre, C 2000, 'Effects of long-term microgravity exposure on cancellous and cortical weight-bearing bones of cosmonauts'. *The Lancet*, vol 355(9215): p. 1607-1611.

33. Smith, SM, Wastney, ME, O'Brien, KO, Morukov, BV, Larina, IM, Abrams, SA, Davis-Street, JE, Oganov, V & Shackelford, LC 2005, 'Bone Markers, Calcium Metabolism, and Calcium Kinetics During Extended-Duration Space Flight on the Mir Space Station'. *Journal of Bone and Mineral Research*, vol 20(2): p. 208-218.

34. Orwoll, ES, Adler, RA, Amin, S, Binkley, N, Lewiecki, EM, Petak, SM, Shapses, SA, Sinaki, M, Watts, NB & Sibonga, JD 2013, 'Skeletal health in long-duration astronauts: Nature, assessment, and management recommendations from the NASA bone summit'. *Journal of Bone and Mineral Research*, vol 28(6): p. 1243-1255.

35. NASA 2008, *International Space Station Imagery*. NASA Human Space Flight. Available from: http://spaceflight.nasa.gov/gallery/images/station/crew-17/html/iss017e006639.html.

36. Wright, J 2013, *NASA International Space Station*. Available from: http://www.nasa.gov/content/astronaut-rick-mastracchio-with-ared/#.U4FWefmSy-V.

37. Hargens, AR, Bhattacharya, R & Schneider, SM 2012, 'Space physiology VI: exercise, artificial gravity, and countermeasure development for prolonged space flight'. *European journal of applied physiology*, vol: p. 1-10.

38. MacDougall, J, Tuxen, D, Sale, D, Moroz, J & Sutton, J 1985, 'Arterial blood pressure response to heavy resistance exercise'. *Journal of Applied Physiology*, vol 58(3): p. 785-790.

39. Goel, R, Kaderka, J & Newman, D 2012, 'Modeling the benefits of an artificial gravity countermeasure coupled with exercise and vibration'. *Acta Astronautica*, vol 70: p. 43-51.

40. LeBlanc, A, Matsumoto, T, Jones, J, Shapiro, J, Lang, T, Shackelford, L, Smith, S, Evans, H, Spector, E & Ploutz-Snyder, R 2012, 'Bisphosphonates as a supplement to exercise to protect bone during long-duration spaceflight'. *Osteoporosis international*, vol: p. 1-10.

41. Cooper, C & Melton III, LJ 1992, 'Epidemiology of osteoporosis'. *Trends in Endocrinology & Metabolism*, vol 3(6): p. 224-229.

42. Biering-Sørensen, F, Bohr, H & Schaadt, O 1988, 'Bone mineral content of the lumbar spine and lower extremities years after spinal cord lesion'. *Spinal Cord*, vol 26(5): p. 293-301.

43. Minaire, P, Meunier, P, Edouard, C, Bernard, J, Courpron, P & Bourret, J 1974, 'Quantitative histological data on disuse osteoporosis'. *Calcified tissue research*, vol 17(1): p. 57-73.

44. Biering-Sørensen, F, Bohr, H & Schaadt, O 1990, 'Longitudinal study of bone mineral content in the lumbar spine, the forearm and the lower extremities after spinal cord injury'. *European journal of clinical investigation*, vol 20(3): p. 330-335.

45. Feskanich, D, Willett, W & Colditz, G 2002, 'Walking and leisure-time activity and risk of hip fracture in postmenopausal women'. *JAMA: the journal of the American Medical Association*, vol 288(18): p. 2300-2306.

46. Chan, K, Qin, L, Lau, M, Woo, J, Au, S, Choy, W, Lee, K & Lee, S 2004, 'A randomized, prospective study of the effects of Tai Chi Chun exercise on bone mineral density in postmenopausal women'. *Archives of physical medicine and rehabilitation*, vol 85(5): p. 717-722.

47. Shackelford, L, LeBlanc, A, Driscoll, T, Evans, H, Rianon, N, Smith, S, Spector, E, Feeback, D & Lai, D 2004, 'Resistance exercise as a countermeasure to disuse-induced bone loss'. *Journal of Applied Physiology*, vol 97(1): p. 119-129.

48. Loehr, JA, Lee, S, English, KL, Sibonga, J, Smith, SM, Spiering, BA & Hagan, RD 2011, 'Musculoskeletal adaptations to training with the advanced resistive exercise device'. *Med Sci Sports Exerc*, vol 43(1): p. 146-156.

49. Rittweger, J, Beller, G, Armbrecht, G, Mulder, E, Buehring, B, Gast, U, Dimeo, F, Schubert, H, De Haan, A & Stegeman, DF 2010, 'Prevention of bone loss during 56 days of strict bed rest by side-alternating resistive vibration exercise'. *Bone*, vol 46(1): p. 137-147.

50. Currey, J 2009, 'Measurement of the Mechanical Properties of Bone: A Recent History'. *Clinical Orthopaedics and Related Research®*, vol 467: p. 1948-1954.

51. Yang, P, Bruggemann, G & Rittweger, J 2011, 'What do we currently know from in vivo bone strain measurements in humans'. *J Musculoskelet Neuronal Interact*, vol 11(1): p. 8-20.

52. Bennell, KL, Malcolm, SA, Thomas, SA, Wark, JD & Brukner, PD 1996, 'The Incidence and Distribution of Stress Fractures in Competitive Track and Field Athletes A Twelve-Month Prospective Study'. *The American Journal of Sports Medicine*, vol 24(2): p. 211-217.

53. Biewener, AA 1993, 'Safety factors in bone strength'. *Calcified tissue international*, vol 53(1): p. S68-S74.

54. Milgrom, C, Finestone, A, Simkin, A, Ekenman, I, Mendelson, S, Millgram, M, Nyska, M, Larsson, E & Burr, D 2000, 'In vivo strain measurements to evaluate the strengthening potential of exercises on the tibial bone'. *Journal of Bone & Joint Surgery, British Volume*, vol 82(4): p. 591-594.

55. Skerry, TM 2008, 'The response of bone to mechanical loading and disuse: fundamental principles and influences on osteoblast/osteocyte homeostasis'. *Archives of biochemistry and biophysics*, vol 473(2): p. 117-123.

56. Caler, WE, Carter, DR & Harris, WH 1981, 'Techniques for implementing an in vivo bone strain gage system'. *Journal of biomechanics*, vol 14(7): p. 503-507.

57. Milgrom, C, Radeva-Petrova, DR, Finestone, A, Nyska, M, Mendelson, S, Benjuya, N, Simkin, A & Burr, D 2007, 'The effect of muscle fatigue on in vivo tibial strains'. *Journal of biomechanics*, vol 40(4): p. 845-850.

58. Matsuyama, J, Ohnishi, I, Sakai, R, Suzuki, H, Harada, A, Bessho, M, Matsumoto, T & Nakamura, K 2006, 'A new method for measurement of bone deformation by echo tracking'. *Medical engineering & physics*, vol 28(6): p. 588-595.

59. Al Nazer, R, Lanovaz, J, Kawalilak, C, Johnston, J & Kontulainen, S 2012, 'Direct in vivo strain measurements in human bone—A systematic literature review'. *Journal of biomechanics*, vol 45(1): p. 27-40.

60. Smith, E & Gilligan, C 1996, 'Dose-response relationship between physical loading and mechanical competence of bone'. *Bone*, vol 18(1): p. S45-S50.

61. Yang, P-F, Sanno, M, Brüggemann, G-P & Rittweger, J 2012, 'Evaluation of the performance of a motion capture system for small displacement recording and a discussion for its application potential in bone deformation in vivo measurements'. *Proceedings of the Institution of Mechanical Engineers, Part H: Journal of Engineering in Medicine*, vol 226(11): p. 838-847.

62. Ganse, B, Yang, P, Brüggemann, G, Müller, L, Rittweger, J & Koy, T 2014, 'In vivo measurements of human bone deformation using optical segment tracking:

surgical approach and validation in a three-point bending test'. *J Musculoskelet Neuronal Interact*, vol 14(1): p. 95-103.

63. Rittweger, J, Beller, G, Ehrig, J, Jung, C, Koch, U, Ramolla, J, Schmidt, F, Newitt, D, Majumdar, S & Schiessl, H 2000, 'Bone-muscle strength indices for the human lower leg'. *Bone*, vol 27(2): p. 319-326.

64. Bay, BK, Smith, TS, Fyhrie, DP & Saad, M 1999, 'Digital volume correlation: three-dimensional strain mapping using X-ray tomography'. *Experimental Mechanics*, vol 39(3): p. 217-226.

65. Richmond, BG, Wright, BW, Grosse, I, Dechow, PC, Ross, CF, Spencer, MA & Strait, DS 2005, 'Finite element analysis in functional morphology'. *The Anatomical Record Part A: Discoveries in Molecular, Cellular, and Evolutionary Biology*, vol 283(2): p. 259-274.

66. Mackerle, J 1995, 'Some remarks on progress with finite elements'. *Computers & structures*, vol 55(6): p. 1101-1106.

67. Wehner, T, Claes, L & Simon, U 2009, 'Internal loads in the human tibia during gait'. *Clinical Biomechanics*, vol 24(3): p. 299-302.

68. Becher, C, Huber, R, Thermann, H, Paessler, HH & Skrbensky, G 2008, 'Effects of a contoured articular prosthetic device on tibiofemoral peak contact pressure: a biomechanical study'. *Knee Surgery, Sports Traumatology, Arthroscopy*, vol 16(1): p. 56-63.

69. Maletsky, LP & Hillberry, BM 2005, 'Simulating dynamic activities using a five-axis knee simulator'. *Journal of biomechanical engineering*, vol 127(1): p. 123-133.

70. Sharkey, NA & Hamel, AJ 1998, 'A dynamic cadaver model of the stance phase of gait: performance characteristics and kinetic validation'. *Clinical Biomechanics*, vol 13(6): p. 420-433.

71. Mueller, O, Lo, J, Wünschel, M, Obloh, C & Wuelker, N 2009, 'Simulation of force loaded knee movement in a newly developed in vitro knee simulator/Simulation von belastungsabhängigen Kniebewegungen in einem neuartigen Knie-Simulator für In-vitro-Studien'. *Biomedizinische Technik/Biomedical Engineering*, vol 54(3): p. 142-149.

72. Wünschel, M, Leichtle, U, Obloh, C, Wülker, N & Müller, O 2011, 'The effect of different quadriceps loading patterns on tibiofemoral joint kinematics and patellofemoral contact pressure during simulated partial weight-bearing knee flexion'. *Knee Surgery, Sports Traumatology, Arthroscopy*, vol 19(7): p. 1099-1106.

73. Ramappa, AJ, Apreleva, M, Harrold, FR, Fitzgibbons, PG, Wilson, DR & Gill, TJ 2006, 'The effects of medialization and anteromedialization of the tibial tubercle

on patellofemoral mechanics and kinematics'. *The American journal of sports medicine*, vol 34(5): p. 749-756.

74. Yang, P-F, Sanno, M, Ganse, B, Koy, T, Brüggemann, G-P, Müller, LP & Rittweger, J, *Bending and torsion predominate the in vivo human tibia deformation regimes during walking and running.* 'Awaiting publication'

75. Hamner, S 2008, *Gait 2392 Max Isometric Muscle Force*. Available from: http://simtk-confluence.stanford.edu:8080/display/OpenSim24/Gait+2392+Max+Isometric+Muscle+Force.

76. Lieberman, DE, Venkadesan, M, Werbel, WA, Daoud, AI, D'Andrea, S, Davis, IS, Mang'Eni, RO & Pitsiladis, Y 2010, 'Foot strike patterns and collision forces in habitually barefoot versus shod runners'. *Nature*, vol 463(7280): p. 531-535.

77. Orthoload *Knee joint; Walking: in Treadmill; Velocity: 3 km/h; K8:, 34 Months PO,* in Orthoload Database. Online database available from: http://www.orthoload.com/?page_id=7.

78. Thorpe, SK, Li, Y, Crompton, RH & Alexander, RM 1998, 'Stresses in human leg muscles in running and jumping determined by force plate analysis and from published magnetic resonance images'. *The Journal of experimental biology*, vol 201(1): p. 63-70.

79. Martin, D, Medri, M, Chow, R, Oxorn, V, Leekam, R, Agur, A & McKee, N 2001, 'Comparing human skeletal muscle architectural parameters of cadavers with in vivo ultrasonographic measurements'. *Journal of anatomy*, vol 199(4): p. 429-434.

80. Sawbones 2013, *Tibia Fourth Generation*. Available from: http://www.sawbones.com/Catalog/Biomechanical/Composite%20Bones/3402.

81. Festo 2013, *Compact cylinders ADVU/AEVUZ Technical Data,* in Compact cylinders ADVU/AEVU. pg 38. Available from: http://www.festo.com/cat/en-us_us/data/doc_enus/PDF/US/ADVU_ENUS.PDF.

82. Festo 2013, *Compact cylinders ADVU/AEVU Accessories,* in Compact cylinders ADVU/AEVU. pg 55. Available from: http://www.festo.com/cat/en-us_us/data/doc_enus/PDF/US/ADVU_ENUS.PDF.

83. Festo *Rod eyes SGS,* in Piston rod attachments. pg 4. Available from: http://ftp.festo.com/Public/PNEUMATIC/SOFTWARE_SERVICE/PDF_Catalogue/PDF/US/PISTON-ROD-ATTACHMENTS_ENUS.PDF.

84. FormFormForm 2014, *sugru*. Available from: http://sugru.com/.

85. Özkaya, N, Nordin, M, Goldsheyder, D & Leger, D 2012, *Fundamentals of biomechanics: equilibrium, motion, and deformation*. Springer.

86. Anderson, FC & Pandy, MG 1999, 'A dynamic optimization solution for vertical jumping in three dimensions'. *Computer Methods in Biomechanics and Biomedical Engineering*, vol 2(3): p. 201-231.

87. Yamaguchi, G, *Dynamic Modelling of Musculoskeletal Motion: A Vectorized Approach for Biomechanical Analysis in Three Dimensions*. 2001, Kluwer Academic Publishers.

88. Delp, SL, *Surgery simulation: a computer graphics system to analyze and design musculoskeletal reconstructions of the lower limb*. 1990, Stanford University.

89. *item*. Available from: http://www.item24.de/en.html.

90. *Performance,* in FSE Robline World Class Yachting Ropes. pg 30. Available from: http://www.robship.se/wp-content/uploads/pdf/Katalog_2014_Web_SWE.pdf.

91. *segelservice.com*. Available from: http://www.segelservice.com/FSE-Festmacher-Ankerleine-RIO-8mm.html.

92. 2014, *Bowline Knot*. Animated Knots by Grog. Available from: http://www.animatedknots.com/bowline/.

93. 2010, *OR6-6-2000 Specifications*. AMTI Force and Motion. Available from: http://www.amti.biz/AMTIpibrowser.aspx?__VIEWSTATE=%2FwEPDwULLTE0NzQ1NDQ3OTNkZA%3D%3D&iListbox1=350&iListbox2=397&iListbox3=OR6-6&iUnits=&iNewpageURL=&iScrollTop=0&iScrollTop2=0&iScrollTop3=533&iArrImage_URL=.%2FImage%2520file%2Fprogress_1.gif%2C.%2FImage%2520file%2Fprogress_2.gif%2C.%2FImage%2520file%2Fprogress_3.gif%2C.%2FImage%2520file%2Fprogress_4.gif%2C.%2FImage%2520file%2Fprogress_5.gif%2C.%2FImage%2520file%2Fprogress_6.gif%2C.%2FImage%2520file%2Fprogress_7.gif%2C.%2FImage%2520file%2Fprogress_8.gif%2C.

94. 2014, *57 mm Cheek Block*. Harken. Available from: http://www.harken.com/productdetail.aspx?id=4725&taxid=418.

95. burster *Model 8523 Model 8531,* in Tension-Compression Load Cells. pg 2. Available from: http://www.burster.com/fileadmin/Documents/Products/Data_Sheets/Section_8/8523_EN.pdf.

APPENDICES

Appendix A: Design Specification List

Table 17 illustrates the Alpha rack design solutions for the specified component requirement.

Table 17: Alpha test rack specifications and design solutions

Component	Specification	Solution
	Attachment of tibia/mounting	
Proximal Fixture	Proximal tibia movable, similar to physiology.	Large plate secured to a small plate that is fixed to the proximal tibia via four M8 bolts so that weights can be stacked on top of the plate. The small plate between the top plate and tibia allows for fast disassembly.
Distal Fixture and Mounting	Distal tibia head firmly fixed to prevent any movement or rotation. May be positioned on a force plate. Mechanical decoupling of tibia fixation and any downward pulling force sources.	Distal tibia fixed to base plate with one M12 bolt as modelling a particular part of body movement under static conditions. Thick base plate to ensure the high loads do not cause it to bend. Gecko tape used to secure base plate to force plate. The tibia is facing the left and is positioned just forward of centre, in line with the pulleys positioned on the front edge of the pillars.

Component	Specification	Solution
	Forces/Control	
Forces and muscles	Four downward forces, modelling the muscles Soleus, Tibialis Posterior, Tibialis Anterior and Flexor Digitorium Longus, applied using pneumatic actuators. Orientation of muscle force vectors close to anatomical orientations. Magnitude of force in range zero to maximum isometric force of each muscle. Speed and force with respect to time behaviour close to physiological conditions.	Actuators (Festo, Compact Cylinder AEVU/AEVUZ, piston side: 100mm, 80mm, 50mm, 32mm) with 4000N, 2733N, 999N and 382N max force, respectively and a small stroke (10 mm). The downward body weight force for body movements applied with weights stacked onto tibia top plate. Force can be applied to the top of the tibia in the y-direction with a rope tied around the top plate and fed through a pulley positioned on the front of the test rack. The other end of the rope has a weight secured to it and is slowly released. Force plate used to position weights and ensure no unwanted moments. Actuators controlled using solenoid valves and control system. Rope (FSE Coppa 3000 Dyneema, 6 mm) with high maximum load (17 kN) and low elasticity to transmit force from actuator to tibia specimen. Ropes secured using bowline knots, rope fasteners and rope tighteners with a preload as the actuator stroke is small and do not want a decrease in force.

Component	Specification	Solution
Tendon	Force transfer to one point on tibia for each muscle to replicate tendon attachment.	One M8 bolt positioned in the centre of tendon area for each muscle to act as the muscle attachment to the tibia.
User Interface	Test rack setup is simple.	Test rack setup can be found in Section 4.1.
Control System	Actuator vibration caused by stroke should not affect tibia deformation. Easily regulated pneumatic control system.	Actuators on same structure but different platform to tibia. Platform thick with nine attachment points to hold the strong forces. Pneumatic control system on a completely separate structure so it can be easily regulated.
	Specimen	
Type of bone	Validation using simple structure with known mechanical properties that is straightforward to model on a computer and has known mechanical properties. Tibia bone replica that is physiologically similar to bone.	Validation using a PVC cylinder Using a tibia bone specimen (SawBone, Composite Bone, Fourth Generation, Size: Large) that has known mechanical properties similar to actual bone
Number of joints	No joints	Tibia firmly fixed to base and not mechanism above tibia to model knee or upper leg
	Optical Measuring System	
Axis and Accuracy	High accuracy and can measure displacement along the x, y and z axis.	Vicon system Cluster markers attached to the tibia specimen for the Vicon system to read the displacement in three locations similar to the MUST study.

Component	Specification	Solution
	Mechanism for optical measuring system to detect bone deformation.	
Visibility	The optical measuring system requires high visibility.	The test rack is designed with only two structural pillars.
	Force Measurement System	
Reaction Force	Measure forces and moments along the x, y and z axis.	Force plate (AMTI OR-6-6-2000) to measure the reaction force at the ankle. Can read forces and moments up to 8896 N (Fz), 4448 N (Fx and Fy), 2258 Nm (Mx, My) and 1129 Nm (Mz)
Muscle Force	Mechanical load cells to measure actuator force.	Mechanical load cells (Burster, models 8531-2000 and 8531-5000) are setup in the rope connection to measure the actuator forces. These are connected to the computer software LabView to read the measurements.
	Test Rack	
Support Structure	Allow for various size elements. Be able to withstand the high forces applied to it	Adjustable height with 1.5 m pillars to allow for more elements to be attached above and below the tibia specimen. Structural components (item) of the test rack constructed with thick beams (80x80 mm) and large brackets (160x160mm).
Safety	Implementations to prevent injury in case of malfunction.	Automatic stop button for the pneumatic system to prevent air flow to the entire system in case of an emergency. Safety glass to prevent any materials from the test rack flying around and

Component	Specification	Solution
		hurting people whilst the actuators are functioning. Rope (FSE Rio white, 8mm) fed through top plate and eyebolts positioned on pillars to prevent weight and plates falling and causing damage to the experimental apparatus.
Whole Test Rack	Simple disassembly. Cost kept at minimum.	All components secured with bolts. No items are welded or permanently fastened together. Reduced cost by, when applicable, using equipment and materials already at DLR.

Appendix B: Isometric Forces of the Lower Leg

The isometric forces of the muscles in the lower leg, used to select the size of actuators and load cells for the test rack, were taken from Gait2392 data (Table 18). This information was developed by OpenSim (Standford University, CA, USA). The Gait2392 maximum isometric forces were scaled, using the method of "strength scaling" [86, 87], from the isometric forces determine by Delp [88] from cadaver muscle cross-sections, which can be relatively.

Table 18: Isometric forces of the muscles in the lower leg; yellow: modelled upward forces, green: modelled downward force. Adapted from [75]

Joint / Type		Muscle	Gait2392, max isometric force (N)	Delp, max isometric force (N)	Scale factor
HIP/ KNEE	h_flex, k_ext	rect_fem	1169	780	1.50
	h_flex, h_add, k_flex	gracilis	162	110	1.47
	h_flex, h_abd, k_flex	sartorius	156	105	1.49
	h_flex, h_abd, h_inrot	tfl	233	155	1.50
	h_ext, h_add, k_flex	semimem	1288	1030	1.25
	h_ext, h_add, k_flex	semiten	410	330	1.24
	h_ext, h_add, k_flex	bi_fem_lh	896	720	1.24
KNEE	ext	vast_med	1294	1295	1.00
	ext	vast_int	1365	1235	1.11
	ext	vast_lat	1871	1870	1.00
	flex	bi_fem_sh	804	400	2.01
KNEE/ ANKLE	k_flex, a_pf	med_gas	1558	1115	1.40
	k_flex, a_pf	lat_gas	683	490	1.39
ANKLE	pf, ev	per_brev	435	350	1.24
	pf, ev	per_long	943	755	1.25
	pf	soleus	3549	2830	1.25
	pf, inv	tib_post	1588	1270	1.25
	pf, inv	fl_dig_long	310	310	1.00
	pf, inv	fl_hal_long	322	320	1.01
	df, inv	tib_ant	905	600	1.51
	df, ev	ext_dig_long	512	340	1.51
	df, inv	ext_hal_long	162	110	1.47
	df, ev	per_tert	180	90	2.00

Appendix C: Beta Rack Specifications

The Beta Test Rack, an advanced proposed design, aims to achieve dynamic movements across a vast range of motion. It is higher cost and larger construction times than the Alpha test rack. Table 19 summaries the specifications for the Beta Test Rack.

Table 19: Beta Test Rack Specifications

Component	Specification
Movement	Dynamic. Static (optional).
Joints	Ankle joint – 2 degrees of freedom (rot x, rot y). Knee joint – 1 degree of freedom (rot x). Hip joint – 5 degrees of freedom (rot x, rot y, rot z, move x, mov z).
Joint positioning	Ankle joint attached between tibia specimen and force plate, with the joint is fixed to the force plate with Gecko Tape. Knee joint between proximal tibia and 'green box' – where actuators modelling upward forces are held.
Forces	Downward muscles implemented using pneumatic actuators. Upward muscles implemented using air muscles. Leg motion and possibly downward force applied using linear actuator attached to the top plate and base. Patella modelled with a pulley.
Structure	Two pillars to allow for stability, high visibility and potential movement along an axis via a pulley system. The same structure from the Alpha rack can be used for the Beta design.
Additional design possibilities	Incorporate a gastrocnemius muscle, a compressive force, using air muscle attachment to the bottom plate and 'green box'. Have the force plate, downward pulleys and ankle joint move along a sliding mechanism at the base (mov y)

Appendix D: List of Products

D1. Structural Components

All but one of the structural components of the test rack were purchased from item (item Industrietechnik GmbH, Solingen, Germany) (Table 20). Further information on the specific components can be found on the item webpage [89].

Table 20: List of structural components of the test rack

Component description	Position in test rack	Article number	Quantity	Additional information	Material
Profile 8, 80x80 (mm) beams	Front and back base beams and top beam for between pillars	0.0.026.03	3	Length: 750 mm	Al, anodised
Profile 8, 80x80 (mm) beams	Left and right base beam	0.0.026.03	2	Length: 910 mm	Al, anodised
Profile 8, 80x80 (mm) beams	Two vertical pillars	0.0.026.03	2	Length: 1500 mm	Al, anodised
Profile 8, 40x40 (mm) beams	Small structure above force plate	0.0.026.27	2	Length: 910 mm	Al, anodised
Profile 8, 40x40 (mm) beams	Small structure above force plate	0.0.026.27	2	Length: 200 mm	Al, anodised
Profile 8, 40x40 (mm) beam	Holds Tibialis Anterior redirection eyebolt	0.0.026.27	1	Length: 100 mm	Al, anodised
Profile 6 30x30 (mm) beams	Holds the other three redirection eyebolts	0.0.419.01	2	Length: 100 mm	Al, anodised
Angle Bracket 8 160 x 160 (mm)	Brackets positioned between two vertical pillars and top beam	0.0.602.36	2	With accessory 0.0.479.96	Die-cast Al

Component description	Position in test rack	Article number	Quantity	Additional information	Material
Angle Bracket Set 8 160 x 80 (mm)	Attachment pillars and base structure, front base	0.0.436.24	4		Zn
Angle Bracket Set 8 80 x 80 (mm)	Connection between four base beams	0.0.411.32	4		Zn
Angle Bracket Set 8 40 x 40 (mm)	Connection for small beams and to base structure	0.0.411.15	16		Zn
Angle Bracket Set 6 30 x 30 (mm)	Attachment of small beams holding redirection bolts to supporting structure	0.0.419.67	2		Zn
Custom designed, manufactured at DLR	Further support to secure the base beams	(Not item)	4	Catia drawing: Base bracket	St

D2. Support Components

Various components were designed for specific purposes (Table 21). They were designed on Catia (Appendix F) and were manufacture by the Institute of Aerospace Medicine workshop, DLR.

Table 21: List of custom designed support components of the test rack

Component description	Purpose	Reference (Catia Drawing)
Actuator platform	Secure actuators to this plate and align with redirection eyebolts.	Actuator Platform (Original)
Plate between actuator plate and base beam	Actuators raised to the same level as the redirection eyebolts	Plate to Raise the Actuator Platform
Recommended actuator plate	A new plate design, manufactured after this thesis. It is thicker and with more attachment points to prevent from unwanted movement	Actuator Plate (New Version)
Initial tibia base plate	A fixture for the distal tibia to the force plate.	Base Tibia Plate (Original)
Tibia base plate used in testing	The plate was adjusted prior to testing so bending would occur.	Base Tibia Plate (New)

Component description	Purpose	Reference (Catia Drawing)
Tibia top plate	Thick, heavy plate secured to the proximal tibia to support weights modelling body forces.	Top Plate
Tibia top plate attachment	Positioned between the top plate and tibia specimen.	Top Plate Attachment

D3. Devices Used

Devices applied forces to the tibia specimen, read those forces and recorded the reaction force at the base of the tibia (Table 22).

Table 22: List of devices used in the test rack

Component description	Purpose	Model	Brand
Actuator	Model the Soleus muscle.	Compact Cylinder AEVU/AEVUZ Piston size: 100 mm	Festo
	Model the Tibialis Posterior muscle.	Compact Cylinder AEVU/AEVUZ Piston size: 80 mm	Festo
	Model the Tibialis Anterior muscle.	Compact Cylinder AEVU/AEVUZ Piston size: 50 mm	Festo
	Model the Flexor Digitorum Longus muscle.	Compact Cylinder AEVU/AEVUZ Piston size: 32 mm	Festo
Load cell	Measure the forces transmitted by actuators.	3 x 8531-2000 1 x 8531-5000	burster
Force plate	Measure forces and moments at the base of the tibia along three axes.	OR-6-6-2000	AMTI

D4. Additional Components

Table 23 lists other components were used when in the setup of the test rack. The PVC cylinder and Gecko Tape were already property of DLR, and hence the brand is not known. Bolts and eyebolts were purchased from Bauhaus (Bauhaus, Zug, Switzerland), with only the size specified.

Table 23: List of other components used in the test rack

Component description	Purpose	Model	Brand
Tibia specimen	Resemble a tibia bone, experience forces and deform accordingly	Fourth generation, large sized	Sawbones
PVC cylinder	Manipulated in the Initial Test, use in the validation test	Known mechanical properties	N/A
Bolts inserted in the specimen	Bolts to attach the top plate, base plate and muscle attachment to the tibia	Top plate: 4 x M8 Base plate: 1 x M12 Muscle attachment points: 4 x M8	Bauhaus
Gecko Tape	Fix the tibia base plate to the force plate	N/A	N/A
Actuator rope	Connection between actuator and tibia specimen	Coppa 3000 Dyneema, 6mm	FSE
Safety rope	Prevents top plate from falling	Rio white, 8mm	FSE
Large eyebolts	Provide attachment points on the pillars for safety rope	4 x M8	Bauhaus
Pulley	Redirect forces applied to the top plate	Carbo AirBlock, 57 mm Cheek Block	Harken
Eyebolts with bolt attachment	Redirection mechanism for muscle forces	4 x M6	Bauhaus

An overview of the various nuts, bolts and washers are not included in this thesis. Many structural components purchased come with appropriate bolts and washes. In general, the profile 8 item beams and brackets used M8 sized bolts and profile 6 used M6 bolts. The components that were specifically designed and manufactured for the current setup were attached to the test rack using corresponding buts, bolts and washers purchased from Bauhaus.

D5 Safety Shielding Components

The components used for the safety shielding were purchased from item and are listed in Table 24. The holes were cut into the safety glass in the Institute of Aerospace Medicine workshop. Appendix F has engineering drawings of the safety shielding assembly and safety glass component

Table 24: Safety shielding components

Component description	Position in test rack	Article number	Quantity	Additional information	Material
Safety Glass	Protection safety shielding	0.0.428.23	1	Dimension: 1500x1500x 5 mm	Poly-carbonate
Profile 8, 40x40 (mm) beams	Two vertical support pillars	0.0.026.27	2	Length: 1500 mm	Al, anodised
Profile 8, 40x40 (mm) beams	Two base support beams	0.0.026.03	2	Length: 500 mm	Al, anodised
Angle Bracket Set 8 40 x 40 (mm)	Connection between pillars and base	0.0.411.15	2		Zn

Appendix E: Specifications of Purchased Components

E1. Tibia Specimen

The tibia specimen was purchased from Sawbones (Pacific Research Laboratories, WA, USA), who is a worldwide leader in orthopaedic and medical models. The fourth generation, large sized tibia was used [80]. Mechanical properties of the specimen are listed in Table 25 and Table 26.

Table 25: Simulated cortical bone (short fibre filled epoxy)

Density	**Longitudinal Tensile**		**Compressive**	
	Strength	Modulus	Strength	Modulus
g/cc	MPa	GPa	MPa	GPa
1.64	106	16.0	157	16.7
Density	**Transverse Tensile**			
	Strength	Modulus		
g/cc	MPa	GPa		
1.64	93	10.0		

Table 26: Simulated cancellous bone (rigid polyurethane bone)

		Compressive	
	Density	Strength	Modulus
	g/cc	GPa	MPa
Solid	0.27	6.0	155
Cellular	0.32	5.4	137

E2. Actuator Rope

The ropes used in this test rack were purchased from a sailing store in Cologne, Germany.

Table 27: Actuator rope specifications [90]

Parameter	Specification
Rope type	FSE Coppa 3000 Dyneema
Diameter	6 mm
Maximum breaking load	17 kN
Material	Dyneema with polyester surroundings

Figure 57: Actuator rope, layouts of material [90]

E3. Safety Rope

The safety rope was required to have some stretch properties so that if the top plate tilted or the tibia specimen broke, and the safety rope came into plate, the test rack would not experience an abrupt jolt.

Table 28: Safety rope parameters [91]

Parameter	Specification
Rope type	FSE Rio white
Diameter	8 mm
Maximum breaking load	14 kN
Material	Polyester

E4. Bowline Knot

The bowline knot was used to secure the safety rope to the top plate, connect the rope to the muscle attachment bolts and connect one end of the rope to the top plate for the y-direction test. It was selected as, when tied firmly, it is not expected to slip or bind. The steps for tying a bowline knots are below (Figure 58).

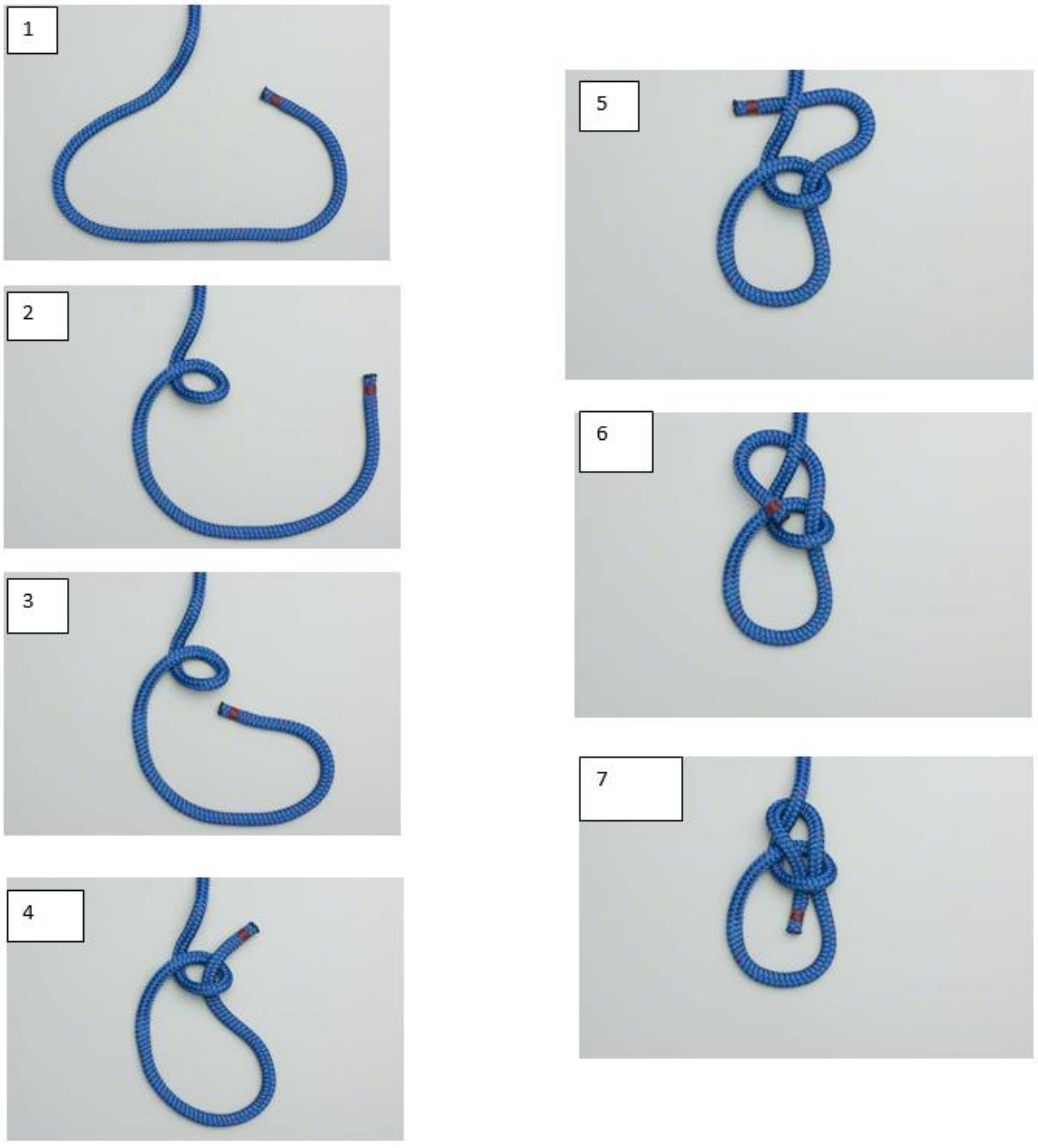

Figure 58: Steps to tie a bowline knot [92]

E5. Force Plate

The AMTI OR-6-6-2000 force plate (Advanced Mechanical Testing, Inc., MA, USA) (Table 29) was selected as it was capable of measuring forces and moments along three axis with the maximum capacity above the maximum isometric force (Table 30). The dimensions of the force plate are shown in Figure 59.

Table 29: AMTI OR-6-6-2000 Force Plate specifications [93]

Specifications	
Dimensions (WxLxH)	464 x 508 x 83 mm
Weight	18.18 kg
Channels	Fx, Fy, Fz, Mx, My, Mz
Top plate material	Composite
Temperature range	-17.78 to 51.67°C
Excitation	10V maximum
Fx, Fy, Fz hysteresis	± 0.2% full scale output
Mounting hardware	Recommended
Sensing elements	Strain gage bridge
Amplifier	Required
Analog outputs	6 Channels
Digital outputs	None
Crosstalk	< 2% on all channels
Fx, Fy, Fz non-linearity	± 0.2% full scale output

Table 30: AMTI OR6-6-2000 Force Plate Capacity, Sensitivity and Frequency [93]

Channel	Fx	Fy	Fz	Units	Mx	My	Mz
Capacity (N-m)	4448	4448	8896	N	2258	2258	1129
Sensitivity (µv/v-N-m)	0.337	0.337	0.0843	µv/v-N	0.797	0.797	1.68
Natural frequency (Hz)	550	550	1000	Hz	-	-	-

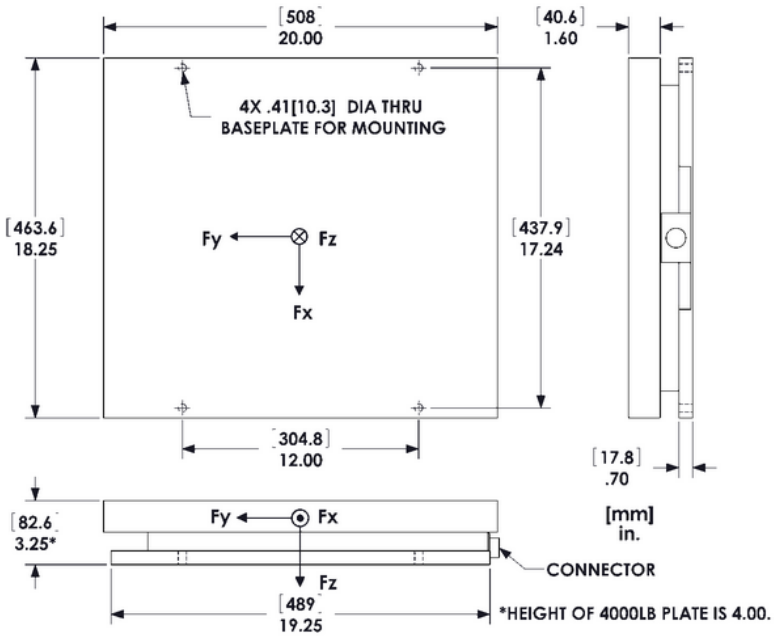

Figure 59: AMTI OR6-6-2000 Dimensions [93]

E6. Pulley

Two pulleys are attached to the front side of the test rack's vertical pillars. They have low friction, are lightweight and strong. These were, like the ropes, purchased from a sailing store in Cologne, Germany.

Table 31: Harken Pulley Specifications [94]

Parameter	Specification
Pulley type	Harken Carbo AirBlocks, 57 mm Cheek Block
Sheave diameter	57 mm
Maximum line diameter	10 mm
Maximum working load	359 kg
Breaking load	1079 kg
Weight	68 g

Figure 60: Harken 57 mm Cheek Block [94]

Appendix F: Test Rack Engineering Designs

The following pages include the engineering drawings of the assembly, including the test rack structural shell, plate alignment and re-direction mechanism positioning. The engineering drawings of individual components design for specific purposes of this study are presented: base brackets, tibia base plates 'original' (used in Initial Test setup) and 'new' (used in other three tests), top plate, top plate attachment (positioned between the top plate and tibia specimen) and actuator platforms: 'original' (used in all tests) with a corresponding plate below to raise the platform by 5mm, and 'new' (manufactured after this project). The 'original' actuator platform material was reused from DLR, hence it came with some extra holes and cut-outs that are not required for stabilisation or fixing the actuators. The assembly drawing of the safety shielding and the component drawing of the safety glass are presented.

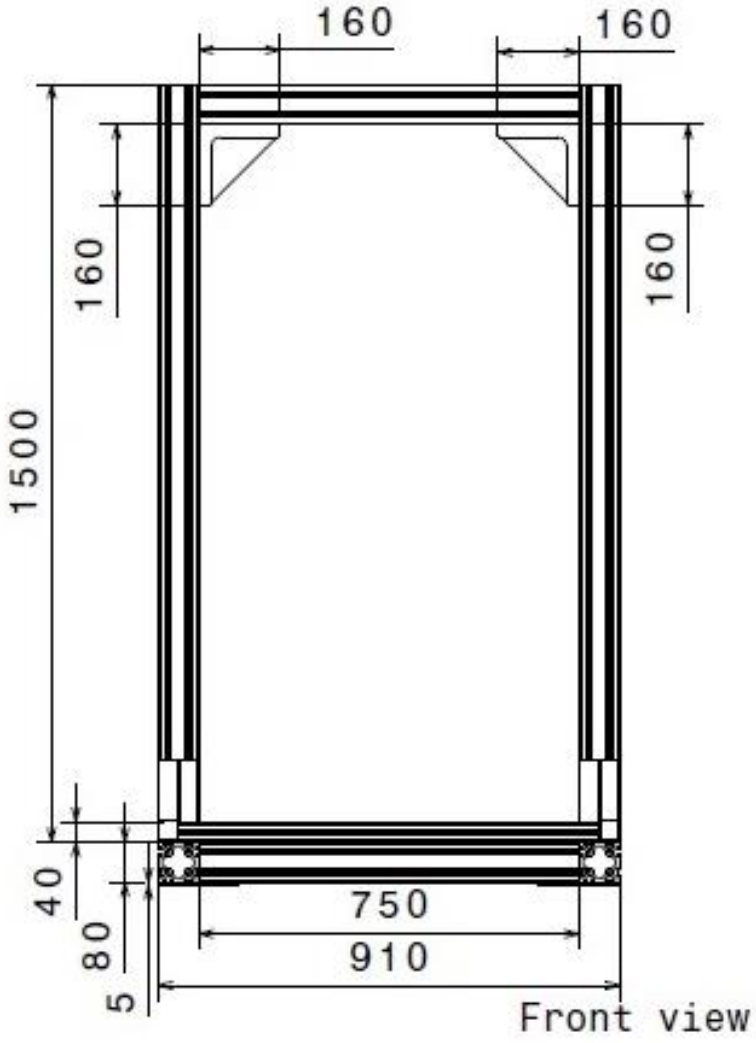

Front view

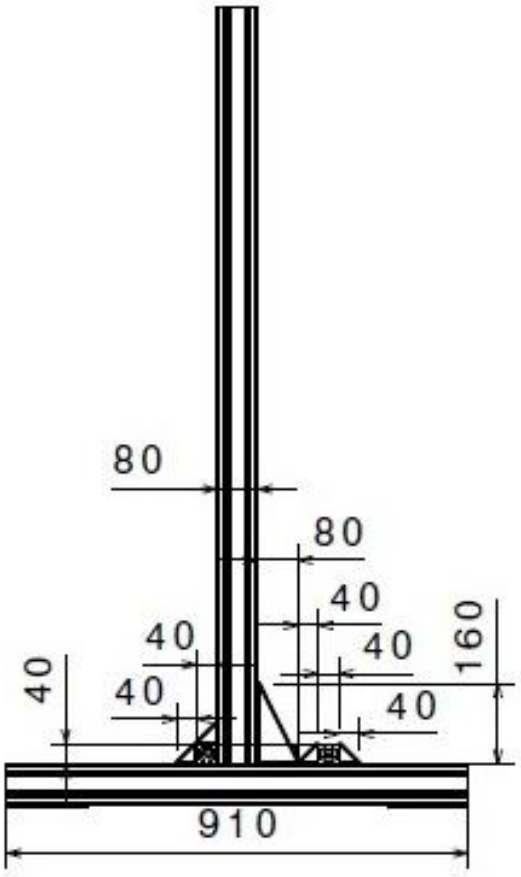

Left view

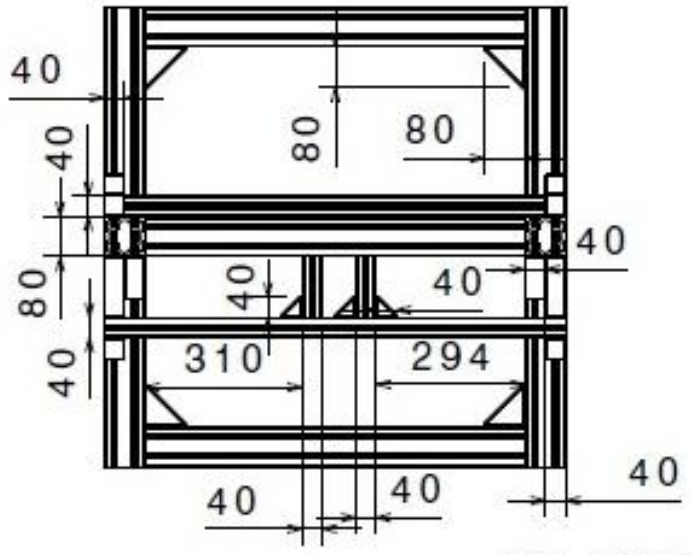

Top view

TITLE: Test Rack Shell	DRAWN BY: Natalie Bennell	DATE: 15/12/2013
Assembly Dimensions	PRODUCTS: item	SCALE: 1:15
	SHEET: 1 OF 1	UNITS: mm

DLR

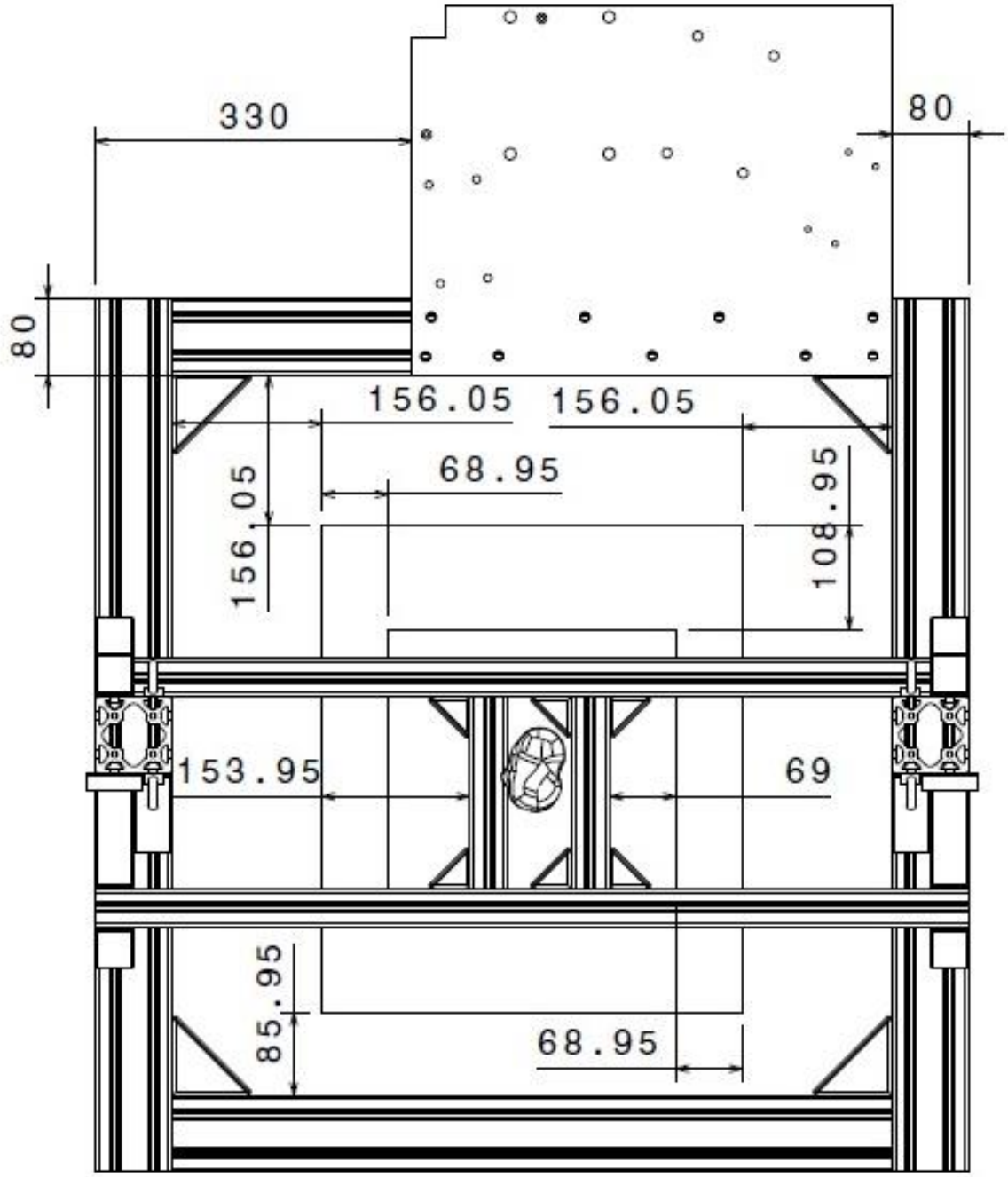

Top view

TITLE: Force, Base and Actuator Plate Positioning	DRAWN BY: Natalie Bennell	DATE: 10/01/2014
Assembly Dimensions	PRODUCTS: item, AMTI, Sawbone	SCALE: 1:7
	SHEET: 1 OF 1	UNITS: mm

DLR

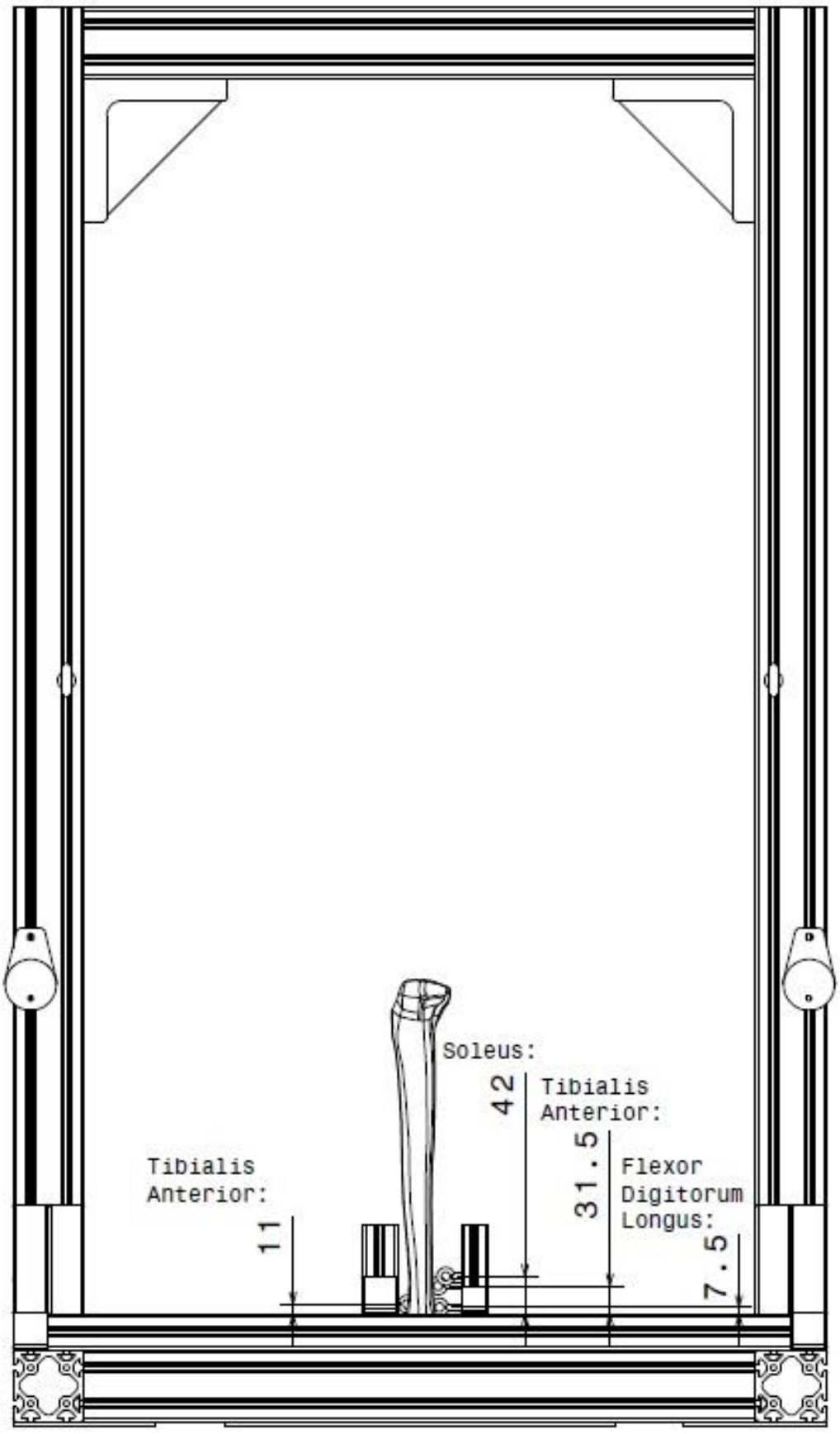

Front view

TITLE: Eyebolt Positioning	DRAWN BY: Natalie Bennell	DATE: 10/01/2014
Assembly Dimensions	PRODUCTS: item, Sawbone	SCALE: 1:7
	SHEET: 1 OF 1	UNITS: mm

DLR

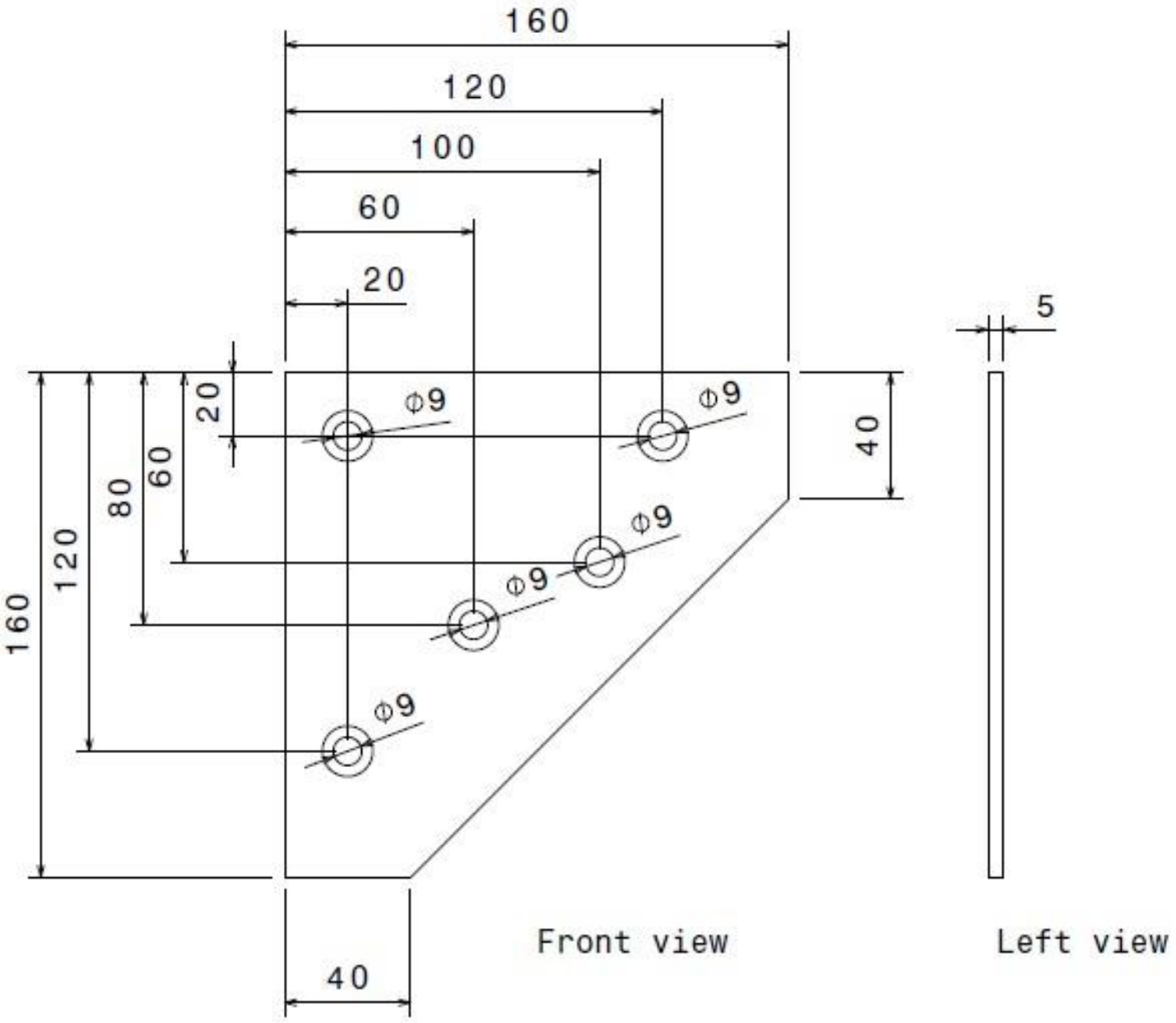

Holes: sunken for M8 bolts

TITLE: Base Bracket (Front left/Back right)	DRAWN BY: Natalie Bennell	DATE: 15/12/2013
Part Dimensions (Quantity: 2)	MATERIAL: Steel	SCALE: 1:2
	SHEET: 1 OF 1	UNITS: mm

DLR

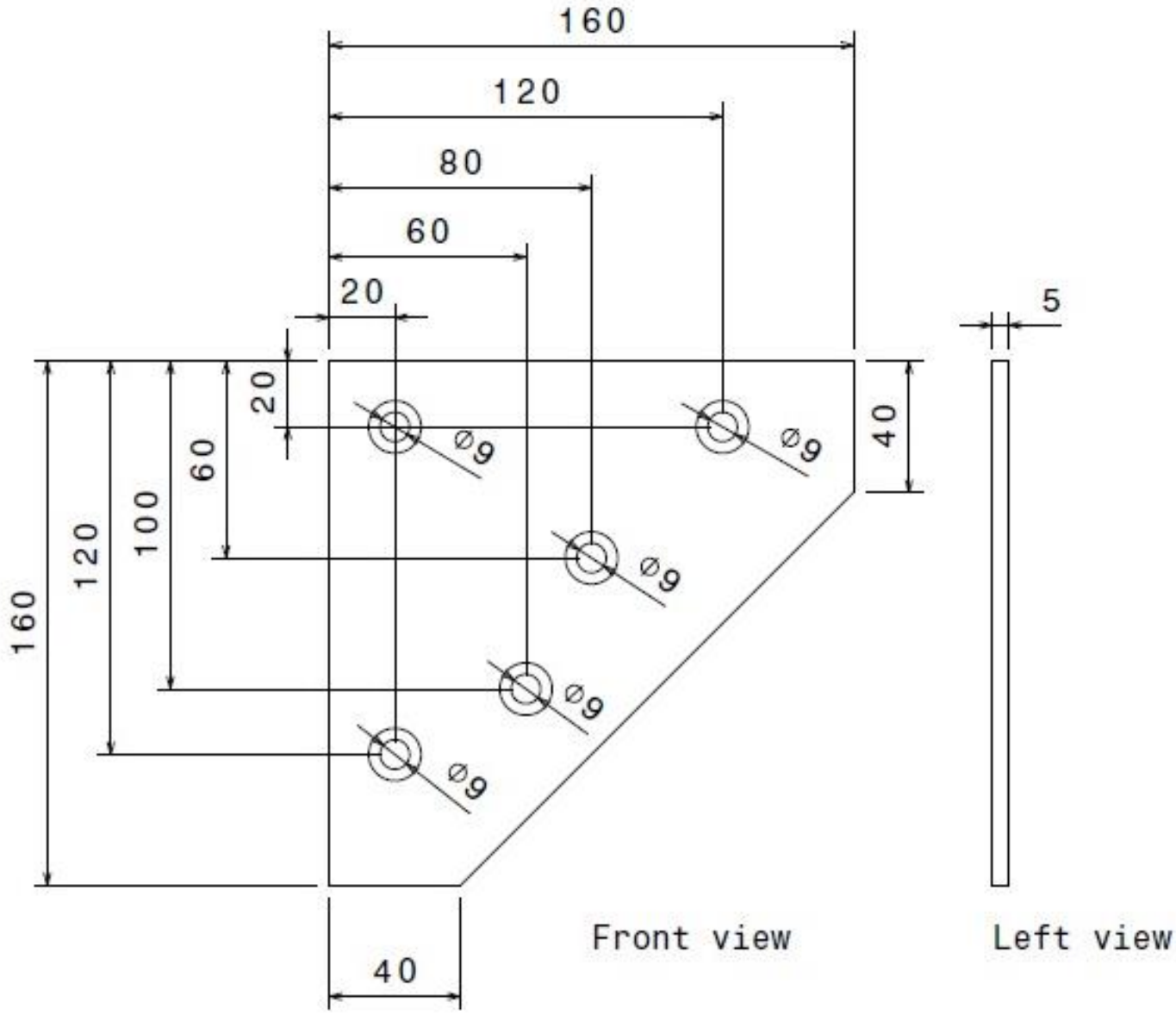

Holes: sunken for M8 bolts

TITLE: Base Bracket (Front right/Back left)	DRAWN BY: Natalie Bennell	DATE: 15/12/2013
Part Dimensions (Quantity: 2)	MATERIAL: Steel	SCALE: 1:2
	SHEET: 1 OF 1	UNITS: mm

DLR

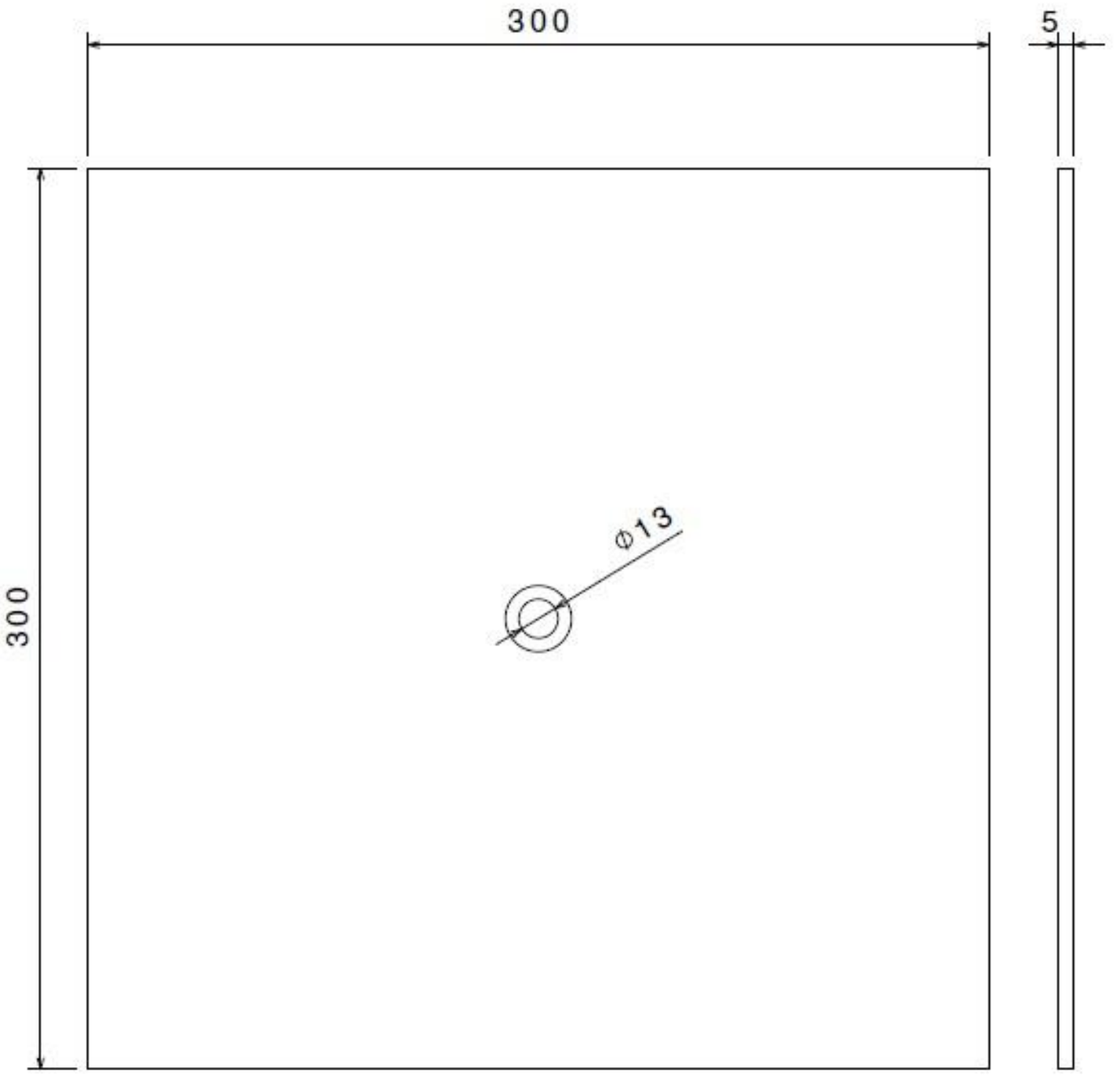

Hole: sunken for M12 bolt

TITLE: Base Tibia Plate (Original)	DRAWN BY: Natalie Bennell	DATE: 10/01/2014
Part Dimensions	MATERIAL: Steel	SCALE: 1:2
	SHEET: 1 OF 1	UNITS: mm

DLR

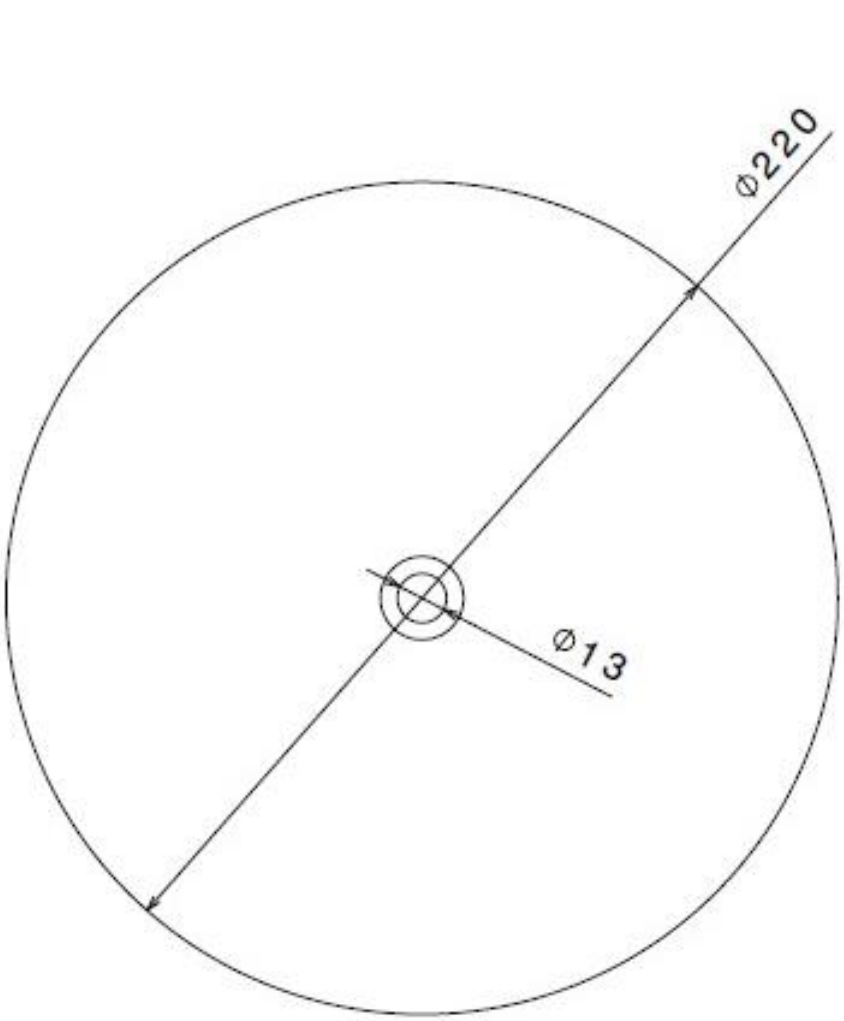

Front view

Left view

Hole: sunken for M12 bolt

TITLE: Base Tibia Plate (New)	DRAWN BY: Natalie Bennell	DATE: 03/02/2014
Part Dimensions	MATERIAL: Steel	SCALE: 1:2
	SHEET: 1 OF 1	UNITS: mm

DLR

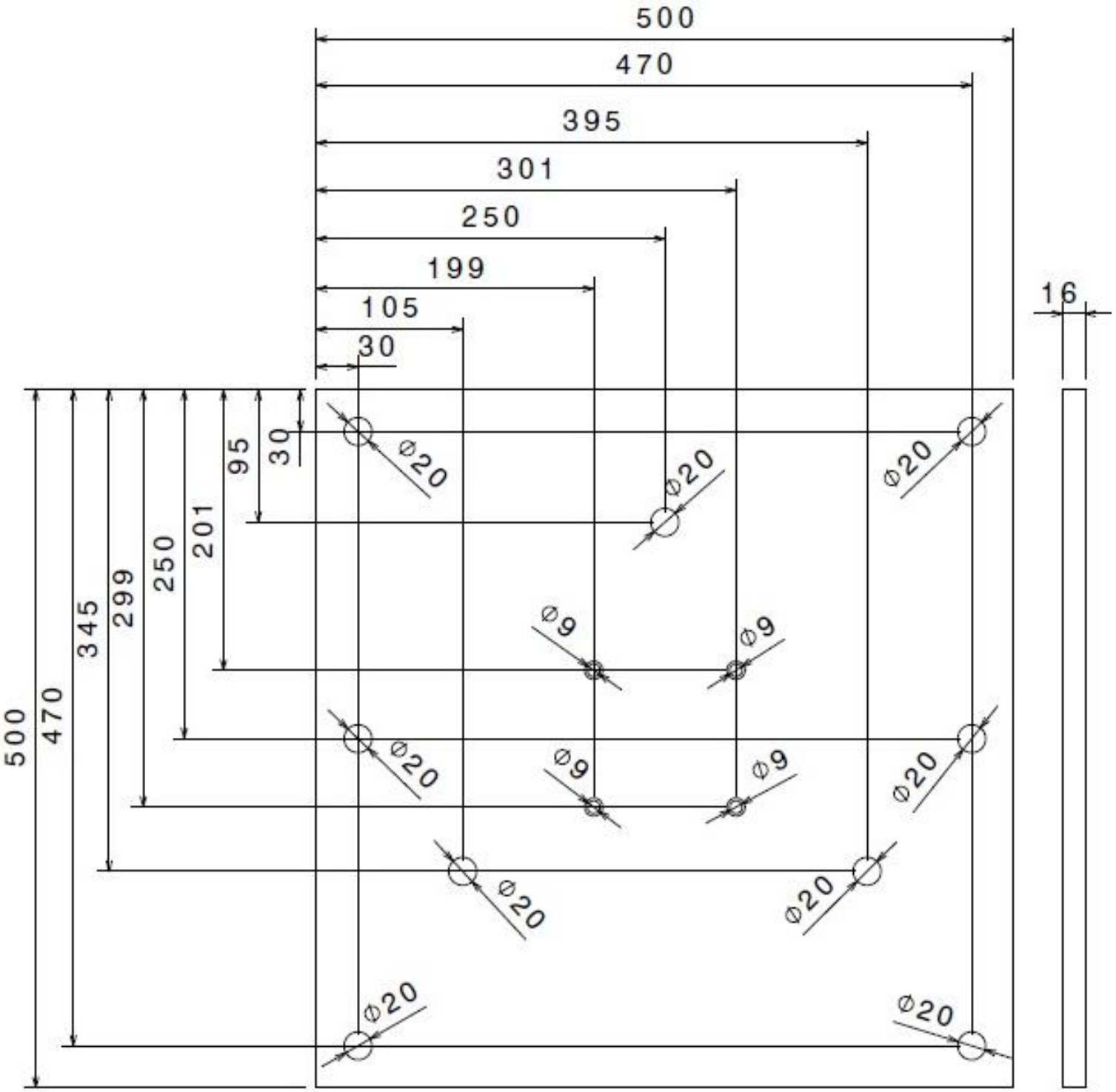

Inner four holes: sunken for M8 bolts

TITLE: Top Plate	DRAWN BY: Natalie Bennell	DATE: 10/01/2014
Part Dimensions	MATERIAL: Aluminium	SCALE: 1:4
	SHEET: 1 OF 1	UNITS: mm

DLR

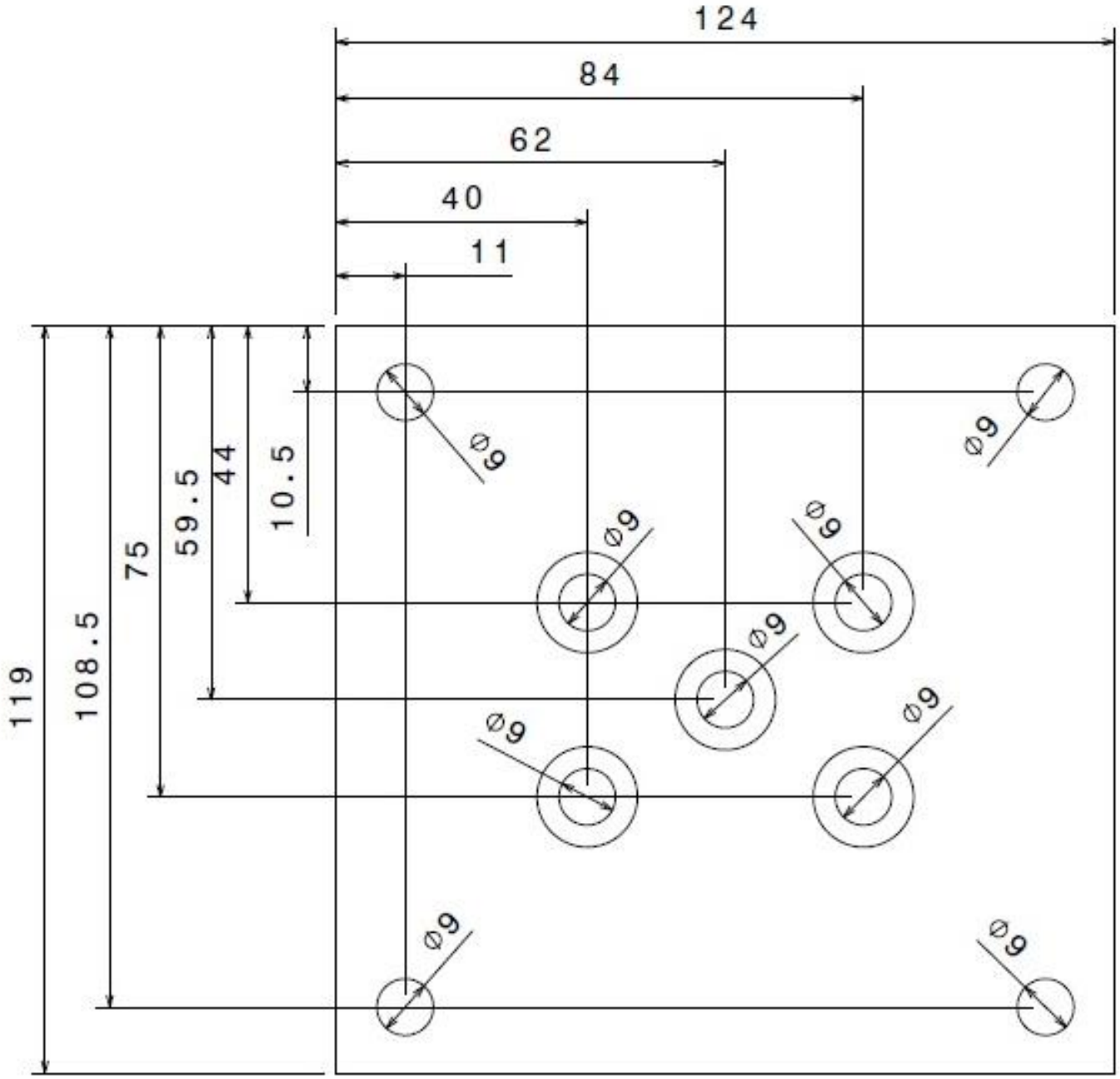

Front view

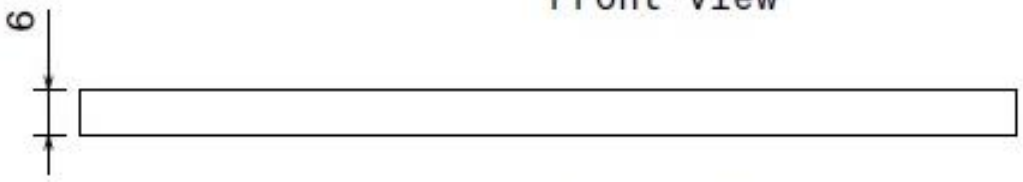

Top view

Inner five holes: sunken for M8 bolts

TITLE: Top Plate Attachment	DRAWN BY: Natalie Bennell	DATE: 10/01/2014
Part Dimensions	MATERIAL: Aluminium	SCALE: 1:1
	SHEET: 1 OF 1	UNITS: mm

DLR

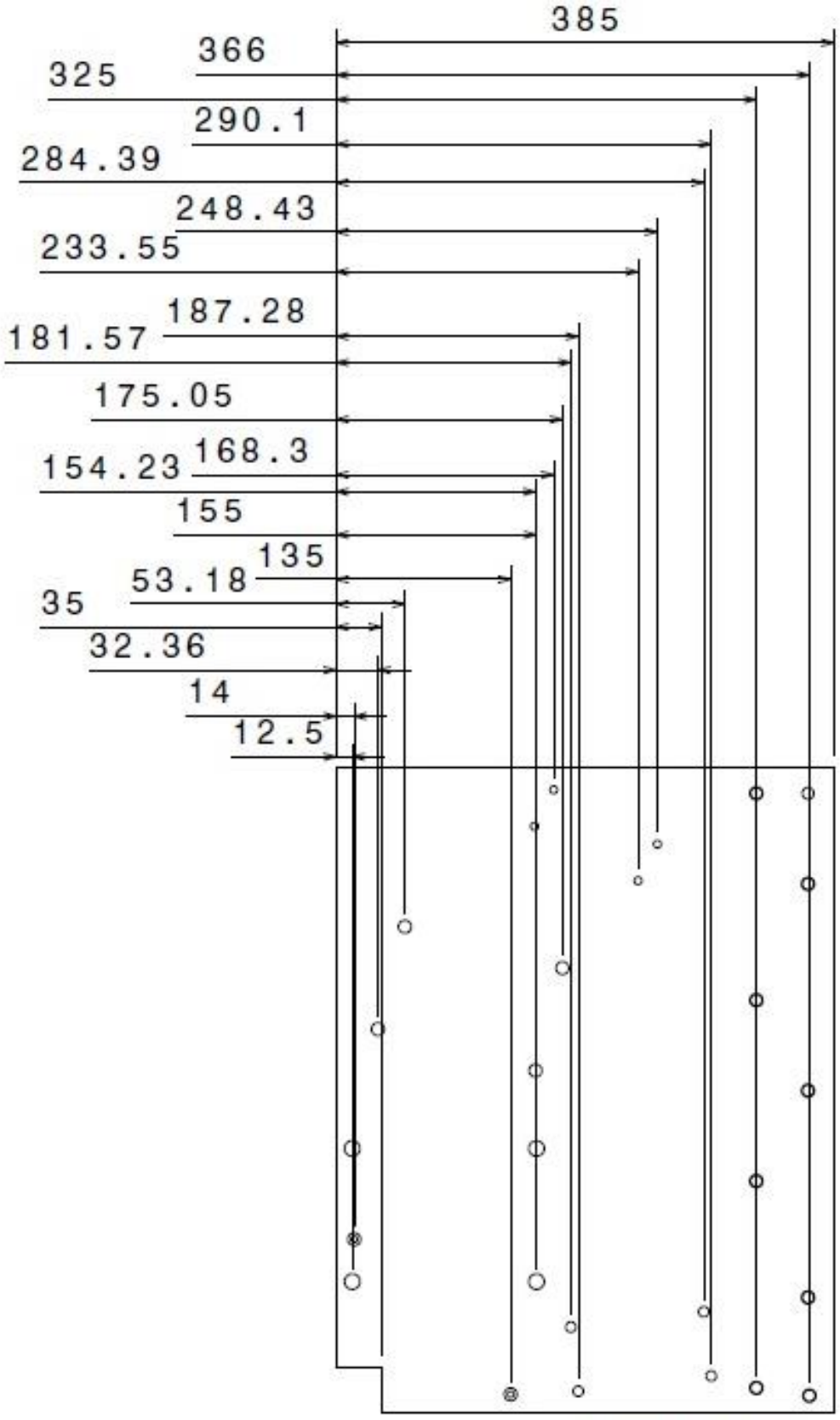

Front view

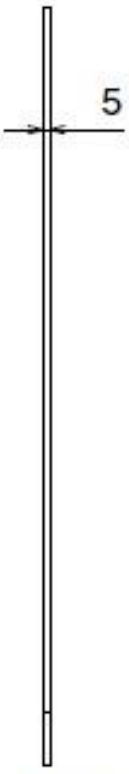

Left view

TITLE: Actuator Platform (Original)	DRAWN BY: Natalie Bennell	DATE: 10/01/2014
Part Dimensions (Hole Locations 1)	MATERIAL: Steel	SCALE: 1:5
	SHEET: 1 OF 3	UNITS: mm

DLR

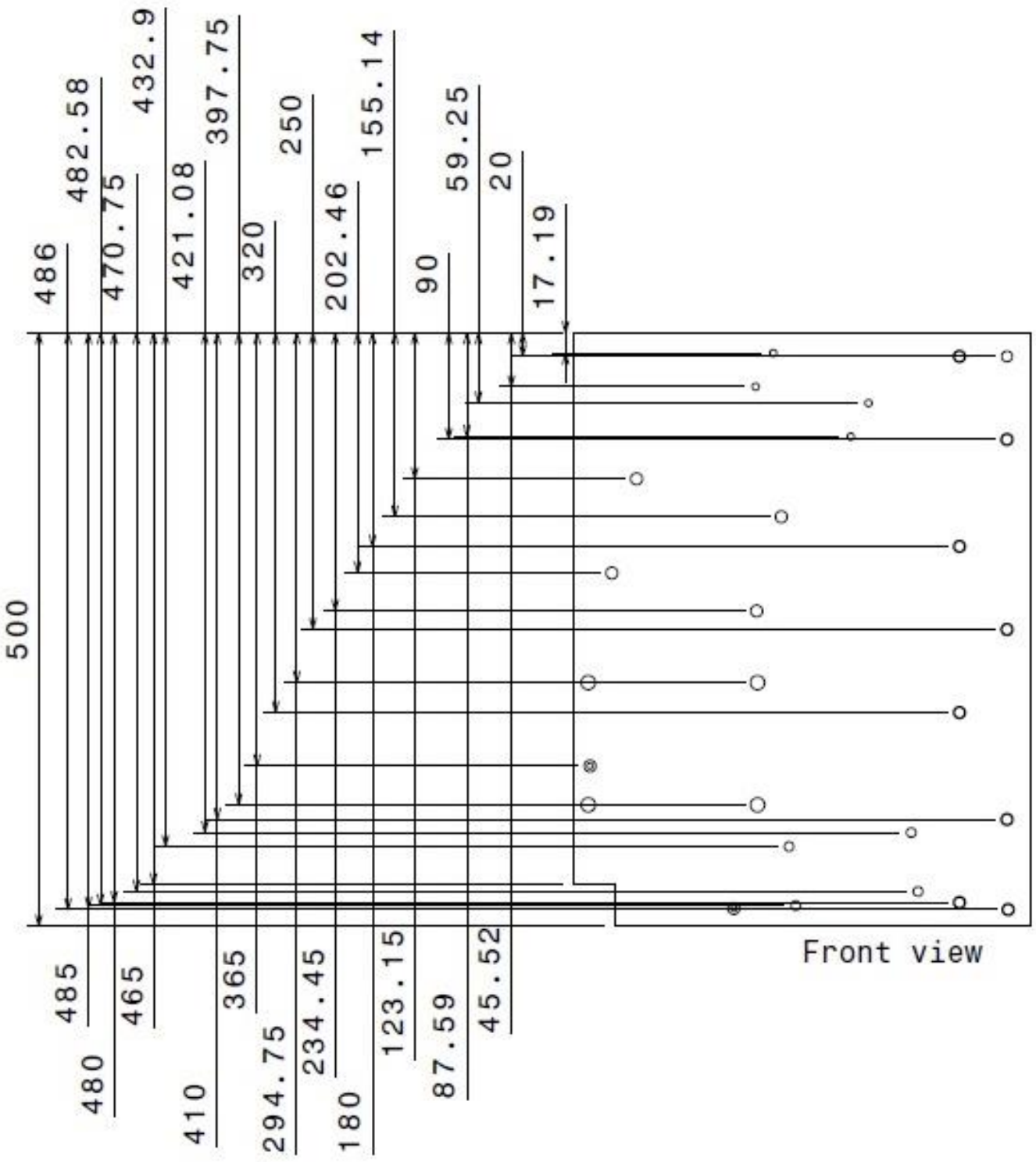

TITLE: Actuator Platform (Original)	DRAWN BY: Natalie Bennell	DATE: 10/01/2014
Part Dimensions (Hole Locations 2)	MATERIAL: Steel	SCALE: 1:5
	SHEET: 2 OF 3	UNITS: mm

DLR

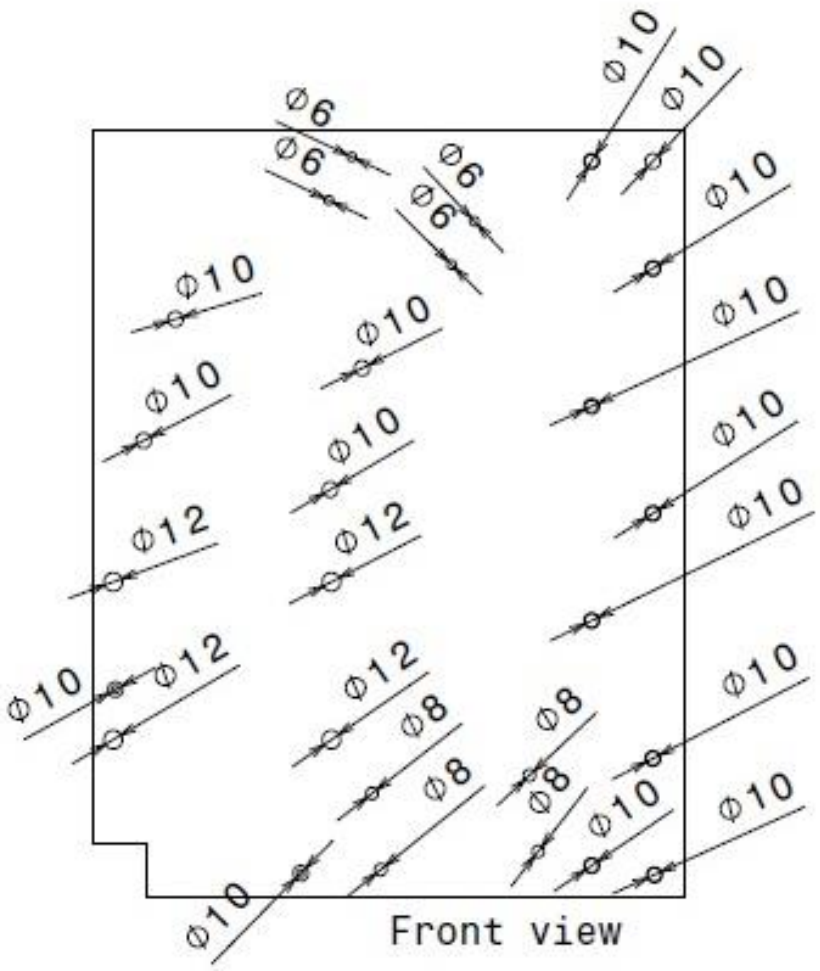

TITLE: Actuator Platform (Original)	DRAWN BY: Natalie Bennell	DATE: 10/01/2014
Part Dimensions (Hole Dimensions)	MATERIAL: Steel	SCALE: 1:5
	SHEET: 3 OF 3	UNITS: mm

DLR

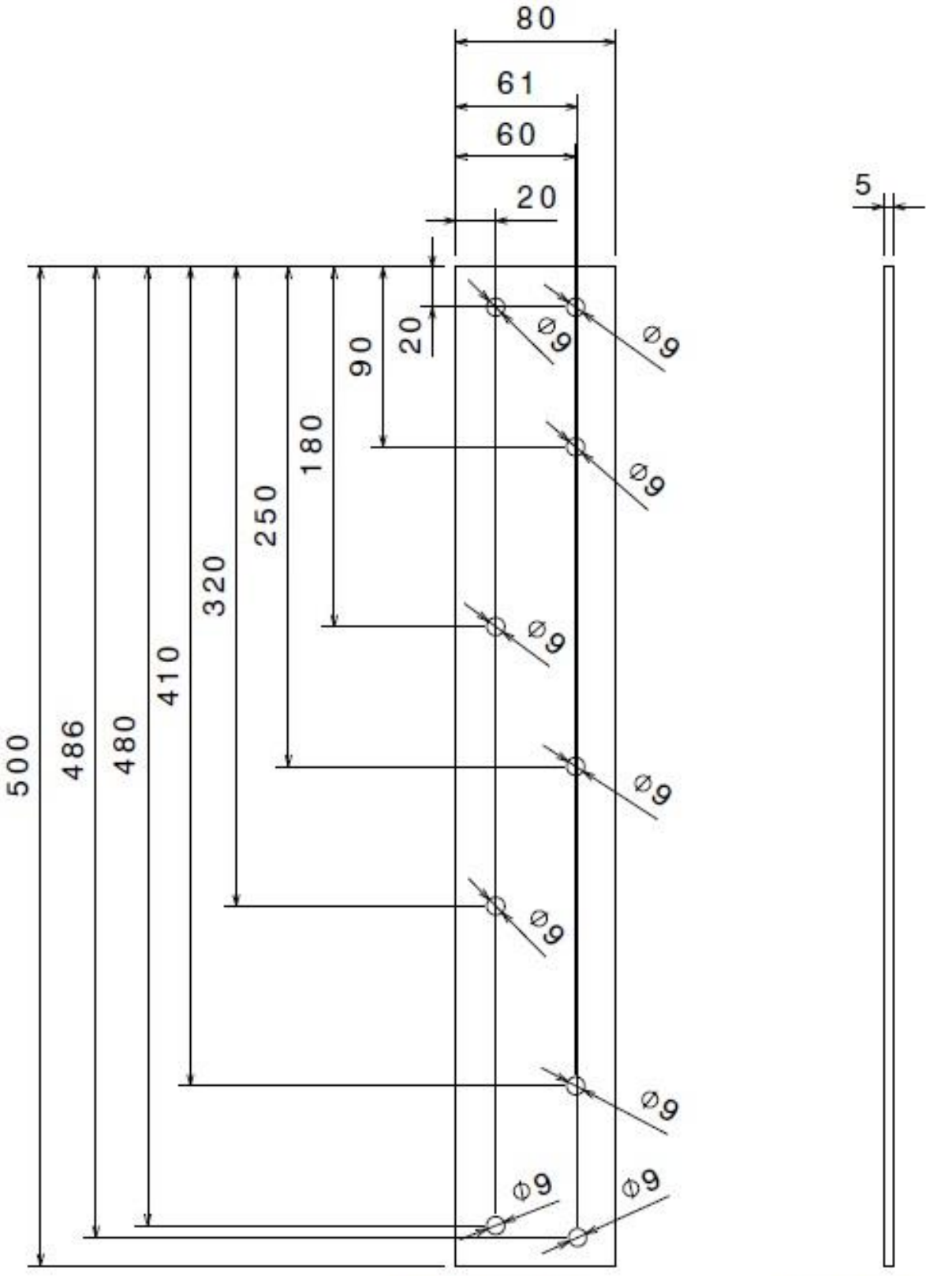

TITLE: Plate to Raise the Actuator Platform	DRAWN BY: Natalie Bennell	DATE: 10/01/2014
Part Dimensions	MATERIAL: Steel	SCALE: 1:3
	SHEET: 1 OF 1	UNITS: mm

DLR

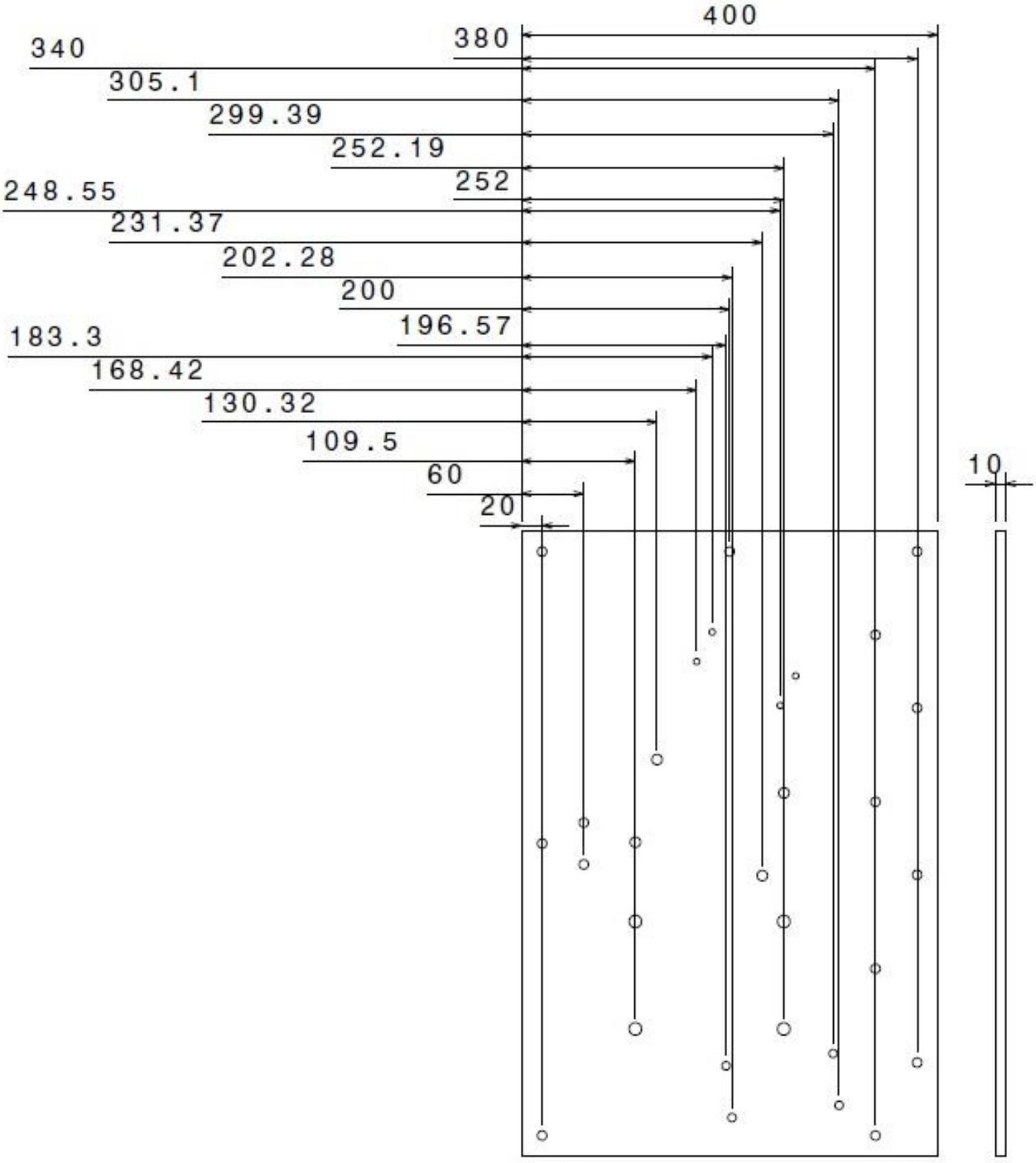

TITLE: Actuator Platform (New Version)	DRAWN BY: Natalie Bennell	DATE: 17/02/2014
Part Dimensions (Hole Locations 1)	MATERIAL: Steel	SCALE: 1:5
	SHEET: 1 OF 3	UNITS: mm

DLR

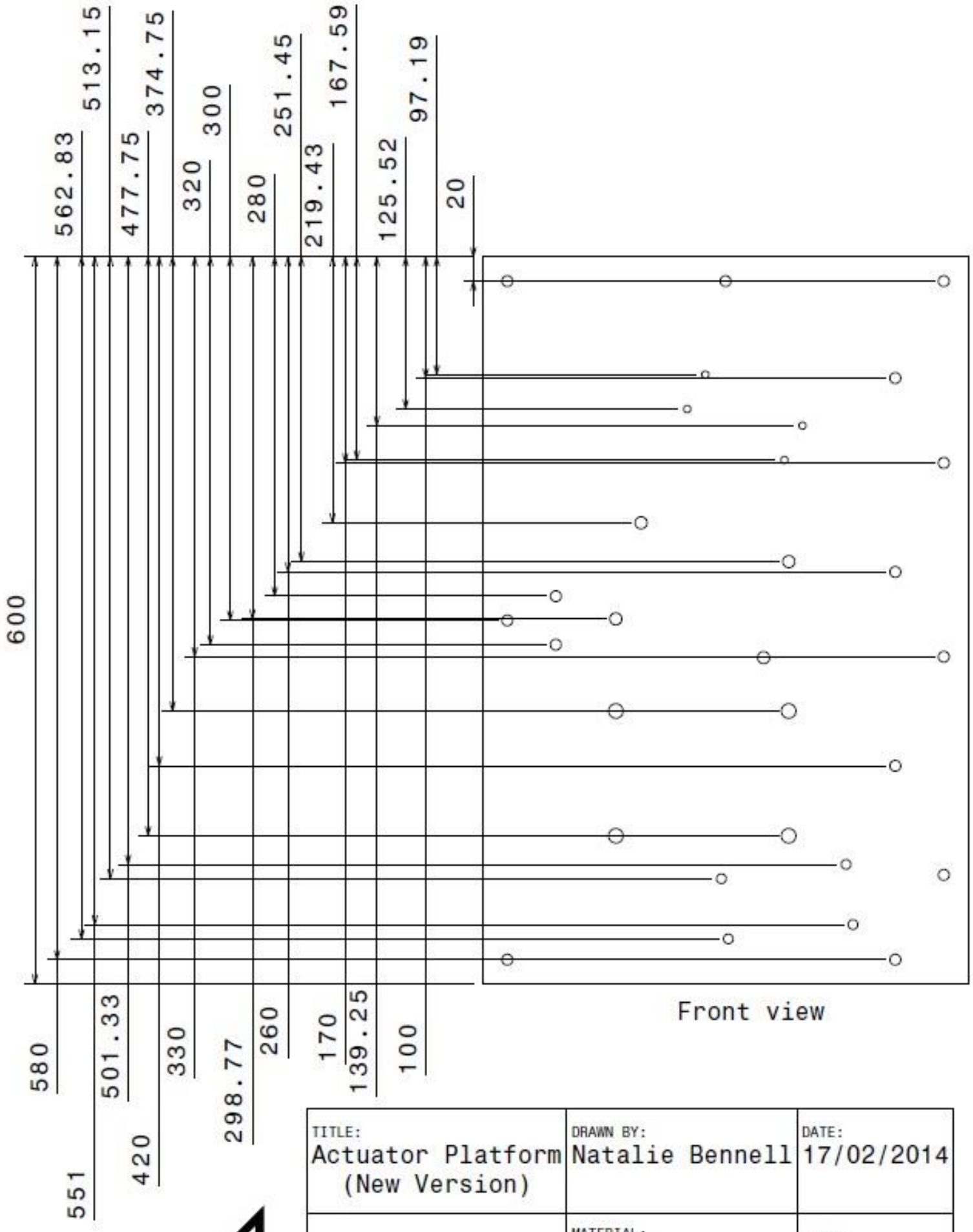

TITLE: Actuator Platform (New Version)	DRAWN BY: Natalie Bennell	DATE: 17/02/2014
Part Dimensions (Hole Locations 2)	MATERIAL: Steel	SCALE: 1:5
	SHEET: 2 OF 3	UNITS: mm

DLR

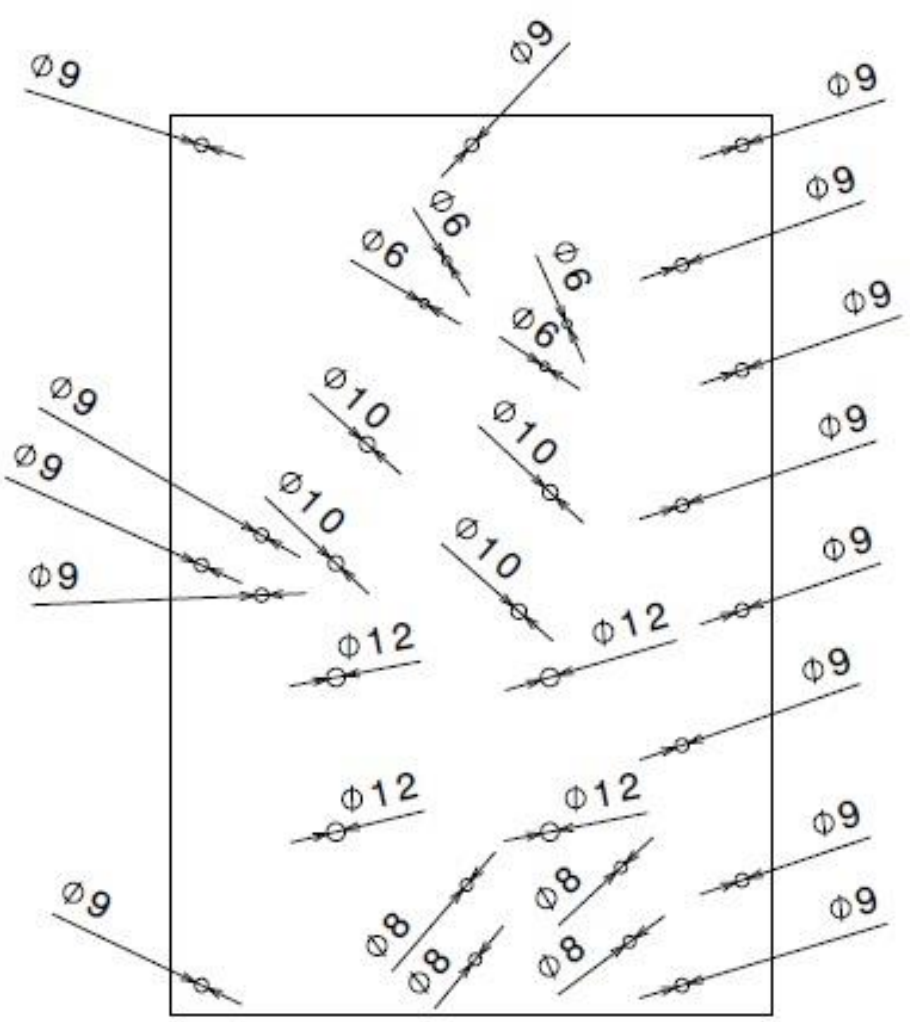

Front view

Left view

TITLE: Actuator Platform (New Version)	DRAWN BY: Natalie Bennell	DATE: 17/02/2014
Part Dimensions (Hole Dimensions)	MATERIAL: Steel	SCALE: 1:5
	SHEET: 3 OF 3	UNITS: mm

DLR

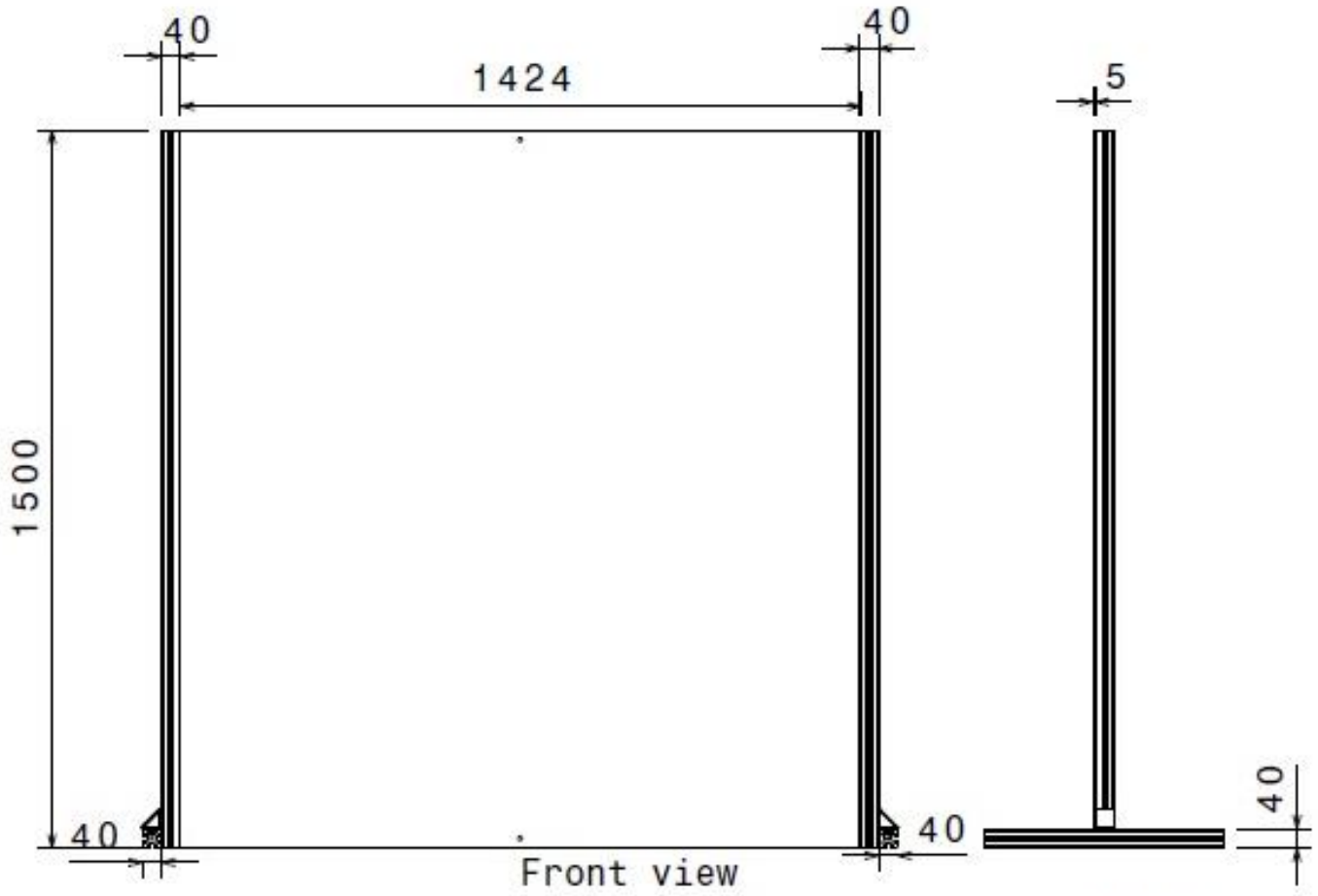

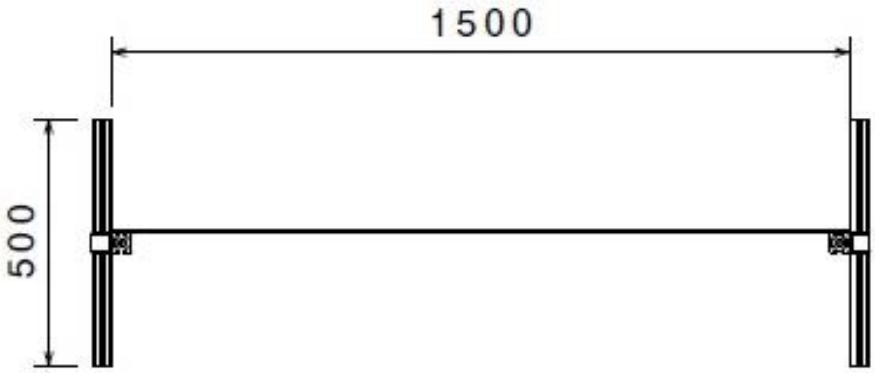

Top view

TITLE: Safety Shielding	DRAWN BY: Natalie Bennell	DATE: 14/01/2014
Assembly Dimensions	PRODUCTS: item	SCALE: 1:15
	SHEET: 1 OF 1	UNITS: mm

DLR

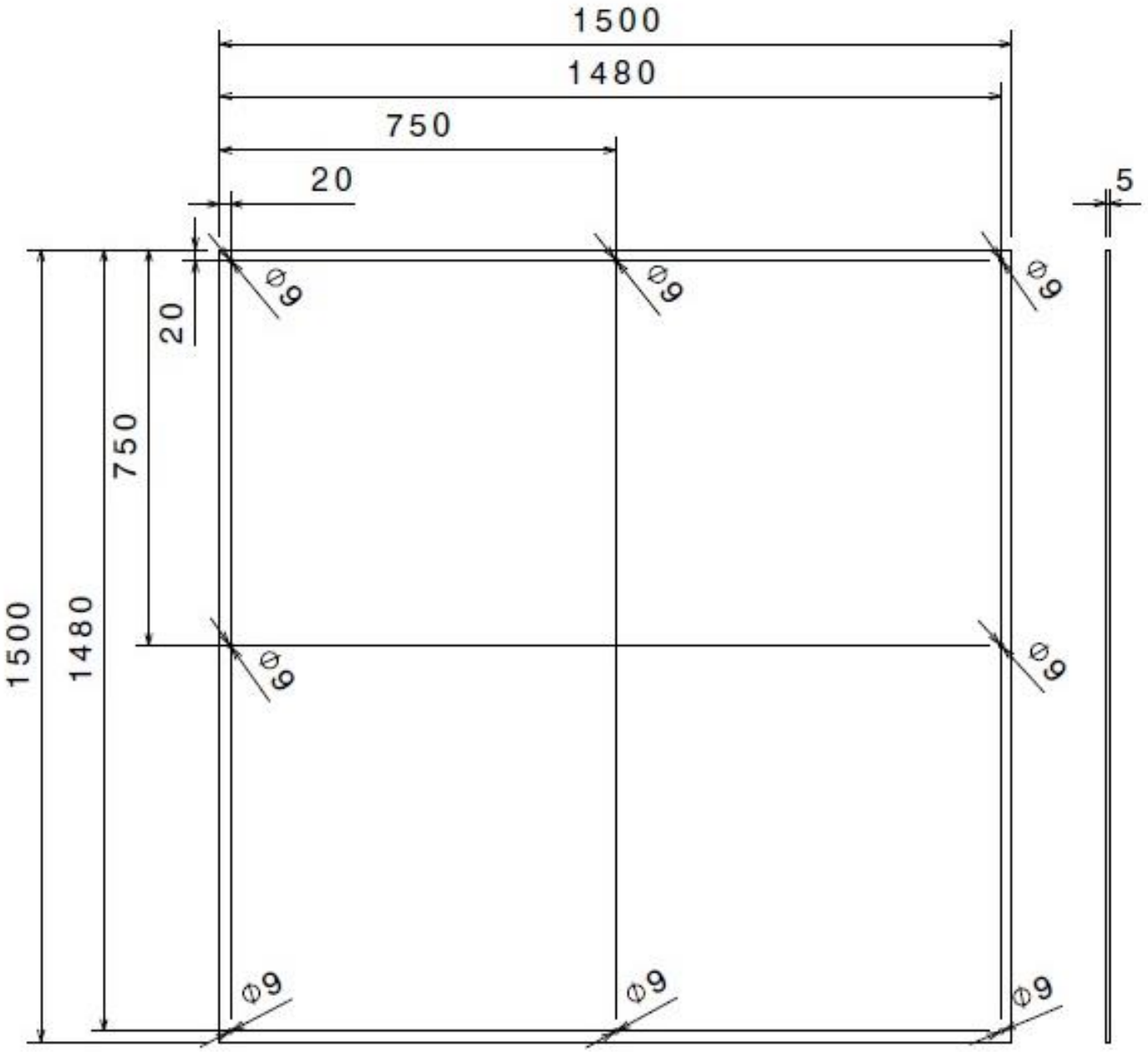

TITLE: Safety Glass	DRAWN BY: Natalie Bennell	DATE: 14/01/2014	
Part Dimensions	MATERIAL: Polycarbonate	SCALE: 1:12	
	SHEET: 1 OF 1	UNITS: mm	

DLR

Appendix G: Control System

G1. Device Specifications

G.1.1 Actuators

Four compact cylinders AEVU/AEVUZ actuators from Festo (Festo AG & Co, Esslingen, Germany) were used in this test rack. Each actuator mimics a muscle by applying force to one muscle attachment on the tibia specimen. Consequently, the actuators were selected to have a fast reaction time and a force magnitude that reaches the corresponding muscle's isometric force. All actuators had a short stroke of 10 mm. Table 32 illustrates the muscles that are simulated with the corresponding actuator piston size and Figure 61 explains the cylinder's materials. Figure 62 and Table 33 show the dimensions of the four selected actuators.

Table 32: Muscle modelled compared with actuator piston size

Muscle	Isometric Force (N) [75]	Piston Size (mm)	Theoretical actuator maximum force (N)
Soleus	3,549	100	4,000
Tibialis Posterior	1,588	80	2,733
Tibialis Anterior	905	50	999
Flexor Digitorum Longus	310	32	382

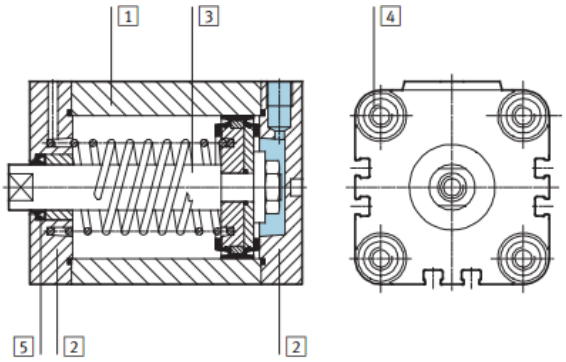

Compact cylinder		Basic version	S6
1 Cylinder barrel		Wrought aluminium alloy	Wrought aluminium alloy
2 End cap		Wrought aluminium alloy	Wrought aluminium alloy
3 Piston rod	∅ 12 ... 32	High-alloy stainless steel	High-alloy stainless steel
	∅ 40 ... 100	High-alloy steel	High-alloy steel
4 Flange screws	∅ 12 ... 16	High-alloy stainless steel	High-alloy stainless steel
	∅ 20 ... 100	Galvanised steel	Galvanised steel
5 Dynamic seals		Polyurethane	Fluorocarbon rubber

Figure 61: Materials of compact cylinders AEVU/AEVUZ [81]

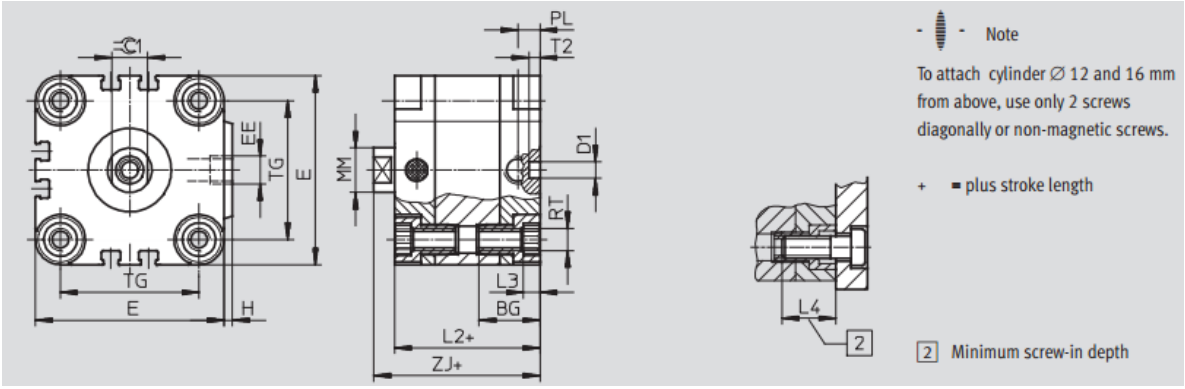

Figure 62: Dimensions of the compact cylinders AEVU/AEVUZ) [81]

Table 33: Dimensions for the four compact cylinders AEVU/AEVUZ used (mm). Adapted from [81]

Piston Ø	BG	D1 Ø	E	EE	H	L2	L3	L4	MM	PL	RT	T2	TG	ZJ	1
32	21.5	6	50	G⅛	2	44.5	5	20	12	8	M6	4	32	50.5	10
50	22	6	68	G⅛	3	45.5	6	20	16	8	M8	4	50	53	13
80	27.5	8	107	G⅛	4	56	8	25	20	8.5	M10	4	82	64	17
100	32.5	8	128	G¼	5	66.5	8	25	25	10.5	M10	4	103	76.5	22

G.1.2 Actuator Lever Arms

Rob eyes SGS from Festo acted as lever arms were attached to the actuators. Four rob eyes (material: galvanised steel) were purchased, one for each of the actuators. The dimensions of the rob eye are shown in Figure 63 and Table 34.

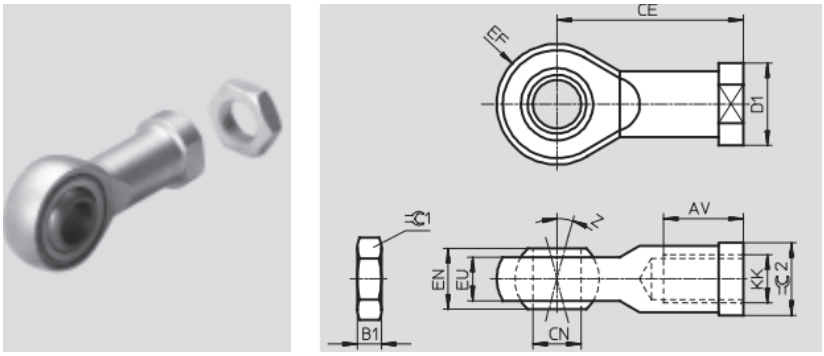

Figure 63: Rob eye SGS dimensions [83]

Table 34: Dimensions for the four rob eyes SGS used (mm). Adapted from [83]

Piston Ø	KK	AV	B1	CE	CN Ø	D1 Ø	EF	EN	EU	Z °	1	2
32	M10x1.25	20	5	43	10	19	14	14	10.5	13	17	17
50	M12x1.25	22	6	50	12	22	16	16	12	13	19	19
80	M16x1.5	28	8	64	16	27	21	21	15	15	24	22
100	M20x1.5	33	10	77	20	34	25	25	18	15	30	30

G.1.3 Actuator Mounting Support

Mounting apparatuses was purchased for each actuator, from Festo, to position the actuators on a horizontal plate. Dimensions are displayed in Figure 64 and Table 35.

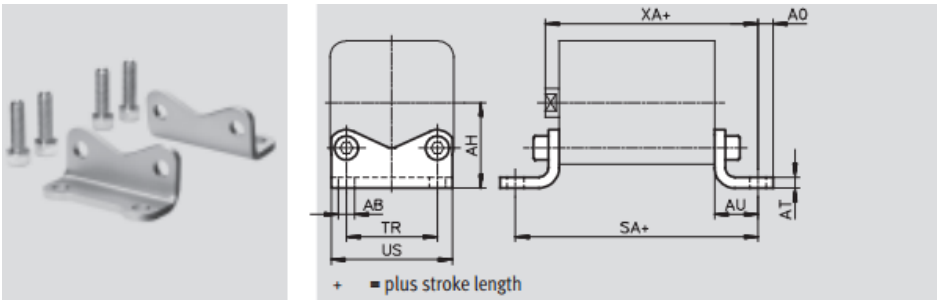

Figure 64: Mounting apparatus dimensions [82]

Table 35: Dimensions for the four actuators mounting apparatus (mm). Adapted from [82]

Piston Ø	AB Ø	AH	AO	AT	AU	SA	TR	US	XA
32	6.6	34	8.25	5	18	80.5	32	48	68.5
50	9	47	8.25	6	24	93.5	50	66	77
80	11	68.5	11.75	8	30	116	82	105	94
100	13.5	81	11.75	8	33	132.5	103	126	109.5

G.1.4 Load Cells

Model 8523-2000 and 8531-5000, burster load cells (burster präzisionsmesstechnick gmbh & co kg, Gernsbach, Germany) were used in the configuration of the test rack. The dimensions and specifications can be found in the Figure 65 and Table 36.

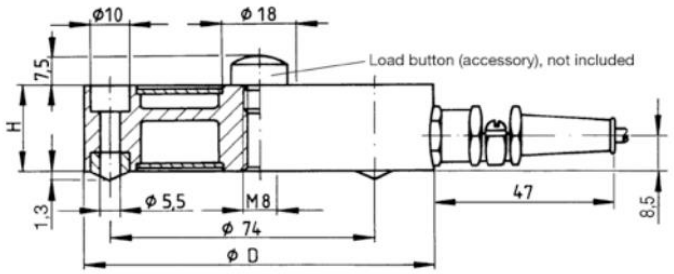

Figure 65: Dimensional drawing of burster load cell, model 8531 [95]

Table 36: Corresponding dimensions and specification for the load cell. Adapted from [95]

Order code	Load Range (N)	Accuracy (%v.E)	Sensitivity (mV/V)	∅ D (mm)	H (mm)	Natural Frequency (kHz)	Weight (kg)
8531-2000	0-2000	≤ ± 0.15	Standardised 1.5 ± 0.2%	99.5	30	1.8	0.35
8531-5000	0-5000	≤ ± 0.15	Standardised 1.5 ± 0.2%	99.5	30	3.0	0.35

G2. Pneumatic Control System Layout

The pneumatic system was controlled by manually adjusting air valves and programing with the software LabView (National Instrument, NI, USA). Figure 66 shows the LabView coding (left) and the individual devices (all purchased from Festo) (right) used in the pneumatic system setup.

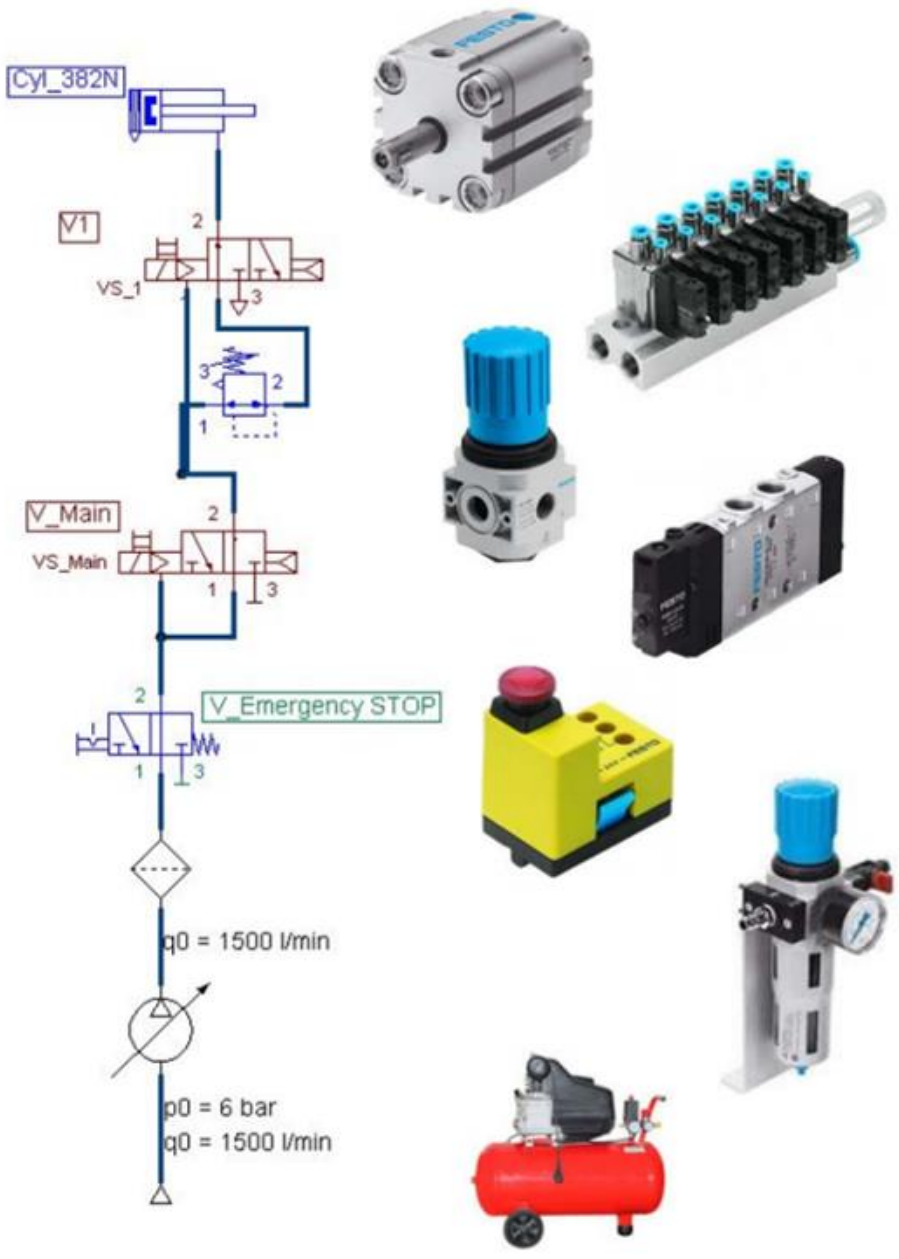

Figure 66: Individual components of the control system

Figure 67 displays the LabView setup for the entire pneumatic system. The system is arranged with the smallest actuator on the left and largest actuator on the right (maximum force displayed). See Table 32 for a list of the actuator maximum forces corresponding to the muscle they are representing.

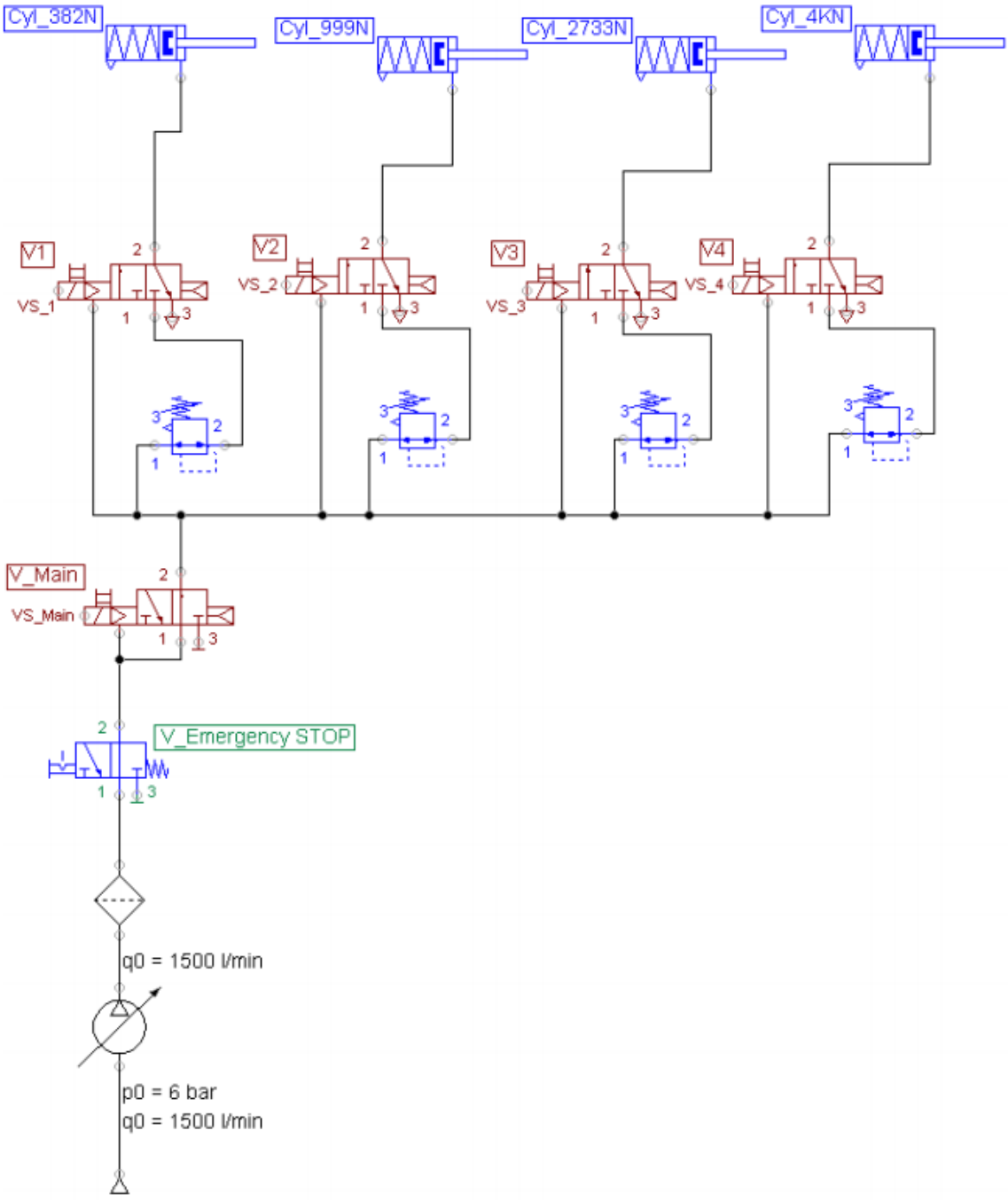

Figure 67: LabView layout of the entire pneumatic system

Appendix H: Test Rack Results Summary

Overview of the test rack specifications and results for stating if the solution 'achieved' its purpose or if it encountered 'problems'.

Table 37: Summary of test rack specifications and the results of this project

Component	Specification	Solution	Results
		Attachment of tibia/mounting	
Proximal Fixture	Proximal tibia movable, similar to physiology.	Large plate secured to a small plate that is fixed to the proximal tibia via four M8 bolts so that weights can be stacked on top of the plate.	Achieved
		The small plate between the top plate and tibia allows for fast disassembly.	Achieved
Distal Fixture and Mounting	Distal tibia head firmly fixed to prevent any movement or rotation.	Distal tibia fixed to base plate with one M12 bolt as modelling a particular part of body movement under static conditions.	Problems Too much pressure at the one point.
	May be positioned on a force plate.	Thick base plate to ensure the high loads do not cause it to bend.	Achieved
	Mechanical decoupling of tibia fixation and any downward pulling force sources.	Gecko tape used to secure base plate to force plate.	Achieved
		The tibia is facing the left and is positioned just forward of centre, in line with the pulleys positioned on the front edge of the pillars.	Problems Tibia twisted during tests so was not aligned with the pulleys.

Component	Specification	Solution	Results
		Forces/Control	
Forces and muscles	Four downward forces, modelling the muscles Soleus, Tibialis Posterior, Tibialis Anterior and Flexor Digitorium Longus, applied using pneumatic actuators.	Actuators (Festo, Compact Cylinder AEVU/AEVUZ, piston side: 100mm, 80mm, 50mm, 32mm) with 4000N, 2733N, 999N and 382N max force, respectively and a small stroke (10 mm).	Problems Small stroke, resulting in a limited force transfer to the specimen.
	Orientation of muscle force vectors close to anatomical orientations.	The downward body weight force for body movements applied with weights stacked onto tibia top plate.	Achieved
	Magnitude of force in range zero to maximum isometric force of each muscle.	Force can be applied to the top of the tibia in the y-direction with a rope tied around the top plate and fed through a pulley positioned on the front of the test rack.	Problems Crack occurred during test.
	Speed and force with respect to time behaviour close to physiological conditions.	The other end of the rope has a weight secured to it and is slowly released.	Achieved
		Force plate used to position weights and ensure no unwanted moments.	N/A
		Actuators controlled using solenoid valves and control system.	Achieved
		Rope (FSE Coppa 3000 Dyneema, 6 mm) with high maximum load (17 kN) and low elasticity to transmit force from actuator to tibia specimen.	Achieved

Component	Specification	Solution	Results
		Ropes secured using bowline knots, rope fasteners and rope tighteners with a preload as the actuator stroke is small and do not want a decrease in force.	Problems Ropes were not secured tightly for complete force transfer to specimen.
Tendon	Force transfer to one point on tibia for each muscle to replicate tendon attachment.	One M8 bolt positioned in the centre of tendon area for each muscle to act as the muscle attachment to the tibia.	Achieved
User Interface	Test rack setup is simple.	Test rack setup can be found in Section 4.1.	Achieved
Control System	Actuator vibration caused by stroke should not affect tibia deformation.	Actuators on same structure but different platform to tibia.	Achieved
		Platform thick with nine attachment points to hold the strong forces.	Problems Platform bent.
	Easily regulated pneumatic control system.	Pneumatic control system on a completely separate structure so it can be easily regulated.	Achieved
		Specimen	
Type of bone	Validation using simple structure with known mechanical properties that is straightforward to model on a computer and has known mechanical properties.	Validation using a PVC cylinder	N/A
		Using a tibia bone specimen (SawBone, Composite Bone, Fourth Generation, Size: Large) that has known mechanical properties similar to actual bone	Achieved

Component	Specification	Solution	Results
	Tibia bone replica that is physiologically similar to bone.		
Number of joints	No joints.	Tibia firmly fixed to base and not mechanism above tibia to model knee or upper leg.	Problems fixture resulted in incorrect for transfer through the specimen.
	Optical Measuring System		
Axis and Accuracy	High accuracy and can measure displacement along the x, y and z axis. Mechanism for optical measuring system to detect bone deformation.	Vicon system Cluster markers attached to the tibia specimen for the Vicon system to read the displacement in three locations similar to the MUST study.	N/A N/A
Visibility	The optical measuring system requires high visibility.	The test rack is designed with only two structural pillars.	Achieved
	Force Measurement System		
Reaction Force	Measure forces and moments along the x, y and z axis.	Force plate (AMTI OR-6-6-2000) to measure the reaction force at the ankle. Can read forces and moments up to 8896 N (Fz), 4448 N (Fx and Fy), 2258 Nm (Mx, My) and 1129 Nm (Mz)	N/A
Muscle Force	Mechanical load cells to measure actuator force.	Mechanical load cells (Burster, models 8531-2000 and 8531-5000) are setup in the rope connection to measure the actuator forces. These are connected to the	Problems Issues occurred in both the setup of the load cell and with

Component	Specification	Solution	Results
		computer software LabView to read the measurements.	the computer scaling.
		Test Rack	
Support Structure	Allow for various size elements.	Adjustable height with 1.5 m pillars to allow for more elements to be attached above and below the tibia specimen.	Achieved
	Be able to withstand the high forces applied to it	Structural components (item) of the test rack constructed with thick beams (80x80 mm) and large brackets (160x160mm).	Achieved
Safety	Implementations to prevent injury in case of malfunction.	Automatic stop button for the pneumatic system to prevent air flow to the entire system in case of an emergency.	Achieved
		Safety glass to prevent any materials from the test rack flying around and hurting people whilst the actuators are functioning.	Achieved
		Rope (FSE Rio white, 8mm) fed through top plate and eyebolts positioned on pillars to prevent weight and plates falling and causing damage to the experimental apparatus.	Achieved
Whole Test Rack	Simple disassembly.	All components secured with bolts. No items are welded or permanently fastened together.	Achieved
	Cost kept at minimum.	Reduced cost by, when applicable, using equipment and materials already at DLR.	Achieved

Appendix I: Validation Test Protocol

Aim:

To validate the test rack by comparing the deformation of a PVC cylinder applied using pneumatic actuators with a computer model.

Hypothesis:

All components of the test rack will function as expected and will experimentally produce the same deformation in the PVC cylinder as the computer model.

Materials:

- Test Rack and components
- PVC cylinder with known mechanical properties
- Computer model, using the software system Ansys (Ansys, Inc., PA, USA)
- Optical measuring system: Vicon (Vicon Motion System Ltd, LA, USA)
- Cluster markers

Safety:

- Ensure safety shielding is positioned between test rack and people
- Have an automatic stop button for the pneumatic system
- All sharp edges on the test rack should either have shielding or have the edges smoothed
- Tie ropes through the top plate and eyebolts positioned on the pillars to hold the top plate if it slants or the PVC cylinder breaks

Method:

Setup Procedure:

- Setup the test rack (Section 4.1). However, instead of a tibia specimen, use a PVC cylinder
- Insert an M8 bolt half way up the PVC cylinder

- Attach a cluster marker in the top third of the PVC cylinder, ensuring the location is reordered so later displacement measurements can be compared to the computer model
- Secure the PVC cylinder to the force plate and tie the rope (using a bowline knot) around the bolt
- Connect the rope to a load cell and attach the other end to the largest pneumatic actuator
- Setup and calibrate the optical measuring system
- Turn on the pneumatic system, ready for actuator operation

Experimental Method:

Along with recording force magnitude of the actuator and displacement of the PVC cylinder, observations of the test rack should be noted. If an issue is raised, tests should cease and the problem should be addressed. Only once a solution has been acquired and verified can the tests resume, and the tests should restart from the beginning.

The measurements should be recorded in the table displayed in the Results.

(1) Low force application

1. Provide 2 bar of pressurised air to the largest actuator;
2. Hold for 5 seconds;
3. Record the load cell force reading on the computer program LabView;
4. Record the PVC cylinder displacement;
5. Repeat 3 times to procure average force and displacement measurements.

(2) Medium force application

1. Provide 4 bar of pressurised air to the largest actuator;
2. Hold for 5 seconds;
3. Record the load cell force reading on the computer program LabView;
4. Record the PVC cylinder displacement;
5. Repeat 3 times to procure average force and displacement measurements.

(3) High force application

1. Provide 6 bar of pressurised air to the largest actuator;
2. Hold for 5 seconds;

3. Record the load cell force reading on the computer program LabView;
4. Record the PVC cylinder displacement;
5. Repeat 3 times to procure average force and displacement measurements.

Computer modelling

The average forces recorded for each force application should be modelled on the software computer program Ansys. The system should include the constraints set on the PVC cylinder, including the base fixation and the large top plate's weight.

Displacement at the same location as the marker cluster should be determined from the model. The software tool used should be the same as that used for future movement tests.

Results:

Test	*Measurement*	*Repetition*			*Average*
		1	**2**	**3**	
Low force application	Force (N)				
	Displacement				
Medium force application	Force (N)				
	Displacement				
High force application	Force (N)				
	Displacement				

Comparison:

A comparison should be made of the PVC displacement between the experimental and computed data. If the experimental displacement is within a chosen range, set by the researches, of the computer model, then the test rack is valid, it accurately simulates the requested functions and is ready for the next phase of testing: body movement testing. If the data is not comparable, depending on the error either or both the test rack and the computer model will need to be adapted. Following amendments, the validation test protocol should be repeated until the displacement of the PVC cylinder is within the chosen range determined by the computer model.